https://ntrs.nasa.gov/search.jsp?R=19670006112 2020-03-16T18:48:45+00:00Z

Akademiya Nauk Ukrainskoi SSR

V.P. Konopleva, Editor

PHYSICS OF COMETS AND METEORS

GPO PRICE $ _____
CFSTI PRICE(S) $ _____
Hard copy (HC) 3.00
Microfiche (MF) 1.30
ff 653 July 65

FACILITY FORM 602
N67 15441 (ACCESSION NUMBER)
110 (PAGES)
(NASA CR OR TMX OR AD NUMBER)
N67 15454 (THRU)
1 (CODE)
30 (CATEGORY)

Translated from Russian

Published for the National Aeronautics and Space Administration, U.S.A.
and the National Science Foundation, Washington, D.C.
by the Israel Program for Scientific Translations

AKADEMIYA NAUK UKRAINSKOI SSR
RESPUBLIKANSKII MEZHVEDOMSTVENNYI SBORNIK

Academy of Sciences of the Ukrainian SSR · Ukrainian Interdepartmental Collection

Series: *Astronomy and Astrophysics*

V. P. Konopleva, Editor

PHYSICS OF COMETS AND METEORS

(Fizika komet i meteorov)

Izdatel'stvo "Naukova Dumka"
Kiev 1965

Translated from Russian

Israel Program for Scientific Translations
Jerusalem 1966

NASA TT F-340
TT 67-51213

Published Pursuant to an Agreement with
THE NATIONAL AERONAUTICS AND SPACE ADMINISTRATION, U. S. A.
and
THE NATIONAL SCIENCE FOUNDATION, WASHINGTON, D.C.

Copyright © 1966
Israel Program for Scientific Translations Ltd.
IPST Cat. No. 1816

Translated by Z. Lerman

Printed in Jerusalem by S. Monson
Binding: Wiener Bindery Ltd., Jerusalem

Price: $ 4.00

Available from the
U. S. DEPARTMENT OF COMMERCE
Clearinghouse for Federal Scientific and Technical Information
Springfield, Va. 22151

x/14/3. 5

Table of Contents

EXPLANATORY LIST OF ABBREVIATIONS OF USSR INSTITUTIONS AND PERIODICALS APPEARING IN THIS BOOK

Abbreviation	Full name (transliterated)	Translation
ATs	Astronomicheskii Tsirkulyar	Astronomical Circular
AZh	Astronomicheskii Zhurnal	Astronomical Journal [Soviet Physics]
DAN UkrSSR	Doklady Akademii Nauk Ukrainskoi SSR	Proceedings of the Academy of Sciences of the Ukrainian SSR
Izv. AN SSSR	Izvestiya Akademii Nauk SSSR	Bulletin of the Academy of Sciences of the USSR
Izv. KrAO	Izvestiya Krymskoi Astronomicheskoi Observatorii	Bulletin of the Crimean Astronomical Observatory
KGU	Kievskii Gosudarstvennyi Universitet	Kiev State University
Publikatsii KAO	Publikatsii Kievskoi Astronomicheskoi Observatorii	Transactions of the Kiev Astronomical Observatory
Trudy AN TadzhSSR	Trudy Akademii Nauk Tadzhikskoi SSR	Transactions of the Academy of Sciences of the Tadzhik SSR
UFN	Uspekhi Fizicheskikh Nauk	Advances in Physical Sciences [Soviet Physics—Uspekhi]
ZhETF	Zhurnal Eksperimental'noi i Teoreticheskoi Fiziki	Journal of Experimental and Theoretical Physics [Soviet Physics—JETP]
ZhFKh	Zhurnal Fizicheskoi Khimii	Journal of Physical Chemistry

D. A. Rozhkovskii

N67 15442

PHOTOMETRY OF COMETS USING 1963—1964 PATROL PHOTOGRAPHS

It has been repeatedly observed that comparatively weak comets with an intrinsic brightness of $8-10^m$ and less are the most frequent ones. The aspect of these comets and some of their properties have been described by B. A. Vorontsov-Vel'yaminov /1/. During the International Year of the Quiet Sun, observers participating in the comet survey will apparently have to deal with these faint objects, applying photographic techniques of observation, photographic photometry in particular.

However, even a careful photometry of a comet, which is quite a time-consuming procedure, gives a fairly limited amount of information. It is obviously desirable to simplify the most tedious stages of the job, without, however, detracting from the value of the results. This particularly applies to the patrol program, based on numerous observations of comets. Our presentation is intended to throw light on the possible solution of the above problem, but the procedure can be adopted in its entirety for other purposes as well.

1. METHOD OF OBSERVATION

Systematic observations of weak comets at the Kazakh Astrophysical Institute are carried out with Maksutov's high-power menisc telescope ($D = 50$ cm, 1 : 2.4), whose optical properties meet the requirements of the patrol program. The tight schedule of the telescopes unfortunately restricts the flexibility of cometary observations.

Comets are photographed on Astro Special or Kodak OaO plates without filter, permitting exposures of up to 12—15 min with a well-exposed background sky. Application of filters substantially increases the exposure time and on the whole is of fairly limited value /11/.

The photographs are standardized by means of extrafocal stellar images obtained with a diaphragmed menisc. The full aperture gives a ring image with a complex diffraction pattern which is inadequate for photometry /6/.

The "double-decker" method is unsuitable for the same reasons. Stars of open galactic clusters, which have been investigated by many authors, and particularly in /10/, are used as standards. Since weak stars predominate in these clusters, minimal extrafocality is applied in standardization. With an extrafocal disk of 0.3 mm diameter, the cluster

photograph will generally show a dozen or more stars of known magnitudes B.

Microphotometric treatment of these standardization photographs requires precision measurements of the area of the extrafocal images. The extrafocal disks of the brighter stars are generally enlarged to a considerable extent by the effect of photographic irradiation, so that measurements are made by means of nearby, possibly faint, stars.

The photographs are calibrated with the aid of bright-ups from a tube photometer illuminated directly by the night sky. During exposure, the photometer is rotated by a small motor, to ensure perfect smoothing of the illumination. Repeated tests have shown that the resulting bright-up photometric scale is virtually identical with the scale of the photometric system B, and also with the international photometric scale. To illustrate this agreement, we have plotted in Figure 1 the P_{pg} from /9/ for some stars in the Hyades against the magnitudes m obtained in photometric treatment of an extrafocal photograph of the cluster, calibrated with the photometer scale.

Additional focal images of the standard stars have often to be considered when estimating the brightness of the starlike condensation in the comet's head (the nucleus). However, brightness estimates of the nucleus obtained by comparison with ordinary "point" images of stars are invariably burdened with errors. The following technique seems to be more accurate. The telescope is diaphragmed so that the comet's head gives a substantially attenuated image with the given exposure. The comet is then photographed on a plate slightly out of focus. The comet's nucleus on this photograph shows as a disk, analogous to ordinary extrafocal stellar disks (Figure 2), and its brightness can be estimated in the usual way.

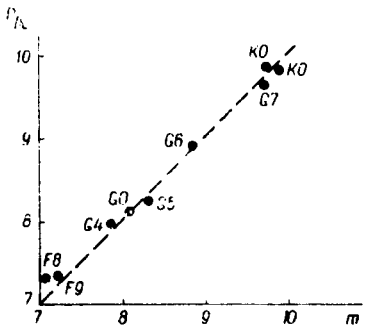

FIGURE 1. The stellar magnitudes obtained from an extrafocal photograph of the Hyades against the data in Eggen's catalog

For example, 15-min exposure on the menisc telescope diaphragmed to 1/10 of its aperture will give an image of a nucleus no fainter than 13^m on a sensitive plate 3 mm out of focus.

It follows from the preceding that the observation of a weak comet following a procedure not much different from the conventional can be completed roughly in 1 hour. The subsequent photometric treatment is much more tedious and time-consuming. Most of the time is taken up by the examination of the comet's photometric structure, which is generally deduced from a set of detailed measurements covering the entire image with a fairly dense mesh.

Isophotometers have been applied in this field in individual instances only. A new isophotometric technique based on the Sabattier effect /12/ has recently been proposed, which seems to be most promising. It requires, however, fairly high contrast and density of the photographic image, so that it appears to be applicable to bright comets only.

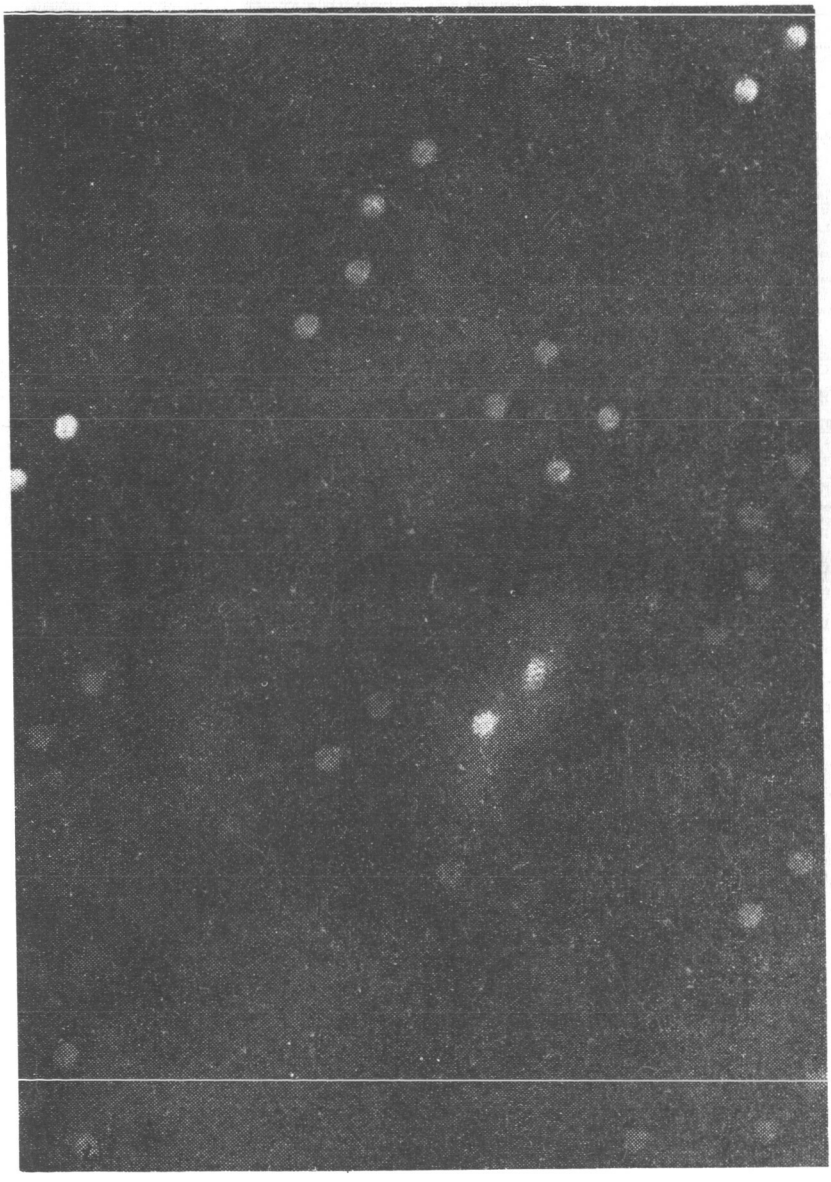

FIGURE 2. An extrafocal photograph showing a comet

We shall discuss an alternative method, whose applicability to the study of the photometric properties of weak comets is backed by considerable experience.

2. REVOLVING-TABLE PHOTOMETRY OF COMETS

The moving stage of any microphotometer can be easily equipped with a small round table with a central hole several centimeters in diameter, where a precision bearing is fitted to ensure smooth and rapid rotation of the negative in the course of measurements. Some of the advantages of this setup are described in /7, 8/. These papers also suggest the application of rapid rotary motion in the microphotometry of certain astronomical photographs. Let us briefly describe the photometry of a comet on a microphotometer equipped with this attachment.

As an example, consider the determination of brightness distribution and the intrinsic brightness of a typical weak comet. In most cases, these comets show as a nebulous spot with a more or less distinct nucleus and a faint tail, or rather several tail "rudiments". According to B.A. Vorontsov-Vel'yaminov, these comets have comas of common structure: brightness falling off monotonically with the distance from the nucleus, the spherical coma lacking a distinct outer boundary /1/.

The photographs of some comets for the years 1963-1964 which will be discussed in the following in general agree with this description. To be on the safe side, we may assume that within the region being investigated the coma is, say, twice as long in one direction as in the other.

Photographs of comets meeting these specifications can be measured without much difficulty. The photograph is spread on the table and is fastened with special clamps, but it may nevertheless be slightly moved to and fro relative to the surface to permit adjustment. The table should then be set in the initial position, the center of rotation coinciding with the comet's nucleus and the two points showing at the center of the microphotometer diaphragm (or square slit); their position should not change when the table is rotated. Once the operator has acquired some experience, this setting can be performed rapidly and reliably, but we may nevertheless offer two practical suggestions:

a) the image of the center of rotation is made to coincide with the diaphragm by alternately moving (i) the carriage on which the table with the negative is mounted and (ii) the negative relative to the surface of the table. The adjustment is made by a succession of steps (i) and (ii) above, each displacement covering a smaller distance;

b) the precision of the initial setting can be controlled photometrically; the galvanometer reading should correspond to maximum density, remaining constant when the table is rotated by hand.

The microphotometer diaphragm or slit should be as small as possible. The granular composition of the emulsion does not influence the results of measurements, while a small diaphragm brings the photometric resolution to the desired level. All these requirements are satisfied by a photometer with a photomultiplier.

A high-resolution photomultiplier photometer designed by A. V. Kurchakov at our Institute has been in operation for a fairly long time. Once the

running-in has been completed, successive measurements are all a matter of routine. The table with a clamped negative is rapidly rotated, by motor or manually. Galvanometer readings are taken, corresponding to equidistant concentric circles: these photometric sections are fixed by the operator, who moves the carriage with a simple micrometric screw. The measurements covering the entire region from the densest sections of the coma (of course excepting the nucleus, which is a "point", and not a "surface", object) to the faintest envelopes merging with the background sky take very little time, and can be repeated as many times as desired.

The measurements are highly reproducible, and the results obtained by different operators are found to be in excellent agreement. When the table is rotated by hand (i.e., moderately fast), the readings slightly fluctuate about a mean, which can be unambiguously established by eye. A high-resistance shunt (some 20 kohm) will substantially reduce the amplitude of these fluctuations, simplifying the measurements.

The procedure gives a sequence of mean densities $D(r_1)$, $D(r_2)$, $D(r_3)\ldots$ on circular sections of the radii r_1, r_2, $r_3\ldots$, all centered at the comet's nucleus. Calibration and standardization by ordinary means give the relative illuminances E_1, E_2, E_3 .... and the absolute mean luminances I_1, I_2, I_3 , ... corresponding to the given distance from the nucleus. However, the absolute brightness of individual points is of no significance in the study of comets, since the variation of brightness with distance can be established by relative measurements. Standardization is essential for the determination of the intrinsic brightness of the coma or the head. We first calculate the flux Φ_c in relative units; this can be done by simple trapezoid integration:

$$\Phi_c=\pi\sum\frac{E_i+E_{i+1}}{2}(r_{i+1}^2-r_i^2); \tag{1}$$

we then find the stellar magnitude m_c of the corresponding section of the comet, applying all the n standard stars:

$$\bar{m}_*-m_c=2.5\lg\frac{s}{S}+2.5\lg\Phi_c-\frac{2.5}{n}\sum\lg\sigma_i-\frac{2.5}{n}\sum\lg e_i, \tag{2}$$

where $\bar{m}_*$ is the arithmetic average of the magnitudes of the standard stars, e_i the illuminance in the extrafocal disk of the i-th star, σ_i the corresponding disk area, S the effective aperture area of the telescope used in photographing the comet, s the same area for the extrafocal photograph.

The last part of the description above is not intended as a photometric novelty: its aim is to emphasize that the subsequent treatment follows the conventional procedure. Whether the results obtained reflect the actual photometric characteristics of the comet should be decided by comparison with the accepted methods of photometric measurements. We can only quote the successful application of the revolving-table technique to the photometry of reflection nebulae /8/, whose structure is much more regular than the structure of comets, and also the favorable experience of other persons who have used it. Furthermore, there is a record of a comparison of two different methods recently applied to comet Kopff, which was observed systematically at our Institute during August 1964.

One of the photographs (No. 2564) of this comet was suitably standardized and calibrated, and then subjected to detailed photometry at some 1500 points. The same photograph was independently measured by the revolving-table technique in 50 circular sections. The first method gave the true isophotes of the comet and made it possible to determine its intrinsic brightness by summing up the illuminances measured for all the 1500 areas covering the comet's image, i.e., the mean illuminance for each circular section; it also enabled the intrinsic brightness to be found for the same image area.

The true and the mean isophotes are plotted in Figure 3, where the former are traced by dashed lines, and the latter are the solid circles.

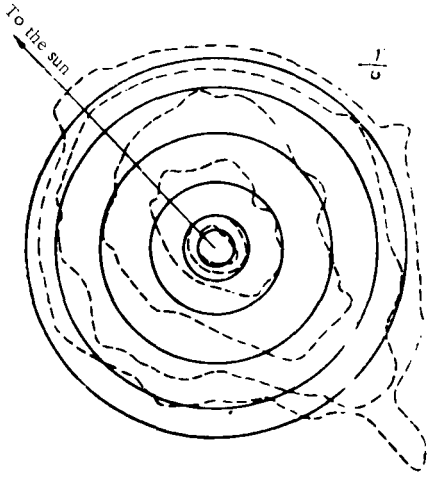

FIGURE 3. True and mean isophotes of comet Kopff (plate No. 2564)

The small circle gives the relative size of the diaphragm. Each set of isophotes clearly corresponds to the same set of measured illuminances. Quantitative comparison can be made by averaging the illuminance distribution over the areas of the true isophotes and comparing the result with the mean isophotes, as has been previously done in /8/. The fit is generally satisfactory.

The fit between the integrated fluxes is illustrated by the following figures:

Method of measurement	Flux Φ (arbitrary units)
conventional	0.923
rapid	0.941

Both figures refer to the same image area, that limited by the outermost circular isophote (Figure 3). The results are fairly satisfactory.

In conclusion we should again dwell on the significance to be attached to the mean brightness distribution obtained in this way. Near the nucleus,

the true coma isophotes will virtually coincide with the mean lines. As the radii of the mean isophotes are proportional to the square root of the areas enclosed by the true isophotes, the divergence in shape and position of the two systems will become noticeable starting with a true isophote which is twice as large in one direction as in the other. However, this divergence is not excessively pronounced for the weak comets with their characteristic "onion" shapes. Here circular symmetry prevails even at considerable distances from the nucleus. The mean brightness distribution obtained in this way can be applied for various purposes, and in particular to study the volume density.

3. RESULTS OF THE PHOTOMETRY OF SOME COMETS OBSERVED IN 1963—1964

Photographs of some objects whose apparent structure was suitable for revolving-table photometry were picked out from among the negatives available at the Institute. Three fairly weak comets were distinctly onion-shaped, in keeping with our observation at the end of the last section. The results of the photometry made by E.S.Eroshevich and the author are arranged in the Table. Columns 6, 7, 8, 9 give estimates of the intrinsic brightness of the coma for circular concentric areas of different angular diameters (centered at the nucleus). The brightness of the nucleus is not included in this estimate. These data can be applied for purposes of comparison with other observations.

Revolving-table photometry brings out the paradoxically slow reduction of coma brightness at large distances from the nucleus. Nevertheless, this technique gives a much more certain estimate of the maximum mean angular subtent of the coma than all the conventional measurements.

Figure 4 (a—f) shows graphs of brightness distribution (in arbitrary units) in the comets investigated. In Figure 4, e the crosses and the dots represent the results obtained independently by two different persons.

Note that the brightness in the immediate proximity of the nucleus varies approximately as r^{-1}. On the other hand, the integrated flux of the coma must be a finite quantity. Hence it follows that at large distance the brightness should fall off faster than $r^{-n}(n=2)$. Our present graphs apparently cease just on the verge on the region of these n. A similarly slow darkening is observed in reflection nebulae of roughly spherical shape and constant density. Seeing that the conditions of illumination for a comet and a reflection nebula are different (E = const for the former and $E \sim r^{-2}$ for the latter), we may conclude that the density of matter in comets varies approximately as ρ^{-2}, where ρ is the linear distance to the nucleus.

The observational data and the theoretical results for comets lead exactly to this conclusion /3, 5/. This aspect of our photometric observations deserves a more detailed discussion.

Date, U.T.	Plate No.	Emulsion	Exposure, min	Comet	Photographic magnitude of nucleus	Intrinsic brightness of coma in stellar magnitudes				$2r_{max}$	Observers	Remarks
						$r_1 = 1'$	$r_2 = 2'$	$r_3 = 3'$	r_{max}			
11.577 March 1963	2400	OaO	5	Ikeya	—	—	—	—	—	16'	A.V.Kurchakov	Poor seeing; telescope diaphragmed to 1/10 aperture, tail 0°.5.
23.730 May 1963	2424	Astr. uns.	5	Alcock	—	9.09	8.15	7.79	7.26	18 8	D.A.Rozhkovskii	Onion shaped, faint tail.
11.697 June 1964	2542	OaO	15	Humason	12	11.08	10.48	10.17	10.09	7.2	V.S.Mityagin and D.A.Rozhkovskii	Diffuse spot with a distinct nucleus
7.816 August 1964	2564	Astr. Spec.	15	Kopff	13.2	11.58	10.74	10.32	9.80	10.7	Yu.I.Glushkov	Diffuse spot with a distinct nucleus
13.908 August 1964	2600	Astr. Spec.	15	Kopff	—	11.54	10.67	10.22	9.36	15	Yu.I.Glushkov	Some brightening at the periphery
15.798 August 1964	2602	Astr. Spec.	15	Kopff	—	11.63	10.77	10.33	9.59	15	D.A.Rozhkovskii	Diffuse object, weak nucleus

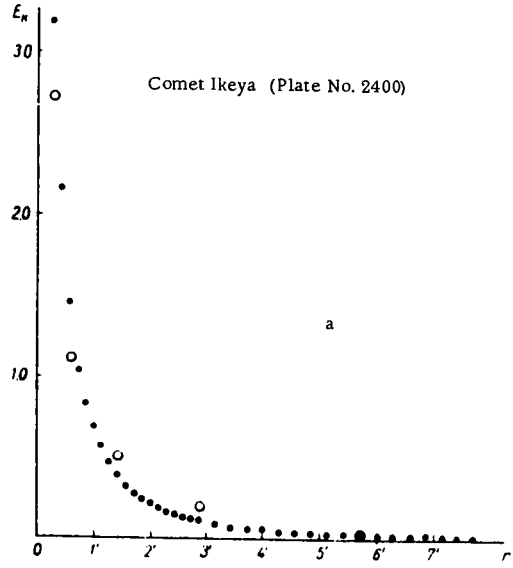

FIGURE 4. Brightness distribution in heads of comets

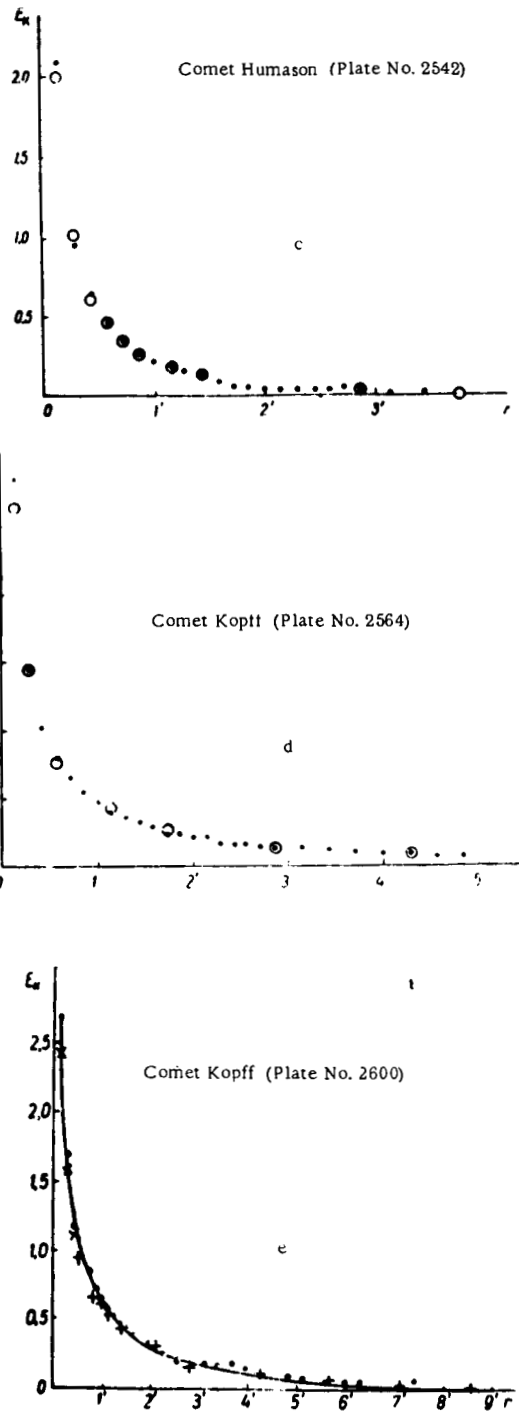

FIGURE 4. Brightness distribution in heads of comets

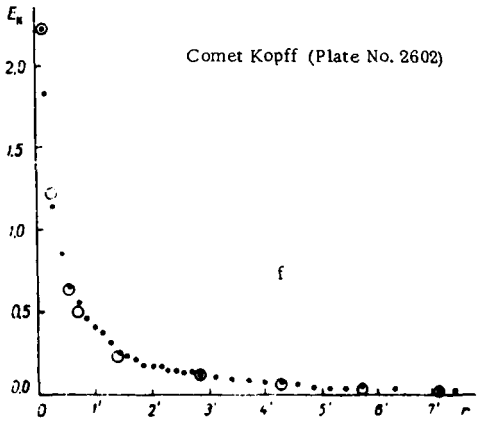

FIGURE 4. Brightness distribution in heads of comets

4. THE LUMINOSITY OF THE COMET'S DUST ENVELOPE

We shall assume that the luminosity of the coma is entirely due to the dust component of the cometary atmosphere. This assumption is apparently true without reservation at large distances /2, 3/. However, lacking adequate spectral observations, we cannot rule out the possibility of fluorescence as well (mostly CN and C_3). This uncertainty may only influence our estimate of the mass of the dust component, whereas its effect on the space distribution of dust is negligible: the dust particles are entrained by the moving gas atmosphere.

The brightness distribution and the luminous flux (the intrinsic brightness) of the comet which are known from observations can be applied to investigate the distribution of volume density and to estimate the dust mass enclosed within the volume of the coma accessible to photometry.

We shall assume a non-absorbing spherically symmetric coma. The illuminance set up by the sun at the comet's distance is $E_\odot$, the diffusion indicatrix is defined by the function $X(\Theta)$ (Θ the angle of scattering), $\alpha(\rho)$ is the extinction coefficient, where ρ is the distance from the nucleus, and μ is the albedo of dust particles. The surface brightness at a certain angular distance from the nucleus is described by the integral

$$I = E_\odot \mu \frac{X(\Theta)}{4\pi} \int_{-S_0}^{+S_0} \alpha(\rho)\, dS, \qquad (3)$$

where $2S_0$ is the linear path traversed by the line of sight in the spherical coma at the given angular distance from the nucleus.

The dust particles can be regarded on the average as identical spheres of radius a having an extinction efficiency Q. Then applying the accepted

definition of the extinction coefficient, we may write

$$\alpha = \pi a^2 Q N(\rho), \tag{4}$$

where $N(\rho)$ is the number of dust particles in unit volume at the given distance from the nucleus. The volume density in the coma is generally assumed to fall off as

$$N(\rho) = \frac{C}{\rho^n}, \quad n > 0. \tag{5}$$

Taking this relation and setting for brevity $\pi a^2 QC = A$, we find

$$I = E_{\odot} \mu A \frac{X(\Theta)}{4\pi} \int_{-S_0}^{+S_0} \frac{dS}{\rho^n}, \tag{6}$$

which can be written as

$$I = E_{\odot} \mu \frac{X(\Theta)}{4\pi} \frac{A}{R^{n-1} \sin^{n-1} \varphi_0} \int_{\varphi_0}^{\pi - \varphi_0} \frac{d\varphi}{\sin^{2-n} \varphi}, \tag{7}$$

substituting $S = r \operatorname{ctg} \varphi$, $\rho = \sqrt{r^2 + s^2}$, $r = R \sin \varphi_0$ (r the distance of the particular point from the nucleus in the image plane, R the linear radius of the envelope). Clearly, $\sin \varphi_0$ is the distance of the point being considered from the nucleus expressed in fractions of the radius r_{max}.

Let us first apply relation (7) to investigate the space distribution, i.e., to estimate the index n. This problem is generally solved by writing an Abel's integral equation satisfying the observations /1, 5/. Within the framework of our model, there is no need to follow this tedious course. Let us assume that the index n varies between 1.5 and 2.0, which is consistent with various observations. The angular distribution of brightness according to (7) is given by the function

$$F(\varphi_0, n) = \frac{1}{2} \sin^{1-n} \varphi_0 \int_{\varphi_0}^{\pi - \varphi_0} \sin^{n-2} \varphi \, d\varphi, \tag{8}$$

which is the one to be compared with the observed brightness distribution (Figure 4, a—f) by means of the relation

$$r = r_{max} \sin \varphi_0.$$

Limiting the analysis to three values of n (1.50, 1.75, and 2.00, seeing that in the last case (8) is immediately integrable), we can easily perform numerical integration (by the method of the trapezoids) plotting the graphs in Figure 5. These graphs are convenient for direct comparison with the observed curves of Figure 4.

The mass of a dust envelope of a given radius can be found assuming that the density is distributed as ρ^{-2}, i.e., $n=2$. The brightness is then given by

$$I=2E_{\odot}\mu\frac{X(\Theta)}{4\pi}\frac{A}{R}\frac{\frac{1}{2}\pi-\sin\varphi_0}{\sin\varphi_0}. \tag{9}$$

The intrinsic brightness is found by integrating this relation with respect to solid angles and over the surface of the sphere taking φ_0 to vary from $0°$ to $\frac{\pi}{2}$. Omitting the detailed calculations, we write the final expression

$$2.512^{-m_c+m_\odot}=\frac{X(\Theta)}{4\pi}\frac{AR}{r_c^2}\frac{\pi^2}{2}, \tag{10}$$

where r_c is the comet's distance from the sun.

On the other hand, the mass of the luminous coma for the given density variation can be written as

$$M_c=4\pi CR\frac{4}{3}\pi a^3\delta; \tag{11}$$

where δ is the intrinsic density of the dust particles.

Eliminating the unknown constant C between (10) and (11), we find

$$M_c=\frac{128}{3\pi}2.512^{-m_c+m_\odot}\frac{ar_c^2\delta}{\mu X(\Theta)Q}. \tag{12}$$

We see that the mass is independent of the linear size of the coma. On the other hand, it is proportional to the physical properties of the dust particles. The dust characteristics are insufficiently known at present, so that only the order of magnitude of the comet's mass can be estimated.

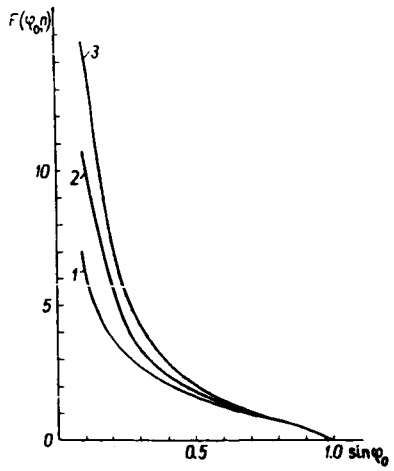

FIGURE 5. The space distribution of dust in a comet's head (curve 1 for $n=1.5$, curve 2 $n=1.75$, curve 3 $n=2.0$)

The brightness of the sun in application to our photographic observations should be expressed in terms of the stellar magnitude B in Johnson—Morgan's system. According to latest data $m_\odot=B_\odot=-26^m.26$ /4/.

In conclusion of this section, we should note that relation (7) applies in the case of fluorescence also, provided that the atmosphere is free from self-absorption. Then $E_\odot$, I should be considered for the frequencies of the corresponding emissions; $\frac{X(\Theta)}{4\pi}$ should be equal to 1, and the albedo must be replaced with the corresponding transition probabilities, etc. This problem is considered in detail in, e.g., /3/.

5. OBSERVED DISTRIBUTION OF VOLUME DENSITY

The observed brightness distribution in the comets investigated (the graphs of Figure 4) can be applied to evaluate the space distribution of density in comets. The dots in the graph mark the observed relative brightness, the circles give the theoretical values calculated from (8). To pass from the theoretical relation to the observation curves, we must know the two quantities r and n, as mentioned in the preceding.

The first quantity was read off the curve, the second was chosen to ensure best fit. This fairly simple procedure gave the following results.

a) Comet Ikeya (Figure 4, a). Brightness distribution more or less follows the theoretical curve with $r_{max} = 7'.3$, $n = 2$.

b) Comet Alcock (Figure 4, b). Theoretical curve having $r_{max} = 10'.2$, $n = 2$. The actual brightness falls off somewhat more steeply. Apparently, $n > 2$.

c) Comet Humason (Figure 4, c). Observations satisfactorily fit the curve with $r_{max} = 3'.8$, $n = 2$.

d) Comet Kopff (Figure 4, d). Satisfactory agreement with $r_{max} = 5'.8$, $n = 1.88$ (the average of $n = 1.75$ and $n = 2.00$).

e) Comet Kopff (Figure 4, e), observed four days later. Observations cannot be represented with any of the n between the chosen limits. The photometry of this photograph was made twice, and in general it is an excellent plate. The photometric results are possibly somewhat distorted by the fairly bright stars in the vicinity of the comet. A more probable explanation: a distinct brightening developed approximately in the EW and NNE directions. In plate No. 2602 (Figure 4, f) the brightening is much less pronounced. The observations fit $r_{max} = 7'.5$, $n = 2$. The series of photographs of this comet, only three of which were investigated, merits further study, since there is a possible indication of a small-sized flare.

The data above demonstrate the adequacy of the rapid revolving-table technique for the treatment of observations. As regards the mass of the comet, only crude estimates can be offered at present. For example, the distance of the comparatively weak comet Humason from the sun can be taken equal to 2 A.U. Assuming $a = 10^{-5}$ cm and isotropically scattering dielectric particles ($\mu = 1$), we find from (12) a mass of the order of magnitude of 10^8 g.

BIBLIOGRAPHY

1. VORONTSOV-VEL'YAMINOV, B. A. — Byulleten' Abastumanskoi Astrofizicheskoi Obs[illegible]orii, Vol. 17: 49. 1954.
2. VSEKHSVYATSKII, S. K. Fizicheskie kharakteristiki komet (Physical Characteristics of Comets). — Fizmatgiz. 1964. [English translation published by Israel Program for Scientific Translations, Jerusalem. 1964 (OTS 62-11031).]
3. DOBROVOL'SKII, O. V. — In: "Trudy AN TadzhSSR", p. 7. Dushanbe. 1961.
4. KARYAGINA, Z. V. and A. V. KHARITONOV. — AZh, Vol. 40: 60. 1963.
5. KONOPLEVA, V. P. — Publikatsii KAO, No. 22: 59. 1962.
6. ROZHKOVSKII, D. A. — Izvestiya Astrofizicheskogo Instituta AN KazSSR, Vol. 1—2. 1953.
7. ROZHKOVSKII, D. A. — ATs, Vol. 207. 1959.
8. ROZHKOVSKII, D. A. — AZh, Vol. 28: 278. 1961.
9. EGGEN, O. J. — Ap. J., Vol. 111: 81. 1950.
10. HOAG, A. A., H. L. JOHNSON, and B. IRIARTE — Publ. of the U. S. Naval Observatory, Vol. 17: 7. 1961.
11. MILLER, F. D. — PASP, Vol. 70: 279. 1958.
12. RICHTER, N. and W. HÖNGER — Mitteil. des K. Schwarzschild Observ., p. 8. 1963.

G. K. Nazarchuk

DETAILED PHOTOMETRY OF COMET AREND-ROLAND 1956 h

N67 15443

DESCRIPTION OF OBSERVATIONAL MATERIAL

Negatives taken on 2 May 1957 on Astro Platten were selected for this study from the large series of photographic observations of comet 1956 h (Arend-Roland) carried out by S. K. Vsekhsvyatskii with the 16" refractor of the Crimean Astronomical Observatory /1/. The negatives showed a sky area for calibration and standardization, as well as the comet proper. The mid-exposure times and the exposure of the photographs are given in Table 1.

TABLE 1

Mid-exposure time (U.T.)		Exposure, min
May 1957	2.8125	81.2
	2.8823	63.0
	2.9335	60.4

All the plates were simultaneously developed under standard conditions in D-19 developer. The exposure was sufficient to give an excellent print of the tail: on the negatives it could be traced to the very edge of the plate. The large magnification (focal distance, 160 cm) made it possible to study the fine details of the tail structure. The head is over-exposed in all the three photographs.

The cometary tail is a system of several streams issuing from the comet's head. Two almost straight streams emerge directly from the head, diverging by a small angle. One of these streams branches into two at a distance of 1°45' from the head, so that over most of its length the tail comprises three streams. The outermost stream is narrow, sharply outlined, and shows to a distance of over 6° from the head. The next stream is straight, broad, and moderately long (3°45'). The third stream is straight, pointing at a large angle to the radius-vector; it is traced to a distance of 4°.5. On the other side of the radius-vector, there is a faint diffuse stream slightly longer than 2°. The deflection of the streams from the radius-vector is 3°, 9°, 18°, and −2°, respectively.

The space structure of the tail was determined with the aid of Kanda's orbital elements:

T	1957, Apr. 8.1 U.T.	
ω	308°.74305	1950.0
Ω	215°.145	1950.0
i	119°.988	1950.0
q	0.31668	
e	1.000178	
$1/a$	−0.00056	

Calculations give $\Delta = 0.769$ A.U. and $r = 0.727$ A.U. for the geocentric and the heliocentric distances, respectively. True anomaly $v = 96°30'$. Phase angle at the time of observations 85°. Angle S between the line of sight and the plane of the cometary orbit 81°. The angle between the axes ξ' and η' of the cometocentric coordinate system in the image plane 57°45'. Angle σ between the projection of the earth—comet line onto the orbital plane of the comet and the radius-vector of the comet nucleus 84°35'.

The deflection of the stream from the radius-vector in the image plane β', the corresponding deflection in space β, the stream length l' calculated neglecting the projection distortion, and the true stream length l are related by the expressions

$$\operatorname{tg}(\sigma-\beta)=\cos S\,\frac{\operatorname{tg}\sigma-\operatorname{tg}\beta'\cos S}{\cos S+\operatorname{tg}\sigma\operatorname{tg}\beta'}, \tag{1}$$

$$l=l'\sqrt{\frac{1+\operatorname{tg}^2(\sigma-\beta)}{\cos^2 S+\operatorname{tg}^2(\sigma-\beta)}}. \tag{2}$$

Applying (1) and (2) we find that the streams are deflected in space from the radius-vector by 19°35', 45°, 62°, and − 3°, respectively, and that projection foreshortened the linear measurements by a factor of 1.106, 1.55, 2.46, and 1.011, respectively.

The first two photographs were treated photometrically, taking into consideration the distortion due to projection.

METHOD AND REDUCTION

The photographs were standardized by the method of extrafocal stellar images. Red stars lying near the center of the plate were applied. Their images are regular circles, so that the brightness in stellar magnitudes per square second of arc is given by

$$M=m+2.5\lg\frac{\pi(d'')^2}{4}.$$

The characteristic curve was plotted by means of the reduced densities, which are related with the ordinary densities S by the expression

$$w=\lg(10^s-1).$$

The microphotometer MF-4 used in this work is suitably calibrated. It is known /4/ that for some emulsions the characteristic curve in integrated light plotted in the coordinates $\lg I$ and w is linear in the region of small and medium densities. Our attempt to linearize the characteristic curve was successful: the readings of extrafocal stars and the scale markings of the tube photometer lie on straight lines. The characteristic line of a standardizing plate (60 min exposure) has the form

$$M=-0.0138\,w+21.87. \tag{3}$$

The equations of the characteristic lines of the comet's photographs taken with different exposures have the form (3) with an additional constant term depending on Schwarzschild's index (we assumed $p = 0.8$). The equations of the characteristic lines of the first and the second plates corrected for Schwarzschild's effect are respectively

$$M = -0.0138\, w + 22.13, \tag{4}$$

$$M = -0.0138\, w + 21.95. \tag{5}$$

For the tail areas adjoining the head, the density is beyond the linearized section. In this case the stellar magnitude is read off the curve $M = f(w)$.

The application of reduced densities has some obvious advantages. Since a straight line can be drawn with a much higher certainty than a curve whose shape is not known beforehand, the linearized characteristic curve is more accurate and enables us to advance far into the region of low densities, i.e., to study the most interesting parts of the tail.

We therefore operated with w-densities exclusively. Photometric measurements were made for sections parallel to the radius-vector, at distances of 0.25 mm from one another. The distance between the adjoining points in each section also was 0.25 mm. On the image of the comet we thus superimposed a square mesh of reduced density readings, covering the entire relevant region without gaps.

The sections were plotted on a single sheet of tracing paper. Individual stars were identified on this photometric chart to avoid possible errors in the superposition of the successive sections. Given a photometric chart, we may investigate a photometric contour of arbitrary shape, in particular, plot the w-isolines which for a variety of reasons do not coincide with the isophotes. The w-isolines are shown in Figure 1.

Because of the large extent of the tail in the sky and on the plates, the simple transition from w to M according to formulas (5), (4) is inadequate for plotting the isophotes, studying the distribution of matter in the streams, or solving other photometric problems. The result of this transformation will be distorted by the photometric field error, background illumination, and differential absorption of light in the atmosphere. Each of these factors requires special consideration and reduction.

The intensity distribution of the objective was determined as follows. When a uniformly luminous body occupying the entire plate is photographed with an astrograph, the density will fall off toward the edges of the plate owing to the photometric field error. Making photometric measurements along the radius of the plate, we find the intensity distribution of the objective.

The sky background was adopted as the internal standard, since the illumination produced by the sky may be assumed constant for a given zenith distance. Photometric measurements of the almucantar through the center of the plate give the correction for the photometric field error.

The background was corrected for by subtracting the background illumination from the total illumination produced by the background and the tail. The reduction was based on the special tables and the technique described in the previously quoted monograph by V.K. Prokof'ev /4/. Background nonuniformity was taken into consideration. To this end

photometric measurements were made over a section parallel to the radius-vector, but lying at a certain distance from the comet.

The differential absorption could not be neglegted since the stars on the standardization photograph and different parts of the tail lie at different zenith distances. No special measurements of atmospheric

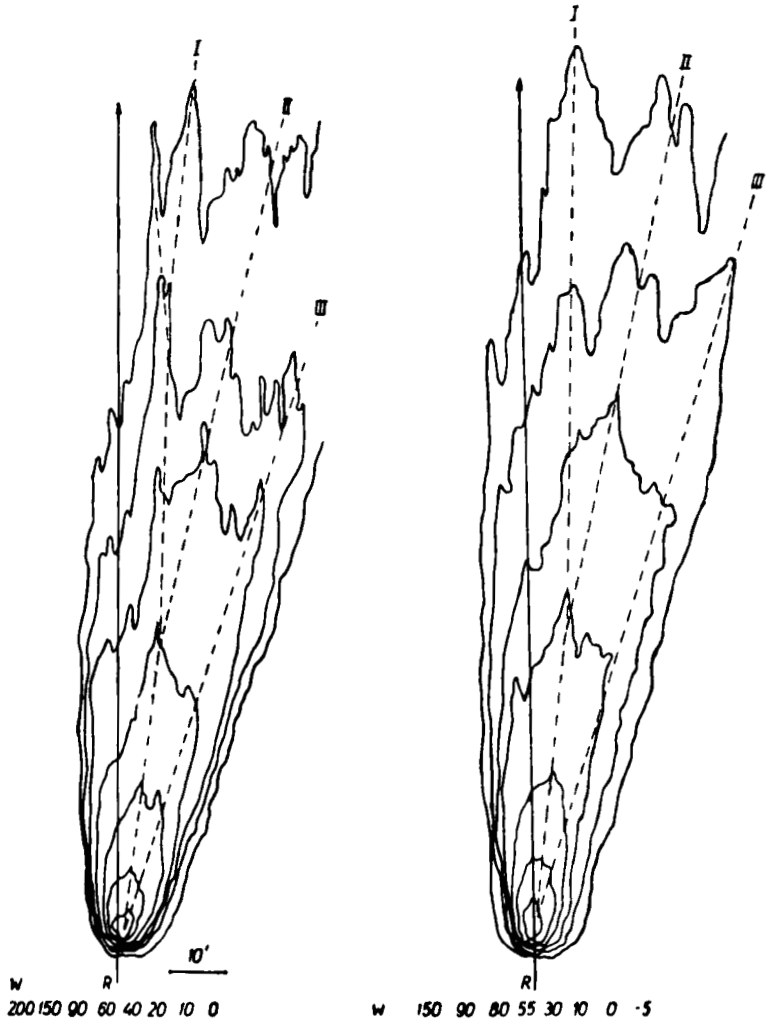

FIGURE 1. Photometric chart of the comet 1956 h

transparency were made when the comet was being photographed, and the corresponding correction factor was therefore borrowed from V. V. Pronik's study /5/. The differential absorption correction was calculated for different zenith distances within the range covered by the tail at intervals of 0°.5. The correction at intermediate points was read off the graph.

BRIGHTNESS DISTRIBUTION ALONG THE STREAMS

Contour lines were traced on the photometric chart outlining each stream, and the readings lying on these lines were picked out. It was remembered that the readings should be maximal in sections perpendicular to the stream. For comparison purposes readings along the radius-vector were selected, since it frequently passes through the minimal readings of the cross sections. Correcting for the various factors considered above, we plotted the brightness distribution along the streams and along the radius-vector. The same technique was applied to the second photograph. The results obtained for the two plates are fully consistent (Figure 2). Repeated attempts to represent the empirical data by inverse power, exponential,

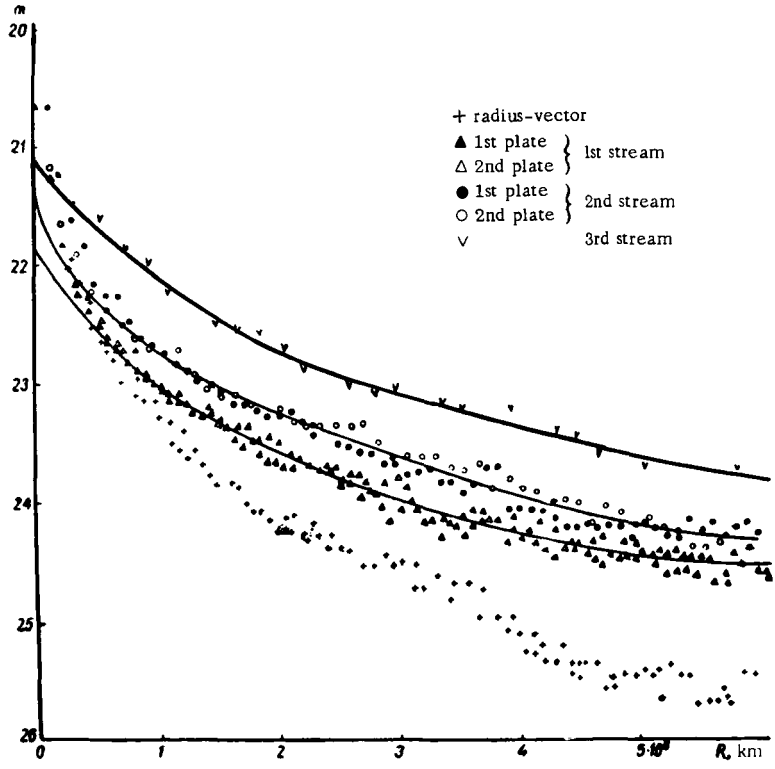

FIGURE 2. Brightness distribution along the streams (comet 1956 h)

and other functions failed. Convenient functional approximations can be fit if each stream is divided into several sections, but the resulting expressions are purely interpolatory: they in no way reflect the physical content of the processes responsible for the reduction of brightness along the stream.

The decrease of brightness along the streams is a joint contribution of several factors: lateral dissipation of matter, acceleration of particles, finite lifetime of optically emitting particles. An exact quantitative theory describing the dynamics and the chemical kinetics of matter in cometary

tails in the field of corpuscular and photon radiation of the sun is at its rudimentary stage at present, and it is therefore interesting to compare the observational data with different simplified theoretical models.

The profiles of the photometric sections perpendicular to the streams are close to Gaussian curves. This similarity suggests that the lateral dissipation of matter can be approximated by a diffusive mechanism. If the origin of the coordinates is placed at the comet's nucleus, the axis Ox is pointed along the stream, and Oy at right angles to the stream, and if the time of observation is regarded as the zero point of the time scale, then the cloud of particles which formed at a time t in the past will show the following distribution at the time of observation:

$$n = \frac{\text{const}}{t} e^{-\frac{x^2}{4Dt}}, \tag{6}$$

where D is the diffusion coefficient.

In fact, the matter which eventually forms the head, the coma, and the tail is released not at the origin, but all over the surface of the nucleus or possibly at certain points on this surface, but since the head is much smaller than the tail, these refinements can be omitted. They will not improve the accuracy of the model, since the tail constituents are chemically different from the matter in the neighborhood of the head. By applying the distribution (6), we do not claim that it describes the early stage of expansion; we only suggest that having been fed into the tail, the matter is distributed as if ejected by a point source located at the center of the nucleus at a time t in the past.

There is no reason to believe that the expansion of the tail is isotropic. The presence of a magnetic field and the anisotropy of the initial velocity distribution of the particles should result in an anisotropic expansion. However, when studying the decrease of brightness along the stream, we may apply distribution (6), since the variation of brightness depends on the diffusion along the axis Ox only: the diffusion coefficients along the other two axes can be shown to enter the constant factor in the right-hand side of (6), and this is clearly of no consequence, since we are only interested in the general form of tail darkening.

If no sharp anisotropy is assumed, the tail matter will not shape into streams by force of expansion alone. The tail structure is apparently decided by the forces of repulsion accelerating the cometary matter. A study of the motion of cloud formations in the tail of comet Arend-Roland revealed the presence of considerable accelerations /3/. Within the framework of the model being discussed, a cloud of particles having the distribution (6) will be displaced downstream by this additional acceleration so that its center occupies the point $x = at^2/2$, where a is the repulsive acceleration. The distribution of particles in the original system of reference will be given by

$$n = \frac{\text{const}}{t} e^{\frac{-\left(x-\frac{at^2}{2}\right)^2}{4Dt}} \tag{7}$$

Note that assuming the diffusive model of expansion, we avoid the difficulties connected with the problem of the initial velocity of ejection

of the particles. We start with a cloud which is initially at rest as a whole, but individual particles in this swarm move with different velocities, so that eventually the cloud will creep and expand. Although the actual law of expansion need not obey (6), this situation is physically probable. A redistribution of velocities will occur once each particle has experienced several collisions. This process may take place near the nucleus only /2/. However, even if collisions become highly improbable, the velocity distribution of particles in the tail will be different from the initial velocity distribution at the time of ejection.

Assuming the tail to be made of identical particles, we shall describe the deexcitation of glowing particles by a single mean lifetime τ. Since all the particles in the "instantaneous" cloud being considered are of the same age, the right-hand side of (7) should be multiplied by $e^{-\tau/t}$. Assuming uniform and continuous ejection of matter from the nucleus, we can find the steady-state distribution of matter along the trajectory described by the centers of the elementary clouds. To this end our expression should be integrated with respect to time from $t=0$ to ∞. Since the brightness of the comet is proportional to the line-of-sight number of luminous particles, the brightness will fall off along the tail with the decrease in the number of particles, thus

$$\frac{n}{n_0}=\int_0^\infty \frac{dt}{t}\exp\left[-\frac{\left(x-\frac{at^2}{2}\right)}{4Dt}-\frac{t}{\tau}\right]. \tag{8}$$

Our problem is to find the longitudinal diffusion coefficient D, the repellent acceleration a and the effective lifetime τ for which the observed tail darkening can be described by expression (8). The freedom in the choice of the parameters a, D, and τ is not as large as could be expected. In particular, it can be shown that the longitudinal expansion of matter is by no means negligible. In the limiting case $D\to 0$, relation (8) takes the form

$$n=\text{const}\left(\frac{x}{L_\tau}\right)^{-3/4}e^{-\frac{x}{L_\tau}}, \tag{9}$$

where $L_\tau=\frac{a\tau^2}{2}$.

The shape of the longitudinal photometric section is now determined by a single parameter L_τ, regardless of the coefficient of transverse diffusion; physically, L_τ is the mean path of a particle to extinction. It was established that relation (9) could not be made to fit the observed darkening irrespective of the particular L_τ chosen.

For simplicity, (8) can be written in the form

$$\frac{n}{n_0}=\int_0^\infty \frac{dt}{t}\exp\left[-\frac{1}{2t}\left(\frac{x}{L}\right)^2-2t-\frac{\Gamma^2}{2}t^2+\Gamma\left(\frac{x}{L}\right)t\right], \tag{10}$$

where $L=2\sqrt{D\tau}$ is a characteristic length (the longitudinal measurement of the elementary cloud acquired on expansion during the lifetime of the

particles), and Γ is a nondimensional constant related with a, D, and τ by the expression

$$\Gamma = a\tau^{3/2}D^{-1/2}. \tag{11}$$

Apart from a constant factor of the order of magnitude of unity, Γ may be regarded as the ratio of L_τ to L. We see from (10) that given the shape of the longitudinal photometric section from observations, we cannot determine the three relevant parameters a, D, and τ; only the two quantities Γ and L expressible in terms of these parameters can be found. Numerical integration was applied to calculate and plot the graphs of n/n_0 as a function of the nondimensional quantity x/L for various values of the parameter Γ.

Comparison of theoretical curves with the observational data gave the values of Γ and L for each stream, which are listed in Table 2. All the brightness points closely fit the theoretical curves, with the exception of several initial observations which fall in the highly overexposed region of the coma.

TABLE 2

Stream	$L\cdot10^{-11}$, cm	Γ	N, cm^{-3}	V, km/sec	$\tau\cdot10^{-5}$, sec	a, cm/sec^2	$D.10^{-17}$, cm^2/sec
I	7.76	5	940 2400	2100 1700	3.8 1.9	14 55	4.0 8.0
II	6.76	4	1100 2800	2200 1800	3.0 1.5	15 60	3.8 7.6
III	7.08	3	1100 2900	2400 1900	2.8 1.4	13 53	4.5 9.0

ESTIMATING THE PARAMETERS OF THE CORPUSCULAR STREAM

Although the observations only give two quantities, which are functions of the unknowns a, D, and τ, the three parameters can be determined in principle, and we shall thus be able to estimate the parameters of the corpuscular stream where the cometary tail has formed. All this is possible since a, D, and τ are not independent quantities, and they can be related by additional equalities.

Indeed, the acceleration and the diffusion coefficient may only depend on the velocity and the concentration of the solar corpuscules moving through the tail, and also on the intensity of the magnetic field. The magnetic field has a substantial influence on the diffusivity only when the transverse component (relative to the tail axis) is large. There is reason to believe that this is not so in our case, since the assumption $D\approx0$, as we have already mentioned, is clearly inconsistent with observations. If the field is directed along the tail, the longitudinal diffusion coefficient is not influenced by the magnetic field: it depends on the velocity and the density of the corpuscules only.

The longitudinal field cannot directly influence the acceleration of cometary ions, either; the indirect influence of the magnetic field shows in the change in the local concentration of the corpuscules, but even in this case the magnetic field strength does not enter the explicit expression for the acceleration:

$$a = \frac{4\pi e^2 \Lambda}{m_e m_i} \frac{w}{V^2} = 6.4 \cdot 10^{14} \frac{N}{V^2}, \tag{12}$$

where N is the concentration, V the velocity of the corpuscular stream. The mean lifetime is defined by

$$\tau = \frac{1}{\sigma_d N V}, \tag{13}$$

where σ_d is the cross section of the inelastic process causing deexcitation of the emitting ions.

The uncertainty in the determination of the diffusion coefficient is much higher than in a and τ. In the following we shall adopt the primitive estimate $D = \frac{1}{3}\bar{v}^2 \tau_D$, where in accordance with our model $\bar{v}^2$ is the mean square (thermal) velocity of a cometary ion, and τ_D is a time interval in which the random component of the longitudinal velocity changes appreciably. By definition,

$$\tau_D = \bar{v}^2 \left(\frac{d\bar{v}^2}{dt}\right)^{-1}. \tag{14}$$

The second factor in (14) can be found from S. Chandrasekhar's result (expression (5.16) in /6/). The final expression for the diffusion coefficient has the form

$$D = \frac{2 m_e k T_i^2 V^3}{3\pi^2 e^4 \Lambda T_s N} = 4.0 \cdot 10^{-9} \frac{T_i^2}{T_s} \frac{V^3}{N}, \tag{15}$$

where T_i is the ion temperature of the tail, T_s the electron temperature of the corpuscular stream.

Substituting (12), (13), and (15) in the expressions for L and I, we obtain a system of equations which is easily solved for N and V. If N and V are then substituted in (12), (13), and (15), the acceleration, the mean lifetime, and the diffusivity can be expressed in terms of the observed quantities Γ and L. The final results are the following:

$$N = 2.0 T_i^{0.8} (10 T_s)^{-0.4} \sigma_d^{-0.8} \Gamma^{-0.2} L^{-1}, \tag{16}$$

$$V = 5.02 \cdot 10^3 T_i^{-0.2} (10 T_s)^{0.1} \sigma_d^{-0.3} \Gamma^{-0.2}, \tag{17}$$

$$a = 5.1 \cdot 10^7 T_i^{-1.2} (10 T_s)^{-0.6} \sigma_d^{-0.2} \Gamma^{0.2} L^{-1}, \tag{18}$$

$$\tau = 10^4 T_i^{-0.6} (10 T_s)^{0.3} \sigma_d^{0.1} \Gamma^{0.4} L, \tag{19}$$

$$D = 2.53 \cdot 10^3 T_i^{0.6} (10 T_s)^{-0.3} \sigma_d^{-0.1} \Gamma^{-0.4} L. \tag{20}$$

Before these expressions can be applied in actual calculations, some information must be available on the temperatures T_i and T_s, and also on the cross section σ_d. As a reasonable estimate of σ_d we shall adopt the dissociation cross section of the molecular ion N_2^+ under proton impact, which can be found from Cherednichenko's formula /7/:

$$\sigma_d = Z\left(\frac{2U_0}{|U_0-U_1|}\right)^{1/4}\exp\left[-\frac{2U_0}{|U_0-U_1|}\right]\cdot 10^{-16}\ \text{cm}^2, \qquad (21)$$

where $Z = 14$ is the number of electrons in the atom of nitrogen, $U_1 = 15.5$ eV the ionization energy of N_2, $U_0 = 24.3$ eV the dissociation energy of the ion N_2^+. Formula (21) gives $\sigma_d = 1.32\cdot 10^{-17}\ \text{cm}^2$.

Since no exact values of the temperatures T_i and T_s are available, calculations using (16)—(20) are made for the two apparently extreme values $T_s = T_i = 10^4$ °K and $T_s = T_i = 10^5$ °K. The results are listed in Table 2, where the upper row figures correspond to the lower temperatures. The considerable scatter in N and V should be attributed to errors in determination. The small accelerations obtained for $T \sim 10^4$ °K suggest that the actual temperatures are close to 10^5 °K.

BIBLIOGRAPHY

1. VSEKHSVYATSKII, S.K. —ATs, Vol. 184, 1957.
2. DOBROVOL'SKII, O.V. Nestatsionarnye protsessy v kometakh i solnechnaya aktivnost' (Nonstationary Processes in Comets and Solar Activity). —Dushanbe, Izdatel'stvo AN TadzhSSR, 1961.
3. NAZARCHUK, G.K. —AZh, Vol. 31: 719, 1959.
4. PROKOF'EV, V.K. Fotograficheskie metody kolichestvennogo spektral'nogo analiza metallov i splavov (Photographic Methods of Quantitiative Spectroscopic Analysis of Metals and Alloys), Vol. II. — Moskva, GITTL, 1951.
5. PRONIK, V.V. —Izv. KrAO, Vol. 20, 1957.
6. SPITZER, L. Physics of Fully Ionized Gases. —Interscience Publ. Inc. 1956. [Russian translation, 1957]
7. CHEREDNICHENKO, V.I. —In: "Issledovanie komet po programme MGSS", p. 73. Kiev, Naukova Dumka, 1964.

V. I. Cherednichenko

N67 15444

THE RADIUS OF EXISTENCE OF C_2 AND C_3 MOLECULES IN COMETS

In a previous paper /14/ it has been shown that molecules of acetylene and propylene participating in various reactions in the heads of comets may produce C_2 and C_3 molecules that can be observed.

We shall calculate the radius of existence of C_2 and C_3 molecules in the field of photon and corpuscular radiation of the sun, comparing our theoretical results with the radii observed in the head of Halley's comet 1910 II.

The energy of dissociation of C_2H_2 by the reaction $C_2H_2 \rightarrow C_2 + H_2$ is $U = D(C_2H_2) - U_0(H_2) = 7 - 4.5 = 2.5$ eV /5, 10/. On the other hand, according to experimental data, the dissociation threshold of C_2H_2 is 5.77 eV /23/. The energy difference $\Delta U = 5.77 - 2.5 = 3.27$ eV is dissipated as the kinetic energy of the dissociation products C_2 and H_2. The C_2 molecules acquire the following amount of kinetic energy:

$$U_{C_2} = \frac{m_{H_2}}{m_{C_2} + m_{H_2}} \cdot \Delta U = \frac{2}{26} \cdot 3.27 = 0.251 \text{ eV},$$

corresponding to a velocity $v_{C_2} = 1.42 \cdot 10^5$ cm/sec.

The C_2H_2 molecule has an initial velocity of 1 km/sec as a dissociation product of C_3H_6 /16/, so that the maximal resulting velocity of the C_2 molecule produced by the chain of dissociations $C_3H_6 \rightarrow C_2H_2 \rightarrow C_2$ is $v_{C_2} = (1.42 + 1) \cdot 10^5 = 2.42 \cdot 10^5$ cm/sec. Taking $\tau_{C_2} = 4.96 \cdot 10^4$ sec for the lifetime of the C_2 molecule, we obtain $R_{C_2} = 1.2 \cdot 10^{10}$ cm for the radius of existence of C_2.

However, the radius of existence of the C_2H_2 molecule having a velocity of 10^5 cm/sec and a lifetime $\tau_{C_2H_2} = 6.95 \cdot 10^3$ sec in the reaction $C_2H_2 \rightarrow C_2 + H_2$ is $R_{C_2H_2} = 6.95 \cdot 10^8$ cm. Consequently, the C_2 boundary will pass at a distance of $6.95 \cdot 10^8$ cm from the comet's nucleus, and $R_{C_2} = 1.27 \cdot 10^{10}$ cm. Furthermore, the C_2 molecules moving sunward are braked by the light pressure. The path covered by a C_2 molecule in the course of its lifetime is therefore given by the formula

$$L_{C_2} = v_{C_2}\tau_{C_2} - \frac{a\tau_{C_2}}{2}, \qquad (1)$$

where a is the acceleration of the molecule due to light pressure; v_{C_2} is the initial velocity of the C_2 molecule forming from a C_2H_2 molecule; τ_{C_2} the lifetime of the C_2 molecule.

The acceleration due to light pressure is found from the relation

$$a = \frac{2\pi^2 e^2 hg}{m_e m_H g_\odot c} \cdot \frac{f}{m_{C_2}\pi^3} \exp\left(-\frac{hc}{kT_0\lambda}\right), \qquad (2)$$

where m_e and m_H are the mass of the electron and the hydrogen atom, respectively; m_{C_2} the mass of the C_2 molecule in atomic units; e the charge of the electron; c the velocity of light; h Planck's constant; λ the wavelength of the strongest absorption band of the C_2 molecule, 4737 Å /7/; $f = 0.024$ /20/ the oscillator strength for this absorption band; k Boltzmann's constant; $T_\odot$ the blackbody temperature of the region of the solar spectrum absorbed by the 4737 Å band of the C_2 molecule ($T_\odot = 5740°K$); $g_\odot = 2.74 \cdot 10^4$ cm/sec^2 the acceleration of the force of gravity on the surface of the sun; $g = 0.593$ cm/sec^2 the acceleration of the force of gravity at a distance of 1 A.U. from the sun.

Substituting in (2) the numerical values of the physical constants and expressing λ in units of 1000 Å and T in units of 1000°K, we find the compact expression

$$a = 1.43 \cdot 10^7 \frac{f}{m_{C_2}\lambda^3} \exp\left(-\frac{144}{\lambda T_\odot}\right) (\text{cm/sec}^2). \qquad (3)$$

Setting

$$f = 0.024,\ m_{C_2} = 24,\ \lambda = 4.74\ \ (\text{in } 10^3\ \text{Å}),\ T_\odot = 5.74\ (\text{in } 10^3\ °\text{K}),$$

we find $a = 0.66$ cm/sec^2.

This acceleration a is consistent with observations of comets /7, 8/, according to which the quantity $1+\mu$ — the ratio of the acceleration due to light pressure to the acceleration of the force of gravity — is of the order of unity. In our case

$$1+\mu = \frac{a}{g} = \frac{0.66}{0.593} = 1.11.$$

Substituting a, τ_{C_2}, and v_{C_2} in (1) and adding the radius of existence of the C_2H_2 molecule, $L_{C_2H_2}$, to the calculated value of L_{C_2}, we find for the radius of existence of the C_2 molecule $R_{C_2} = 11.9 \cdot 10^9$ cm ($r = 1$ A.U.).

For Halley's comet 1910 II at $r = 1$ A.U., $R^{\circ}_{C_2} = 13 \cdot 10^9$ cm /7, 8, 17/. The difference of $1.1 \cdot 10^9$ cm between R_{C_2} and $R^{\circ}_{C_2}$ is quite reasonable on account of the errors in measurements of the apparent size of the comet's head and of its photographs /8, 17/.

Let us further consider the agreement between the calculated data for the molecules C_3H_6 and C_2H_2 /14/ and the observed variation in the head diameter of Halley's comet 1910 II with the distance from the sun /7, 8, 17/ (see Figure). The optical image of the comet's head is mainly determined by the emission $\lambda = 4737$ Å /17/.

It has been established that C_3H_6 goes through the following sequence of reactions:

$$C_3H_6+H^+ \rightarrow 2H_2+H_2^++C_3+H; \quad C_3+H^+ \rightarrow C_3^++H;$$
$$C_3+h\nu \rightarrow C_2+C^+; \quad C_2+H^+ \rightarrow C_2^++H;$$
$$C_2^++h\nu \rightarrow C^++C^*.$$

Assuming that C_3H_6 enters cometary nuclei in the form of ice, we may regard the C_3H_6 molecules as having small initial velocities. In our calculations the velocity of the solar protons in the corpuscular streams will be assumed constant in the range $0.6 \leqslant r \leqslant 3.4$ A.U., being equal to $5 \cdot 10^7$ cm/sec /13/; the concentration of the solar protons is assumed to vary as $n_{H^+}(r) = 6 \cdot 10^2 \cdot r^{-0.5} \text{cm}^{-3}$ /15/.

The radius of existence of the molecules in the sunward direction will be calculated from (1). The deceleration due to light pressure (as the molecule moves sunward) is considered only for C_3 and C_2 molecules since these have resonance absorption lines 4050 Å and 4737 Å in the visual solar spectrum, where the intensity of the light quanta is fairly

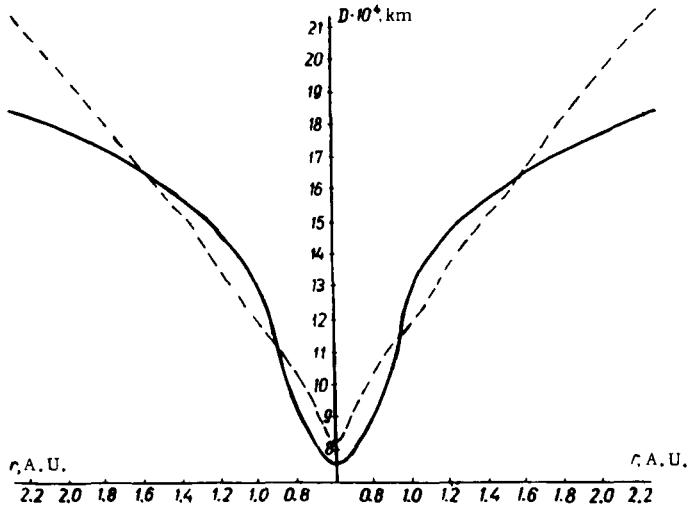

Head diameter (D) of Halley's comet 1910 II and C_2 IV emission as a function of the distance from the sun (r)

high. For other molecules (C_3H_6, C_3^+) the pressure of light is neglected, since their absorption bands lie in the far ultraviolet /11, 19/, where the intensity of solar radiation is low /12, 22, 6/. The acceleration due to light pressure is determined from the expression /2/

$$a = \frac{1{,}19\pi^2 e^2 h}{r^2 m_e m_H g_\odot c} \frac{f}{m_{C_3} \lambda^2} \exp\left(-\frac{hc}{kT_\odot \lambda}\right), \qquad (4)$$

where r is the distance of the comet from the sun, in A.U. The other symbols are as in formula (3).

Substituting the numerical values of the physical constants in (4), we obtain a more compact expression

$$a = 1.43 \cdot 10^7 \frac{f}{r^2 m \lambda^3} \exp\left(-\frac{144}{\lambda T_\odot}\right) (\text{cm/sec}^2), \qquad (5)$$

where m is the molecular mass in atomic units; f the oscillator strength for the absorption band; λ the wavelength in the strongest part of the absorption band (in units of 1000 Å); $T_\odot$ the blackbody temperature corresponding to the spectral region absorbed by the molecule (in units of 1000 °K).

The oscillator strength for the λ 4050 Å band of the molecule C_3 has been calculated assuming that the effective cross section for excitation by electron impact σ_e is equal in this case to 0.1 of the effective cross section σ_s for the scattering of electrons by the C_3 molecule /3/. The effective scattering cross section σ_s for the C_3 molecule is assumed equal to the C_3H_8 cross section, since both have the same number of valent electrons /4/; hence $\sigma_s = 4.8 \cdot 10^{-16}$ cm^2 /21/ at electron energies $U_e = 29$ eV.

Then $\sigma_e(C_3) = 4.8 \cdot 10^{-17}$ cm^2. The oscillator strength f_{C_3} and the $\sigma_e(C_3)$ are related by the expression /1/

$$\sigma_e(C_3) = \frac{\pi e^4}{U_e U_a} f_{C_3} \ln \frac{4U_e}{U_a}, \qquad (6)$$

where $U_a = 3.06$ eV is the excitation potential of the 4050 Å band of C_3, $U_e = 29$ eV the electron energy.

Substituting the numerical quantities in (6), we find $f_{C_3} = 0.018$ (at $\lambda = 4050$ Å), which is close to $f_{C_3} = 0.024$ /8/.

The energy released in the reactions

$$C_3H_8 + H^+ \rightarrow C_3 + 2H_2 + H_2^+ + H \quad (U_1 = U_i(H) - U_a = 3 \text{ eV})$$

and

$$C_3 + H^+ \rightarrow C_3^+ + H \quad (U_2 = U_i(H) - U_i(C_3) = 2.3 \text{ eV}),$$

is dissipated either as the energy of light quanta with the wavelengths λ 4130 Å and λ 5400 Å, respectively, or as the kinetic energy of dissociation or charge-exchange products /1/. We shall assume the latter to be true. The energy U_1 and U_2 is distributed between the reaction products in the following proportion /9/:

$$U_{C_3} = \frac{2m_{H_2} + m_{H_2^+} + m_H}{2m_{H_2} + m_{H_2^+} + m_H + m_{C_3}} \cdot U_1 \text{ and } U_{C_3^+} = \frac{m_H}{m_{C_3^+} + m_H} \cdot U_2. \qquad (7)$$

The intensity of the light quanta required to calculate the lifetime of the C_3^+ molecule in the reaction $C_3^+ + h\nu \rightarrow C_2 + C^+$ at various distances r from the sun is found from the relation

$$Qw = \frac{1.35 \cdot 10^{15}}{r^2} T^3 \exp\left(-\frac{144}{\lambda T}\right) \left[\left(\frac{144}{\lambda T} + 1\right)^3 + 1\right], \qquad (8)$$

where r is in A.U., λ in units of 1000 Å, and T in units of 1000 °K; Q is the flux of photons at the surface of the sun, w dilution ratio.

The results of calculations for C_3H_6 and C_2H_2 are listed in Table 1 and 2. The following symbols are used: R_{C_2} the calculated radius of existence of C_2 molecules, $R^{\circ}_{C_2}$ the observed radius of existence of C_2 molecules /20, 7, 8/; L_{C_3}, $L_{C_3^+}$, L_{C_2} the radii of existence of the molecules C_3, C_3^+, and C_2, respectively: r the distance of the comet from the sun, in A.U.

TABLE 1. The radius of existence of the molecules C_3, C_3^+, and C_2 at various distances from the sun

r, A.U.	0.6	0.7	0.8	0.9	1.0	1.1	1.2	1.5	1.7	2.3
n_{H^+}: 10^3 cm^{-3}	7.75	7.16	6.7	6.3	6.0	5.7	5.45	4.9	4.6	3.95
v_{C_3}: 10^5 cm/sec	1.62	1.62	1.62	1.62	1.62	1.62	1.62	1.62	1.62	1.62
τ_{C_3}: 10^4 sec	2.67	2.89	3.09	3.28	3.45	3.63	3.8	4.22	4.5	5.24
a_{C_3} cm/sec^2	0.61	0.447	0.343	0.271	0.22	0.181	0.152	0.0975	0.076	0.0413
r_{C_3}: 10^9 cm	4.10	4.50	4.85	5.17	5.47	5.77	6.05	6.76	7.22	8.44
$v_{C_3^+}$: 10^5cm/sec	2.21	2.21	2.21	2.21	2.21	2.21	2.21	2.21	2.21	2.21
$\tau_{C_3^+}$: 10^4 sec	0.262	0.358	0.466	0.590	0.730	0.890	1.05	1.65	2.11	3.87
$r_{C_3^+}$: 10^9 cm	0.580	0.791	1.03	1.31	1.61	1.97	2.32	3.65	4.66	8.55
v_{C_2}: 10^5 cm/sec	2.21	2.21	2.21	2.21	2.21	2.21	2.21	2.21	2.21	2.21
τ_{C_2}: 10^4 sec	3.84	4.15	4.45	4.73	4.96	5.22	5.46	6.08	6.48	7.54
a_{C_2} cm/sec^2	1.83	1.35	1.03	0.815	0.66	0.545	0.379	0.242	0.189	0.103
r_{C_2}: 10^9 cm	7.14	8.07	8.81	9.6	10.2	10.8	11.5	12.0	13.9	16.3
R_{C_2}: 10^9 cm	12.8	13.4	14.7	16.1	17.3	18.5	19.9	22.4	25.8	33.3
$R^{\circ}_{C_2}$: 10^9 cm	7.5	8	9.04	10.6	13.2	14.0	14.8	16.0	16.9	18.5

In calculations of R_{C_2} for C_2 molecules produced in the dissociation of acetylene, the C_2H_2 molecules were assumed to have an initial velocity of 1 km/sec as products of corpuscular dissociation of C_3H_6 /16/.

TABLE 2. The radius of existence of the molecules C_2H_2 and C_2 at various distances from the sun

r, A.U.	0.6	0.7	0.8	0.9	1.0	1.1	1.2	1.5	1.7	2.3
n_{H^+}: 10^3 cm^{-3}	7.75	7.16	6.70	6.30	6.00	5.70	5.45	4.90	4.60	3.95
$v_{C_2H_2}$: 10^5cm/sec	1	1	1	1	1	1	1	1	1	1
$\tau_{C_2H_2}$: 10^4 sec	0.250	0.340	0.445	0.564	0.695	0.840	1.00	1.56	2.00	3.68
$r_{C_2H_2}$: 10^9 cm	0.250	0.340	0.445	0.564	0.695	0.840	1.00	1.56	2.00	3.68
v_{C_2}: 10^5 cm/sec	2.42	2.42	2.42	2.42	2.42	2.42	2.42	2.42	2.42	2.42
τ_{C_2}: 10^4 sec	3.84	4.15	4.45	4.73	4.96	5.22	5.46	6.08	6.48	7.54
a_{C_2} cm/sec^2	1.83	1.35	1.03	0.815	0.66	0.545	0.379	0.242	0.189	0.103
r_{C_2}: 10^9 cm	7.95	8.94	9.90	10.6	11.2	11.9	12.6	14.2	15.3	17.9
R_{C_2}: 10^9 cm	8.20	9.28	10.4	11.2	11.9	12.7	13.6	15.7	17.3	21.6
$R^{\circ}_{C_2}$: 10^9 cm	7.50	8.00	9.04	10.6	13.22	14.0	14.8	16.0	16.9	18.5

We see that the radii of existence of C_2 molecules from C_2H_2 are fairly consistent with observations of Halley's comet 1910 II /7, 8, 17/ for $0.6 \leqslant r \leqslant 2.3$ A.U. (see Figure). The sharp reduction in the apparent size of Halley's comet in C_2 light at $r > 2.3$ A.U. can be attributed to the sharp drop in the yield of propylene C_2H_6 and other hydrocarbon molecules which dissociate to give C_2 molecules. The yield of hydrocarbons decreases probably because at distances $r > 2.3$ A.U. the energy of the solar protons and photons is insufficient to detach the parent molecules from the comet's nucleus.

The fact that the calculated radii of existence of C_2 molecules generated in the reactions $C_3H_6 \rightarrow C_3 \rightarrow C_2$ /14/ are considerably higher than the observed radii /7, 8, 17/ does not contradict our concepts on the formation of C_2 and C_3 molecules. Indeed, according to the data of Tables 1 and 2 /14/ the scheme $C_3H_6 \rightarrow C_2H_2 \rightarrow C_2$ is much faster than the scheme $C_3H_6 \rightarrow C_3 \rightarrow$ $\rightarrow C_3^+ \rightarrow C_2$. The concentration of C_2 molecules produced by the second scheme is therefore very small, and the emission of these molecules is hard to observe.

Our approach to the production of C_3 molecules readily explains the contraction of the 4050 Å emission regions of C_3 in cometary heads near the sun /18/ and the excess intensity of λ 4050 Å bands in comparison with CH bands in cometary spectra at large distances from the sun /24, 25, 26/. The size of the 4050 Å emission region of C_3 molecules (4100 – 22,000 km) for the comet 1948 *I* observed as r varied from 0.9 to 2.2 A.U. /27/ is close to the values of L_{C_3} listed in Table 1 for Halley's comet 1910 II /17/.

A study of the dissociation and ionization of other hydrocarbons (C_2H_6, C_2H_4, etc.) producing C_2 molecules will apparently attribute the appearance of halos in various comets to differences in the distance from the comet's nucleus where C_2 molecules start forming and to differences in the radius of existence of these molecules (Table 2).

BIBLIOGRAPHY

1. AMBARTSUMYAN, V. A. et al. Teoreticheskaya astrofizika (Theoretical Astrophysics). —Moskva, GITTL. 1952.
2. DIVARI, N. V. —AZh, 27(6):351. 1950.
3. ZHIGAREV, A. A. Elektronika (Electronics). —Moskva, Gosenergoizdat. 1951.
4. KONDRAT'EV, V. N. Fizicheskie i khimicheskie svoistva molekul (Physical and Chemical Properties of Molecules). —Leningrad. 1928.
5. KONDRAT'EV, V. N. Elementarnye khimicheskie protsessy (Elementary Chemical Processes). —Leningrad, ONTI. 1936.
6. MITRA, S. K. Verkhnyaya atmosfera (The Upper Atmosphere). —Moskva, IL. 1955.
7. ORLOV, S. V. Priroda komet (The Nature of the Comets). —OGIZ. 1944.
8. ORLOV, S. V. Golova komety i klassifikatsiya kometnykh form (The Cometary Head and the Classification of Cometary Forms). —Moskva, Sovetskaya Nauka. 1945.
9. SENA, L. A. Stolknovenie elektronov i ionov s atomami gaza (Collisions of Electrons and Ions with the Atoms of Gases). —Leningrad-Moskva, OGIZ. 1948.
10. Spravochnik khimika (Chemist's Manual), Vol. 1. —Leningrad-Moskva, Goskhimizdat. 1951.
11. TERENIN, A. —ZhFKh, 8(1):160. 1936.
12. FRIEDMAN, H., and H. E. HINTEREGGER. —In: "Ul'trafioletovoe izluchenie Solntsa i mezhplanetnaya sreda", pp. 47, 172. Moskva, IL. 1962.
13. CHAPMAN, S., and E. N. PARKER. —In: "Kosmicheskaya astrofizika", pp. 167, 198. Moskva, IL. 1962.
14. CHEREDNICHENKO, V. I. —In: "Issledovanie komet po programme MGSS". Kiev, Naukova Dumka. 1964.
15. CHEREDNICHENKO, V. I. —Publ. KAO, 11. 1962.
16. YAKOVLEVA, A. V. —ZhETF, 9(3): 302. 1939; 9(1): 10. 1939.
17. BOBROVNIKOFF, N. T. —Lick. Obs. Publ., Vol. 17: 473. 1931.
18. KUIPER, G. P. —The Solar System, New York, Vol. 4: 511. 1964.
19. LANDOLT-BÖRNSTEIN, Zahlenwerte und Funktionen aus Physik. —Astronomie, 1, 3. 1951.
20. LYDDAM, ROGERS and ROACH. —Phys. Rev., Vol. 60: 281. 1941.
21. MASSLY, H. S. W and E. H. S. BURHOB. —Electronic and Ionic Impact Phenomena, London, Oxford University Press, 206. 1952.
22. NEWELL, H. E. High Altitude Rocket Research. —New York. 1953.
23. NORRISCH. —Trans. Farad. Soc., Vol. 30: 103. 1934.
24. SWINGS, P., C. T. ELVEY and H. W. BABCOCK. —Ap. J., Vol. 94: 320. 1941.
25. SWINGS, P. —Ap. J., Vol. 95: 270. 1942.
26. SWINGS, P. —Month. Noties., 103, 2. 1943.
27. SWINGS, P. —La Physico-Chemie des Comets. Conference feinte en Paris, 1951.

V. I. Cherednichenko

N67 15445

DISSOCIATION AND IONIZATION OF WATER MOLECULES IN COMETARY ATMOSPHERES

Spectra of the region near the cometary nucleus show (0,0) bands of the $^2\Sigma \rightarrow {}^2\Pi_{inv}$ system of the molecule OH ($3078 < \lambda < 3100$ Å) and bands of the $A^3\Pi_{verk} \rightarrow X^3\Sigma$ system of the molecule OH^+ ($3695 < \lambda < 3893$ Å) /1,10/.

H_2O is the most probable parent molecule whose dissociation products are OH and OH^+ /2, 11, 12/. Dissociation and ionization processes of water molecules have been studied in sufficient detail /3, 4, 7, 8/. H_2O molecules are destroyed by solar photons and protons in the following schemes /3, 7, 8/:

$$H_2O \rightarrow H_2O^+ + e - 12.6 \text{ eV}; \quad H_2O \rightarrow H_2 + O^+ + e - 18.5 \text{ eV};$$
$$H_2O \rightarrow OH + H^+ + e - 18.9 \text{ eV}; \quad H_2O \rightarrow OH^+ + H + e - 18.9 \text{ eV};$$
$$H_2O \rightarrow OH^* + H - 9 \text{ eV}.$$

The effective cross sections of the various reactions with the participation of water molecules and the corresponding lifetimes in the field of corpuscular solar radiation are calculated on the basis of the data and the relations from /5/.

The effective photoabsorption cross sections adopted for the molecules H_2O, H_2O^+, OH, OH^+ were as follows /6/:

$$\sigma_{ph}(H_2O) \approx \sigma_{ph}(Ne) = 5.8 \cdot 10^{-18} \text{ cm}^2,$$
$$\sigma_{ph}(H_2O^+) \approx \sigma_{ph}(Ne^+) = 4.5 \cdot 10^{-18} \text{ cm}^2,$$
$$\sigma_{ph}(OH) \approx \sigma_{ph}(F) = 6.0 \cdot 10^{-18} \text{ cm}^2,$$
$$\sigma_{ph}(OH^+) \approx \sigma_{ph}(F^+) = 2.5 \cdot 10^{-18} \text{ cm}^2.$$

The following numerical values were applied in the calculation of the dissociation energies and the effective cross sections: energy of the HO − H bond, 5.12 eV; O − H bond, 4.4 eV /4/; $U_0(H_2O) = 9.52$ eV /4,5/; gas-kinetic molecular cross sections $\sigma(H_2O) = 4.05 \cdot 10^{-16}$ cm², $\sigma_2(OH) = 2.96 \cdot 10^{-16}$ cm² /9/; $U_a(H_2O) = 6.96$ eV /5, 7/; $U_a(OH) = 4$ eV /3, 7/; $U_i(OH) = 13.8$ eV /7/; $U_i(H) = 13.5$ eV; $U_i(O) = 13.6$ eV; $U_i(H_2O) = 12.6$ eV; energy to produce a H_2 molecule $U_0(H_2) = 4.5$ eV; excitation energies of O and H atoms $U_a(O) = 2$ eV and $U_a(H) = 10.2$ eV. The dissociation energy of molecular ions was calculated from the relations in /5/ using the

above numerical data. The following dissociation schemes were considered for the molecular ions H_2O^+, OH^+ and for the molecule OH:

$$H_2O^+ \rightarrow O^+ + H_2; \quad H_2O^+ \rightarrow O + H_2^+; \quad H_2O^+ \rightarrow OH^+ + H;$$
$$H_2O^+ \rightarrow OH + H^+; \quad H_2O^+ \rightarrow O^+ + 2H; \quad H_2O^+ \rightarrow O + H + H^+;$$
$$OH^+ \rightarrow O + H^+; \quad OH^+ \rightarrow O^+ + H; \quad OH^+ \rightarrow O^+ + H^*;$$
$$OH \rightarrow OH^+ + e - 13.8 \text{ eV } /7/; \quad OH \rightarrow O^* + H - 6.4 \text{ eV};$$
$$OH \rightarrow O^+ + e + H - 18 \text{ eV}; \quad OH \rightarrow O + H^+ + e - 17.9 \text{ eV}.$$

The dissociation energy for the last three processes was calculated from the relation

$$U = U_0 + U_i + U_a,$$

where U_0 is the energy of the O—H bond, U_i the ionization energy of the atoms H and O, respectively, and U_a the excitation energy of atomic oxygen.

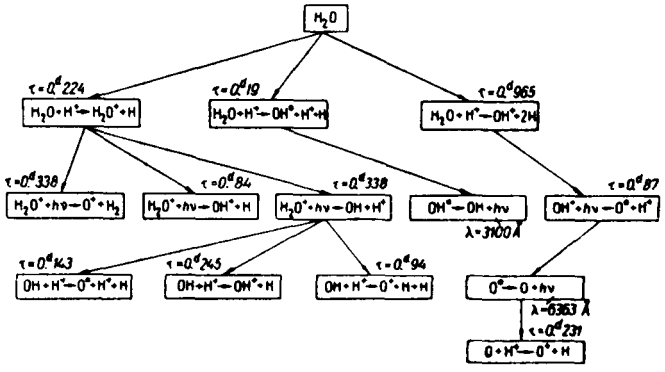

The scheme of the most probable reactions of H_2O in comets ($r = A.U.$)

Table 1 lists the reactions of H_2O in the field of solar photons for comets at a distance of $r = 1$ A.U. from the sun. The second column gives the reaction schemes, the third column the effective emitted wavelength λ (in Å), the fourth column the photon flux Qw of the effective emission through 1 cm² per second at a distance $r = 1$ A.U. from the sun (the corresponding intensity figures have been borrowed from /5/), the fifth column lists the effective cross sections σ_{ph} in cm², the sixth column the lifetime τ_{ph} in days (d) or years.

Table 2 gives the conversions of H_2O molecules produced by solar protons in the corpuscular streams. The second column lists the reaction schemes, the third the effective cross section σ_c in cm², and the fourth the lifetime τ_c calculated from the relations in /5/.

The various effective reactions of H_2O molecules in the field of solar photons and protons are schematized in the figure; it is seen that the prevailing processes are charge exchange with the solar protons and charge exchange on dissociation.

TABLE 1

No.	Scheme	λ, Å	$Q\varphi/10^9$	$\varepsilon_{ph}/10^{-16}$	τ_{ph}
		H_2O			
1	$H_2O+h\nu \rightarrow H_2O^+ + e - 12.6$ eV	983	4.95	50	46.^{d}8
2	$\rightarrow H_2 + O^+ + e - 18.5$ eV	670	3.36	5.8	1.62 years
3	$\rightarrow OH + H^+ + e - 18.9$ eV	656	3.29	5.8	1.66 "
4	$\rightarrow OH^+ + H + e - 18.9$ eV	656	3.29	5.8	1.66 "
5	$\rightarrow OH^* + H - 9$ eV	1380	1.01	5.8	5.42 "
		H_2O^+			
6	$H_2O^+ + h\nu \rightarrow O^+ + H_2 - 6$ eV	2060	7640	4.5	0.^{d} 33
7	$\rightarrow O + H_2^+ - 8.2$ eV	1510	372	4.5	69.^{d} 2
8	$\rightarrow OH^+ + H - 6.3$ eV	1970	3060	4.5	0.^{d} 84
9	$\rightarrow OH + H^+ - 6$ eV	2060	7640	4.5	0.^{d}338
10	$\rightarrow O^+ + 2H - 10.5$ eV	1180	0.163	4.5	43 years
11	$\rightarrow O + H + H^+ - 10.6$ eV	1170	0.123	4.5	57.3 "
		OH			
12	$OH + h\nu \rightarrow OH^+ + e - 13.8$ eV	898	4.52	6	1.16 years
13	$\rightarrow O^* + H - 6.4$ eV	1780	67.1	6	28.^{d} 8
14	$\rightarrow O^+ + H + e - 18$ eV	690	3.47	6	1.52 years
15	$\rightarrow O + H^+ + e - 17.9$ eV	693	3.48	6	1.51 "
		OH^+			
16	$OH^+ + h\nu \rightarrow O^* + H^+ - 6.1$ eV	2030	5300	2.5	0.^{d} 87
17	$\rightarrow O^+ + H^* - 14.4$ eV	860	4.31	2.5	2.92 years

Asterisk * denotes an excited molecule (or atom).

TABLE 2

No.	Scheme	$\varepsilon_c/10^{-16}$	τ_c
	H_2O		
1	$H_2O+H^+ \rightarrow H_2O^+ + e + H^+ - 12.6$ eV	1.91	2.^{d} 03
2	$\rightarrow H_2O^+ + H$	17.2	0.^{d} 224
3	$\rightarrow H_2 + O^+ + e + H^+ - 18.5$ eV	0.115	33.^{d} 6
4	$\rightarrow OH + H^+ + e + H^+ - 18.9$ eV	0.00242	4.37 years
5	$\rightarrow OH^* + H^+ + H - 9$ eV	20.3	0.^{d} 19
6	$\rightarrow OH^+ + H + H - 18.9$ eV	4	0.^{d} 965
7	$\rightarrow OH^* + H + H^+ - 9$ eV	0.91	2.^{d} 66
	H_2O^+		
8	$H_2O^+ + H^+ \rightarrow O^+ + H_2 + H^+ - 6$ eV	2.18	1.^{d} 77
9	$\rightarrow O + H_2^+ + H^+ - 8.2$ eV	0.464	8.^{d} 32
10	$\rightarrow OH^+ + H + H^+ - 6.3$ eV	1.91	2.^{d} 02
11	$\rightarrow OH + H^+ + H^+ - 6$ eV	2.18	1.^{d} 77
12	$\rightarrow O^+ + 2H + H^+ - 10.5$ eV	0.0142	7.4 years
13	$\rightarrow O + H + H^+ - 10.6$ eV	0.115	33.^{d} 5
	OH		
14	$OH+H^+ \rightarrow OH^+ + e + H^+ - 13.8$ eV	1.74	2.^{d} 21
15	$\rightarrow OH^+ + H$	15.7	0.^{d} 245
16	$\rightarrow O^* + H^+ + H - 6.4$ eV	27.1	0.^{d} 143
17	$\rightarrow O^+ + H + e + H^+ - 18$ eV	0.0064	1.64 years
18	$\rightarrow O + H^+ + e + H^+ - 17.9$ eV	0.000835	12.6 "
	OH^+		
19	$OH^+ + H^+ \rightarrow O^* + H^+ + H^+ - 6.1$ eV	1.97	1.^{d} 97
20	$\rightarrow O^+ + H^* + H^+ - 14.4$ eV	$8.59 \cdot 10^{-10}$	$1.23 \cdot 10^7$ years

BIBLIOGRAPHY

1. DOBROVOL'SKII, O. V. Nestatsionarnye protsessy v kometakh i solnechnaya aktivnost' (Nonstationary Processes in Comets and Solar Activity). — Izdatel'stvo AN TadzhSSR. 1961.
2. POLOSKOV, S. M. Elementarnye protsessy proiskhodyashchie v kometakh, i svyazannye s nimi voprosy fiziki komet (Elementary Processes in Comets and the Related Problems of the Physics of Comets). — Summary of Doctorate Thesis, Moskva. 1955.
3. PRINGSHEIM, P. Fluorescence and Phosphorescence. — [Russian translation. 1951.]
4. Spravochnik khimika (Chemist's Manual), Vol. 1. — Moskva, Goskhimizdat. 1951.
5. CHEREDNICHENKO, V. I. — Byulleten' Komissii po Kometam i Meteoram Astronomicheskogo Soveta AN SSSR, No. 2. 1958; In: "Issledovanie komet po programme MGSS", p. 73. Kiev, Naukova Dumka. 1964.
6. BATES. — Monthly Not. Roy. Astron. Soc., 106, 432. 1964.
7. LANDOLT-BÖRNSTEIN. — Zahlenwerte und Funktionen aus Physik, Chemie, Astronomie, 1, 3. 1951.
8. LANDOLT-BÖRNSTEIN. — Physikalisch-chemische Tabellen, 1, 2. 1935.
9. LANDOLT-BÖRNSTEIN. — Zahlenwerte u. Funktionen aus Physik, Chemie, Astronomie, 1961, 1, Atome u. Sonnen, 369.
10. SWINGS P. — Monthly Notices of the R. A. S., 103: 2. 1943; La Physico-Chemie des Comets. 1951.
11. WHIPPLE. — Ap. J., 111(2): 375. 1950.
12. WURM K. — Mitt. Hamb. Berg., 8: 51, 66. 1943.

S. K. Vsekhsvyatskii

N67 15446

INTRINSIC BRIGHTNESS OF COMET IKEYA 1963 a

The comet was discovered on 4 March in evening twilight with binoculars (50 mm, ×7), according to Marsden's ephemerides, at a height of 15° above the horizon. The intrinsic brightness of the comet was estimated with binoculars by means of extrafocal comparison with nearby stars. In what follows, the brightness in stellar magnitudes is given in parentheses.

March 4.715. *a* 8 *K* 5 *b* (4.15 taking differential absorption into consideration; *c* 10 *K* (4.4?). AZT-7 seeker shows a nonspherical nebulosity elongated upward; central condensation 40"; $D \sim 1'.5 - 2'$. 4.729: $K > b$ by $0^m.2$ (4.22). Color bluish. Even at a height of 10° easily visible with a seeker through foliage.

March 6.708. Poor seeing, brightness estimated in twilight *a* 8 *K* 4 *b* (4.36).

March 9.702. *a* 9 *K* 4 *b* (4.49). Color bluish. AZT-7 seeker (×150 magnification) shows a bright central condensation elongated upward. Excellent seeing. Image steady. 9.710: *a* 10 *K* 8 *b*; $a > K$ by $0^m.6 - 0^m.7$(4.39).

March 10.701. On light sky *a* 12 *K* 7 *b* (4.50). Under ×150 magnification, $D \sim 1'.5$; strong central condensation. *K* 3 *d* (4.4). Visible with binoculars through tree branches until March 10.743.

March 19.726. After a cloudy stretch, the comet was easily found with binoculars even in twilight. *e* 7 *K* 3 *f* (4.23). 19.732: *e* 9 *K* 3 *f* (4.15). With seeker shows as a bright disk. Under ×150 magnification a nuclear condensation 0'.3 and faint envelopes up to 1'.5 are visible. Tail not seen either with binoculars or seeker. 19.738: *e* 12 *K* (4.3).

March 20.727. Brightness *e* 12 *K* 5 *f* (4.27). Fairly dense haze.

March 21.715. Comet noticeably fainter and fairly diffuse, but still visible with binoculars. *f* 4 *K* (4.78). 21.729: *f* 4 *K* 2 *d* (4.82); *a* 15 *f* 3 *K* (4.74); *K* 4 *g*; $K > g$ by $0^m.5$ (4.85).

March 24.715. Located with AZT-7 seeker against the light background of the sky. Not seen with binoculars. $K < f$ by $0^m.4 - 0^m.5$ (4.95). 24.726: *f* 8 *K* 4 *g* (4.97). 24.736: seen with binoculars under excellent seeing conditions, *f* 5 *K* 6 *g* (5.1).

Comparison stars:

Symbol	Star	m_v	S_p	Symbol	Star	m_v	S_p
a	α Psc	3.82	A2P	*e*	η Psc	3.72	G5
b	ζ Psc	4.85	KO	*t*	o Psc	4.50	KO
c	δ Ceti	4.04	B2	*g*	64 Ceti	5.72	GO
d	ν Psc	4.68	KO				

N67 15447

S. K. Vsekhsvyatskii

VISUAL OBSERVATIONS OF COMET ALCOCK 1963 b

The comet was found on a plate taken by A. A. Demenko with Astropetsval camera on 6 April 1963; coordinates $\alpha = 19^h4^m.0$, $\delta = +52°24'$ (1950.0). 7 April, invisible with binoculars ($D \sim 70$ mm) under weather conditions characterized by haze and running clouds. 8 April in the evening, photographed with the large astrograph of the Crimean Astronomical Observatory and with the Astropetsval camera; after a lengthy search found with binoculars in the form of a weak diffuse nebulosity of 9^m, 4—5' in diameter.

After a considerable interval, the comet was rediscovered with binoculars according to Marsden's ephemerides on 9.806 May 1963, almost in the zenith. Very difficult to observe against light sky. The comet formed an extended shapeless nebulosity without central condensation.

Below we list our observations of the intrinsic brightness of the comet and of its aspect. All estimates were obtained by extrafocal comparison. The comet's brightness in stellar magnitudes is given in parentheses.

May 9.819. *a* 8 *K* 7 *c*; *K*>*c* by $0^m.7$ (6.33).

May 10.797. Comet faint: *d* 10 *K* 12 *e* (7.03). Highly diffuse head 8 — 10' in diameter. May 10.813, comet visible through AZT-7 seeker (70 mm, X25), but invisible with a telescope owing to the faintness of the central condensation. *d* 10 *K* 6 *e* (7.2).

May 11.792. Located with binoculars, brighter: *f* 6 *K* 10 *e* (6.63).

May 11.300 *f* 8 *K* 5 *e* (6.84). A diffuse patch or a rudimentary tail noticeable at $p = 5°$; $D = 8'.5$.

May 11.813. *f* 9 *K* 3 *e* (6.98).

May 12.899. No central condensation, shape not spherical. *g* 18 *K* 4 *h* (7.18) and *f* 8 *K* 5 *e* (6.86).

May 13.790. Weaker than on 12 May, *g* 9 *K* 6 *i* (7.18); *j* 3 *K* 4 *k* (7.25).

May 13.809. *j* 4 *K* 5 *i* (7.44); *K*=*k* (7.44).

May 14.799. Shows as a diffuse spot against light sky. *m* 2 *K* 3 *h* (6.79).

May 14.806. *m* 5 *K* 2 *j* (6.96); *K* 10 *n*.

May 15.809. High seeing. Comet distinctly visible through binoculars. *o* 4 *K* 6 *p* (7.05); *K*=*q* (6.84).

May 15.813. *o* 5 *K* 2 *j* (6.97); *q* 2 *K* 7 *p* (7.03). *D* corresponding to $^1/_4$—$^1/_5$ of the distance between the stars *q* and *p* (6 — 8'); inhomogeneities noticed in the outer part of the head.

May 16.810. Brighter than the day before: *r*=*K* (6.82); *s* 4 *K* 10 *t* (6.99); *u* 10 *K* 10 *t* (6.75). Central part more condensed than earlier; $D \sim 10 - 13'$.

May 16.816. *r* 2 *K* 10 *t* (6.95).

Since 10 May, the comet was photographed with short-focus cameras in parallel with the visual observations.

May 24.800. After a stretch of cloud, found with binoculars at a distance of 1°.5 from Marsden's ephemerides. $K=v$ (6.8) w 3 K 5 x (6.56)

May 25.806. Despite the very light sky, the comet was instantly found with a 70 mm binocular telescope and it was well visible with 50 mm binoculars (×7). $K=y$ (7.12); y 2 K 7 z (7.21); v 3 K 1 y (7.04).

May 25.823. A 8 K 3 y (6.84); v 3 K 2 y (6.99).

May 26.808. Well visible against the light sky. Head sharply outlined on the southwest, elongated to the northeast. K 1 B (6.85); A 4 K 3 y (6.68). A star cluster (M3) is seen near the comet in the field of vision of the binoculars. The cluster is much brighter than the comet. From comparison with the stars HD 119035 and 119081, the brightness of M3 is $6^m.30$.

May 26.826. $K=B$ (6.95); $K>y$ by 0 2—$0^m.3$ (6.92).

May 27.823. Comet somewhat brighter than on 26 May; C 5 K 5 y (6.76). M3 brighter than the comet by 2 degrees (6.50). Surface brightness of the comet much less than of M3, but the diameter is twice as large.

May 28.809. Comet exceptionally bright even when observed through cirrus clouds: D 2 K 8 C (5.20); $D \approx K$ (4.90). May 28.826: comet brighter by $1^m.5$ than M3 (4.8); $D=1/2$ C ($D \sim 7'$).

May 30.800. Comet easily found on twilight sky; E 6 K 3 D (4.70). May 30.816: a bright central condensation seen with binoculars. Comet brighter than E by $0^m.15$ (4.2). May 30.826: $K=E$ (4.32). Light sky, the moon in its first quarter.

May 31.803. Easily located in bright twilight, in moonlight. E 3 K 6 D (4.50). AZT-7 seeker (×200) shows a bright condensation of 6—7^m and a highly diffuse coma. 31.833: E 5 K 5 D (4.61).

June 1.806. Comet at a distance of 20° from the moon, and yet easily visible with binoculars: K 3 F (4.85); E 6 K 2 D (4.76); $D \sim 7$—10′. Estimates made through gaps in cirrus clouds.

June 2.810. Sky very light, but seeing excellent, moon. Extrafocal comparison with binoculars: F 1 K 9 g (5.0); H 4 K 5 I (4.74); K 4 E (4.70); $D \sim 19'$. Color bluish.

June 3.858. Slight haze. I 3 K 6 J (5.35); 3.864 : I 4 K 6 J (5.42). Central condensation noticeable. D less than on 2 June.

June 4.810. Moon, very light sky; comet fainter, but found with binoculars; $K=L$ (6.2). 4.814: brightness estimated with greater certainty, I 8 K 3 L (5.90).

June 5.311. Comet easily seen with binoculars against very light sky, under good seeing conditions. M 7 K 2 L (6.04).

June 6.808. Full moon, found with difficulty on light sky (binocular telescope). N 2 K 9 O (5.78), star-like central condensation shows occasionally. 6.814 : N 3 K 8 O (5.85).

June 7.813. Full moon. Light sky, but good seeing. With binocular telescope: N 3 K 5 O (5.94); $K>P$ by $0^m.1$ (5.95). 7.830 : with AZT-7 seeker, $K=0$ (6.4); under ×200 magnification, the nucleus is seen to issue a bright elongated condensation (directed roughly away from the sun) in which a second nucleus is outlined.

June 8.817. Comet seen on light sky. Brightness estimated reliably (binocular telescope): P 4 K 6 O (6.20). A highly concentrated nebulosity: $D=8'$.

June 10.814. Light sky. R 6 K 2 S (6.55); $K>S$ by $0^{m}.1$ (6.52). Star-like nucleus and a very faint nebulosity.

June 11.815. $K=S$ or K fainter than S by $0^{m}.05$ (6.65): 11.823 : Q 7 K 1 S (6.52); $K>S$ by $0^{m}.15$ (6.53).

June 12.825. Found with difficulty with a binocular telescope: T 3 K 6 V (6.39); $D \sim 20'$.

June 14.831. Found with binoculars. T 5 K 2.5 V (6.58); $K>V$ by $0^{m}.2$ (6.56).

June 19.844. Found with AZT-7 seeker; not fainter than $7-7^{m}.5$. $K>SS$ Virg by $0.2-0^{m}.3$. $D \sim 3-4'$. Under X240 magnification, a highly elongated central condensation with a nucleus in the western apex. Brightness of the nucleus $=X$ (8.3).

The magnitudes of the comparison stars are listed in the table.

No.	Symbol	HD	m_{vis}	S_p	No.	Symbol	HD	m_{vis}	S_p
1	*a*	136729	5.52	A3	25	*z*	117893	7.54	KO
2	*c*	137895	7.03	K2	26	*A*	119035	6.08	G5
3	*d*	135944	6.52	G5	27	*B*	116287	6.95	KO
4	*e*	135401	7.22	KO	28	*C*	114092	6.40	K5
5	*f*	134493	6.27	KO	29	*D*	113996	4.90	K5
6	*g*	133029 = 44Boo	6.16	AOp	30	*E*	114710 βComB	4.32	GO
7	*h*	133207	7.40	KO	31	*F*	112033	5.10	KO
8	*i*	130582	7.86	F8	32	*G*	113848	6.04	F5
9	*j*	131446	7.11	KO	33	*H*	114378+	(5.22+	F5
10	*k*	131883	7.44	KO			+114379	+5.22)	
11	*l*	130945	5.76	F5	34	*I*	112769	4.96	Ma
12	*m*	128184	6.57	AO	35	*J*	113022	6.12	F5
13	*n*	130987	7.56	F8	36	*L*	111893	6.25	A2
14	*o*	127285	6.62	KO	37	*M*	111067	5.33	K2
15	*p*	129426	7.70	G5	38	*N*	111397	5.64	AO
16	*q*	130044	6.84	FO	39	*O*	111308	6.43	AO
17	*r*	128092	6.82	A2	40	*P*	111164	6.05	A3
18	*s*	127663	6.75	A2	41	*Q*	111028	5.86	KO
19	*t*	126304	7.58	KO	42	*R*	110377	6.33	A5
20	*u*	128902	5.92	KO	43	*S*	109764	6.62	A2
21	*v*	117981	6.80	KO	44	*T*	108985	6.16	K5
22	*w*	119458	5.98	KO	45	*U*	109417	6.85	K2
23	*x*	118643	7.59	K2	46	*V*	108561	6.76	AO
24	*y*	117203	7.12	K2	47	*X*	108263	8.3	KO

N67 15448

E. I. Fialko, I. V. Bairachenko, Yu. V. Chumak, R. I. Moisya, and V. I. Mel'nik

STATISTICAL CHARACTERISTICS OF THE METEOR RADIO ECHO IN THE EPOCH OF THE 1963 GEMINIDS

1. EQUIPMENT AND OBSERVATIONS

The observations were made at the "Tripol'e" station of the Kiev State University im. T. G. Shevchenko in the epoch of the Geminid stream (December 1963) using the radar equipment designed at the Department of General Radio Engineering and described in /5/. The basic parameters of the radar stations:

1) $\lambda = 9.59$ m; $P_u = 20$ kW; $F_u = 500$ c/s; $\tau_u = 10\,\mu$sec; each fifth pulse "double"; four-unit transmitting and receiving antennas raised to $h = \lambda/2$ above the ground.

2) $\lambda = 6.49$ m; the other parameters as at $\lambda = 9.59$ m. The range-amplitude characteristics are photographed off a display screen (time base, 0.11 sec).

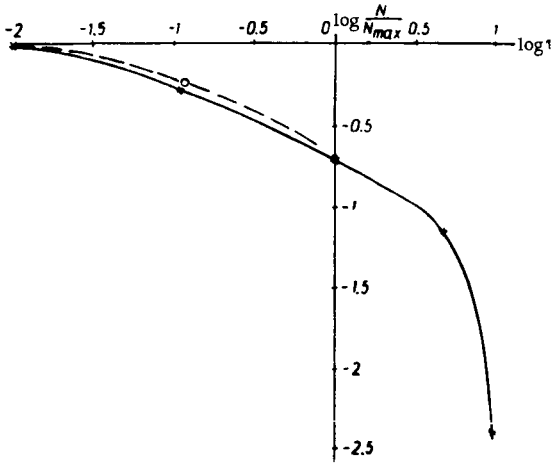

FIGURE 1. Integrated distribution of the meteor radio echo duration

The radar equipment was assembled with the participation of I. V. Bairachenko, R. I. Moisya, V. I. Mel'nik, and others. The observations were made by I. V. Bairachenko with the assistance of V. I. Mel'nik and others. The observational results were treated under the direction of

E. I. Fialko. The statistical characteristics of the meteor radio echo were determined from observations carried out during the half-hour from $\sim 0^h00^m$ to $\sim 0^h35^m$ on 14 December 1963 (local standard time).

During that half-hour, 207 meteor radio echoes were recorded at $\lambda = 9.59$ m (note that the two "slow" time bases are triggered by a signal from the receiving device at $\lambda = 9.59$ m). The hourly rate was thus $N_t = 355$. However, some radio echoes, though range-resolved, "overlapped" on the "diffraction pattern"; for some other reflections, the time of occurrence, the duration, etc., were recorded with inadequate accuracy. The various statistical characteristics were therefore based on a varying number of meteor radio echoes, from 198 to 207.

Determination of the slant range, of the time of occurrence, and of the duration, as well as of the radio echo amplitudes enabled us to derive various statistical characteristics which are interpreted in the following.

2. DISTRIBUTION OF RADIO ECHO DURATION

Figure 1 shows the integrated distribution of radio echo duration at $\lambda = 9.59$ m (dashed line) and $\lambda = 6.49$ m (solid line) normalized to unity for $\tau = 0.01$ sec; N is the number of reflections with a duration of not less than τ, $N_{max} = N(\tau_{min})$. The duration distribution was plotted for 203 meteor radio echoes recorded at $\lambda = 9.59$ m in the range from 0.01 sec to 12.3 sec. Most of the echoes were long enduring, i. e., stable (some 60%); some 10% of the echoes were classified as intermediate, and some 30% unstable. Somewhat fewer reflections were recorded at $\lambda = 6.49$ m, but the choice of recording parameters (0.11-sec time bases intended for separate observations of the amplitude-range characteristics of the meteor radio echo at the two λ were triggered by signals received at $\lambda = 9.59$ m only) is unsuitable for a comparison of the hourly rates at the two wavelengths. The echo at $\lambda = 6.49$ m was often lost in the general noise in range sweeps ("fast" time base), while the signal at $\lambda = 9.59$ m was distinctly recorded. However, with "slow" time bases, almost all the signals of the six-meter station could be analyzed (provided that the corresponding reflection was also recorded at the nine-meter wavelength). Therefore, although the echo duration distribution at the two wavelengths is clearly objective, our results cannot be extended to a general wavelength dependence of the meteor rate.

Let us consider the distribution of the radio echo duration at $\lambda = 9.59$ m. In the range of stable, long enduring radio echo (corresponding to the so-called overdense trains), the curve shows a distinct break in the region $\tau = 5$ sec. The sharp drop in the number of echoes of higher duration is attributable to the characteristic features of the "normal" scattering of radio waves (as has been previously observed in /2/), and to a certain extent also to deionization processes /2/ and, possibly, to the influence of the antenna directivity /1/. In the range of low durations (hundredths and tenths of a second), where unstable meteor radio echoes prevail (corresponding to the so-called underdense trains), the hourly rate falls off less steeply with the decrease in duration than in the range

$\tau \approx 1-5$ sec. This is due to the exponential behavior of the unstable echoes /2/.

We see from Figure 1 that in the region $\tau > 1$ sec the duration distribution at the two wavelengths is virtually the same. This is so because only stable echoes can have these durations (having electron line density $\alpha \gg 10^{12}$ electron/cm), and the corresponding distribution function is written in the approximate form

$$P(\tau) = \frac{N(\tau)}{N(\tau_{min})} = \left(\frac{\tau_{min}}{\tau}\right)^{3/4(s-1)}. \quad (1)$$

The distribution $P(\tau)$ is thus determined only by the index s, characterizing the mass distribution of the meteor bodies, and is independent of the wavelength λ.

In the range of low durations $\tau < 1$ sec, there is a certain divergence between the distributions at $\lambda = 9.59$ m and $\lambda = 6.49$ m. This is so because in the region of τ of the order of 0.1 sec unstable trains prevail, having a different distribution /2/:

$$P(\tau) = \frac{N(\tau)}{N(\tau_{min})} = e^{-\left(\frac{4\pi}{\lambda}\right)^2 (s-1)\, D(\tau - \tau_{min})}, \quad (2)$$

where D is the diffusivity. The somewhat lower rate of echoes with durations of 1 sec observed at $\lambda = 6.49$ m is fully consistent with formula (2). On the other hand, it must be remembered that for τ of the order of 0.1 sec a certain number of intermediate (as well as a limited number of stable) trains may occur. A quantitative discrepancy may thus arise between the experimental data and the approximate formula (2), derived for echo reception from the characteristic height.

3. DISTRIBUTION OF RADIO ECHO AMPLITUDES

Measurements of the radio echo amplitudes, corrected for the nonlinear pulse-height characteristic of the receiver and of the display channel, gave the integrated distribution of meteor radio echo amplitudes at $\lambda = 9.59$ m (Figure 2, a) and $\lambda = 6.49$ m (Figure 2, b).

At $\lambda = 9.59$ m, 203 radio echoes were used in statistical treatment. The relation between the different echo types is as before (see Figure 1). Curve 1 in Figure 2,a gives the integrated amplitude distribution of all the recorded echoes (at $\lambda = 9.59$ m). We see that the rate of strong reflections (with amplitudes $U > 50\,\mu$V) sharply decreases. The trend of curve 1 can be understood if the total population is divided into three echo types: unstable (curve 2), intermediate (curve 3), and stable (curve 4). We see that the distribution of the entire population is largely decided by the height distribution of the stable echoes (since in our case the equipment had relatively low sensitivity: $\alpha_{min} \approx 5 \cdot 10^{10}$ electron/cm).

The height distribution of stable trains in the region of moderate amplitudes is adequately approximated by an inverse power function (see /2/)

$$P(U) \sim U^{-n}. \quad (3)$$

The straight line (a) approximates the left-hand section of the amplitude distribution of stable radio echoes. In the region of large amplitudes, the frequency falls off sharply.

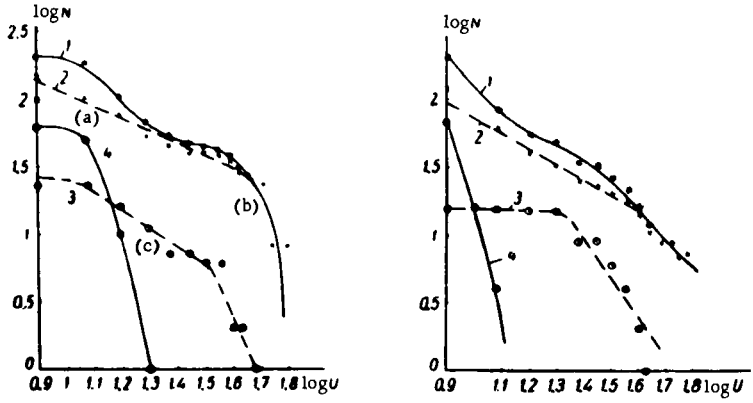

FIGURE 2. Distribution of meteor radio echo amplitudes:

1) * integrated, 2) × stable, 3) ⊙ intermediate, 4) unstable; a at $\lambda = 9.59$ m; b $\lambda = 6.49$ m

Unstable echoes (curve 4) have small amplitudes, but in the region of moderate amplitudes the experimental points closely follow a straight line (section (a) of curve 4). This is so because the amplitude distribution of unstable trains /2/ is also described by an inverse power function:

$$P(U) \sim U^{-n_2}. \tag{4}$$

But since approximately $n_2 \approx s-1$, while $n_1 = 4$ ($s-1$), branch (a) of curve 2 is much steeper than branch (a) of curve 4. The flat section of curve 4 is apparently also attributable to instrumental peculiarities (the measurements were made at the sensitivity threshold). The distribution of intermediate reflections (curve 3) is "intermediate", but clearly closer to the distribution of stable echoes. The departure of curve 1 in the region of small echo amplitudes from the "linear" approximation is attributable to the "contribution" of unstable meteor echoes.

The amplitude distribution at $\lambda = 6.49$ m (Figure 2,b) displays the same features on the whole. The distribution of unstable echoes (curve 4) has predictably shifted to the region of smaller amplitudes. Furthermore, the intermediate trains possess a somewhat different distribution: the left-hand branch of curve 3 is flat; however, at $\lambda = 6.49$ m no more than 15 intermediate trains were recorded, this being quite inadequate for drawing any reliable conclusions. The trend of curve 3 could be merely accidental.

The curves plotted in Figure 2 distinctly point in favor of adopting a differential approach to echoes of different types; furthermore, it is not always possible to consider two groups of trains — overdense and underdense — without distinguishing a third, intermediate type.

4. TIME DISTRIBUTION OF RADIO ECHOES

Figure 3 shows the integrated distribution of the time intervals T between the successive radio echoes (the points correspond to experimental results at $\lambda=9.59$ m). It follows from /2/ and /3/ that the analytical expression for the integrated time distribution has the form

$$P(T)=N_{\Sigma}e^{-\frac{T}{\bar{T}}}, \qquad (5)$$

where N_{Σ} is the overall number of echoes during the time T_{Σ}; $\bar{T}=\frac{T_{\Sigma}}{N_{\Sigma}}$ the mean interval.

In our case, $N_{\Sigma}=205$, $T_{\Sigma}=35$ min, $\bar{T}=10$ sec. The exponential function (5) is plotted as the solid line in Figure 3. We see that the agreement between the experimental and the theoretical results is highly satisfactory. A similar result was found for $\lambda=6.49$ m.

5. RANGE DISTRIBUTION OF RADIO ECHOES

The slant range was measured for 207 radio echoes at $\lambda=9.59$ m. Figure 4 shows the differential range distribution of the radio echoes ($\lambda=9.59$ m).

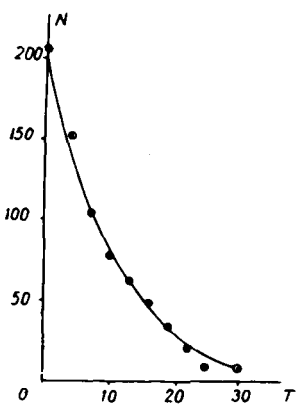

FIGURE 3. Integrated time distribution

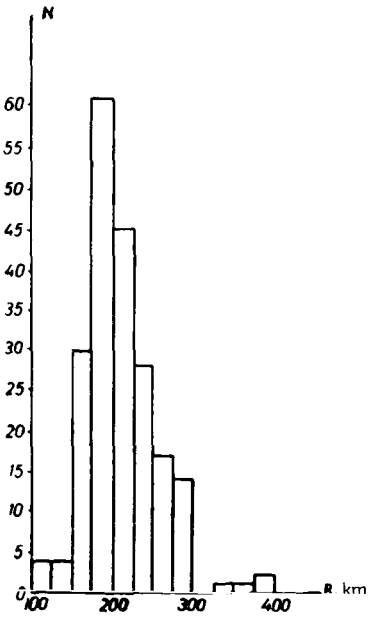

FIGURE 4. Differential distribution of range R

This distribution, as could be expected, is unimodal. Meteors were actually observed at ranges of from 100 to 400 km, the mode of the distribution lying at 175—200 km.

Some 75% of the meteors were observed at R=150—250 km. The range distribution at $\lambda=6.49$ m is similar.

The experimental results on the distribution of R can be easily interpreted, and they confirm the well-known results of /4/.

6. CONCLUSIONS

1) The duration distribution of meteor radio echoes at $\lambda = 9.59$ m and $\lambda = 6.49$ m is virtually the same in the region of high durations ($\tau > 1$ sec), slightly diverging in the range of small durations; a distinct change in the steepness of the curve $N(\tau)$ is observed for the Geminids near $\tau \approx 5$ sec.

2) Three echo types distinctly emerge from the echo amplitude distribution — stable, unstable, and intermediate; the distribution of the intermediate radio echoes is closer to the stable echoes.

3) The time distribution of meteor echoes is exponential.

BIBLIOGRAPHY

1. MOISYA, R.I., V.G. KRUCHINENKO, and I.V. BAIRACHENKO.—In: "Sbornik rabot po MGG", Izdatel'stvo KGU Vol. 2, p. 40, 1963.
2. FIALKO, E.I. Nekotorye problemy radiolokatsii meteorov (Some Problems of Meteor Radar Astronomy).—Izdatel'stvo Tomskogo Universiteta, 1961.
3. BOWDER, K.R. and J.G. Davies.—J. Atm. Terr. Phys., 11(1):62, 1957.
4. KAISER, T.R.—Phil. Mag. Suppl., 2(8):495, 1953.
5. BAIRACHENKO, I.V —Geomagnetizm i Aeronomiya, 5(3):463, 1965.

N67 15449

E. I. Fialko, I. V. Bairachenko, and Yu. V. Chumak

SOME RESULTS OF THE APPLICATION OF INTERMEDIATE-TYPE TRAINS IN MEASUREMENTS OF ELECTRON LINE DENSITY

E. I. Fialko proposed a radio-echo technique for measuring the electron line density α in ionization trains of the intermediate type. The radar approach is possible since the form of the intermediate-type radio echo (α of the order of 10^{12} electron/cm) is highly sensitive to α. In the present paper this technique is applied to obtain the distribution of α in the range $\alpha \approx 10^{12} - 5 \cdot 10^{12}$ electron/cm. The experimental data were supplied by observations of the 1963 Geminids (see preceding paper).

During half an hour (from 0^h0^m to 0^h35^m local standard time) on 14 December 1963, 207 meteor trains were recorded ($\lambda \approx 9.6$ m), 23 of which were classified as intermediate type.

Without repeating the description of the method, we shall confine ourselves to the results of measurements. The observational results were treated by Yu. V. Chumak under the guidance of E. I. Fialko, with the participation of I. V. Bairachenko.

DISTRIBUTION OF α IN INTERMEDIATE-TYPE TRAINS IN THE EPOCH OF THE 1963 GEMINIDS

The figure shows the integrated α distribution of the intermediate-type trains (N being the number of trains where the linear electron density α exceeded a given value). The measured values of α lie between the limits $10^{12} \leqslant \alpha \leqslant 6.10^{12}$ electron/cm. The graph clearly breaks into two parts: the left-hand section (comparatively gently sloping) and the right-hand section (much steeper). Note that, as in the case of long enduring, stable radio echo, the curve of the integrated α-distribution shows a distinct "break". Its origin is by no means obvious, but it may be attributed to various factors: the nature of "normal" scattering of radio waves by the meteor train /3/, the influence of the directivity pattern /1/, etc. Let us try to pass from the distribution of α to the distribution of meteor mass. Setting approximately $\alpha \sim m$ and applying the right-hand branch of the experimental curve $\log N$ vs. $\log\alpha$ (see Figure), we find in accordance with the relations in /3/

$$s \approx 1 + \frac{\log N_2 - \log N_1}{\log \alpha_1 - \log \alpha_2} \approx 1.67.$$

This is somewhat higher than for the Geminids (s= 1.66 /2/). However, remembering that the analysis was based on 23 meteors only (for 10 of which no velocity measurements were made), we may consider this tentative figure as quite satisfactory.

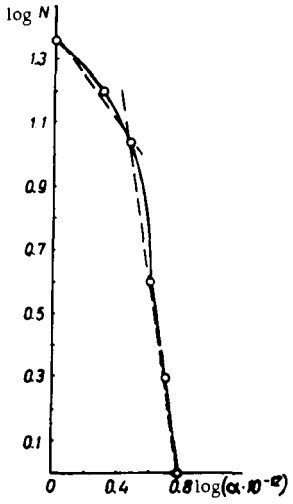

Integrated distribution of the electron line density α in intermediate-type trains

CONCLUSIONS

1) The determination of the electron line density in the epoch of the 1963 Geminids gave the density distribution in the interval

$$\alpha \approx (1 - - 6) \cdot 10^{12} \text{ electron/cm}.$$

2) As with stable trains, the curve of the integrated α-distribution shows a distinct "break".

3) A satisfactory numerical estimate of the index was obtained ($s \approx 1.67$).

BIBLIOGRAPHY

1. MOISYA, R. I., V. G. KRUCHINENKO, and I. V. BAIRACHENKO. — In: "Sbornik rabot po MGG", Izdatel'stvo KGU, Vol. 2, p. 40, 1963.
2. LOVELL, A. C. B. Meteor Astronomy. — [Russian translation. 1954.]
3. FIALKO, E. I. Nekotorye problemy radiolokatsii meteorov (Some Problems of Meteor Radar Astronomy). — Izdatel'stvo Tomskogo Universiteta, 1961.

I. A. Deryugin and V. I. Vorontsov

N67 15450

PROPAGATION OF ELECTROMAGNETIC WAVES IN A MOVING GYROTROPIC MEDIUM

The dynamics of ionized meteor trains and the "winds" in the upper ionospheric layers, starting with the F_2 layer, must sometimes be taken into consideration when investigating the propagation of electromagnetic waves in the ionosphere: the ionospheric "winds" in the neighborhood of the F_2 layers have speeds of some 500 m/sec, and the velocity of the meteor head may reach 70 m/sec. Suitable relativistic corrections must therefore be introduced into the parameters of the radar beam used in observations of a moving ionized gas.

In the present paper we advance a theory of the propagation of plane, and in general inhomogeneous, electromagnetic waves in a moving gyrotropic medium. The case of a gyrotropic medium moving along the forcelines of a constant magnetic field is of the greatest applied significance. The nonmagnetized moving plasma is considered as a particular case of the theory.

1. THE EQUATIONS OF A VARIABLE MAGNETIC FIELD

Maxwell's equations are inherently relativistic, and therefore the linear equations for the components of a variable electromagnetic field

$$a = a_0 \exp\{i\omega(t - \vec{\xi}\cdot\vec{r})\}, \tag{1.1}$$

where $\vec{\xi}$ is the vector of normal refraction, apply in any system of coordinates:

$$[\vec{\xi}\times\vec{H}] + \vec{D} = 0, \tag{1.2}$$

$$[\vec{\xi}\times\vec{E}] - \vec{B} = 0, \tag{1.3}$$

$$\vec{\xi}\cdot\vec{D} = 0, \tag{1.4}$$

$$\vec{\xi}\cdot\vec{B} = 0. \tag{1.5}$$

The two constitutive equations relating the displacement and the induction with the strength of the electromagnetic field are generally replaced with Minkowsky's equations in the electrodynamics of moving media. Minkowsky's equations, however, are not always convenient, and in general they cannot even be solved without resorting to equations (1.2)—(1.5). I. E. Tamm /3/ developed an electrodynamics of moving anisotropic media, where the constitutive equations are written in

tensor form:

$$E^{\mu\nu}=\frac{1}{2}\varepsilon^{\mu\nu,\alpha\beta}E_{\alpha\beta},\quad E_{\mu\nu}=\frac{1}{2}\varepsilon_{\mu\nu,\alpha\beta}E^{\alpha\beta},\quad \frac{1}{2}\varepsilon^{\mu\nu,\alpha\beta}\varepsilon_{\lambda\sigma,\alpha\beta}=\delta^{\mu\nu}_{\lambda\sigma}. \tag{1.6}$$

However, permittivity tensors of fourth valence are much too unwieldy for gyrotropic media. If, on the other hand, we introduce the 6-dimensional bivector space, the constitutive equations (1.6) take a convenient calculational form

$$E^A=\varepsilon^{A,B}E_B,\quad E_A=\varepsilon_{A,B}E^B,\quad \varepsilon^{A,B}\varepsilon_{B,C}=\delta^A_C, \tag{1.7}$$

where the collective indices of the 6-dimensional bivector space are used /2/:

$$A=\{01,\ 02,\ 03,\ 23,\ 31,\ 12\},$$
$$E^A=\{E^{0n};\ E^{mn}\}=\{\vec{D};\ \vec{H}\},\quad E_A=\{E_{0n};\ E_{mn}\}=\{-\vec{E};\ \vec{B}\}. \tag{1.8}$$

In a stationary coordinate system, the 6-dimensional permittivity tensors can be written as square-diagonal matrices:

$$(\varepsilon_{A,B})=\begin{pmatrix}-(\overleftrightarrow{\varepsilon}) & 0\\ 0 & (\overleftrightarrow{\mu})^{-1}\end{pmatrix},\quad (\varepsilon_{A,B})=\begin{pmatrix}-(\overleftrightarrow{\varepsilon})^{-1} & 0\\ 0 & (\overleftrightarrow{\mu})\end{pmatrix}, \tag{1.9}$$

where the 3-dimensional diagonal squares contain the ordinary permittivity tensors of gyrotrpic media /1/.

Equations (1.7) are covariant relative to the bivector Lorentz transformations:

$$L'^{A\cdot}_{\cdot B}=2L'^{[\mu}_{\cdot\alpha}L'^{\nu]}_{\cdot\beta},\quad L'^{A\cdot}_{\cdot B}=L'^{\cdot A}_{B\cdot},\quad L'^{B}_{\cdot A}=L'^{\cdot B}_{A\cdot}. \tag{1.10}$$

For example, the motion of the coordinate system $'K$ relative to another system K along the axis x_3 is described by the following transformations:

$$(L'^{A\cdot}_{\cdot B})=\left(\begin{array}{cccc:cccc}\gamma & 0 & 0 & 0 & \beta\gamma & 0\\ 0 & \gamma & 0 & -\beta\gamma & 0 & 0\\ 0 & 0 & 1 & 0 & 0 & 0\\ \hdashline 0 & -\beta\gamma & 0 & \gamma & 0 & 0\\ \beta\gamma & 0 & 0 & 0 & \gamma & 0\\ 0 & 0 & 0 & 0 & 0 & 1\end{array}\right),\quad \beta=\frac{v}{c},\quad \gamma=\frac{1}{\sqrt{1-\beta^2}}. \tag{1.11}$$

In the natural system of the gyrotropic medium, the 6-dimensional permittivity tensors have the square-diagonal form (1.9). In the laboratory system, with the gyrotropic medium moving parallel to its x_3 axis in the direction of the constant magnetic field, the 6-dimensional permittivity tensors take the form

$$('\varepsilon^{A,B})=\begin{pmatrix}M & i\beta N\\ -i\beta N & \overset{\vee}{M}\end{pmatrix},\quad ('\varepsilon_{A,B})=\begin{pmatrix}\overset{\vee}{M} & -i\beta\overset{\vee}{N}\\ -i\beta\overset{\vee}{N} & \overset{\vee}{M}\end{pmatrix}, \tag{1.12}$$

where the component squares contain the 3-dimensional matrices

$$(M)=-\begin{pmatrix} \gamma^2(\varepsilon-\beta^2\bar{\mu}); & i\gamma^2(\varepsilon_a-\beta^2\bar{\mu}_a); & 0 \\ -i\gamma^2(\varepsilon_a-\beta^2\bar{\mu}_a); & \gamma^2(\varepsilon-\beta^2\bar{\mu}); & 0 \\ 0; & 0; & \varepsilon_{\parallel} \end{pmatrix},$$

$$(\overset{\vee}{M})=-\begin{pmatrix} \gamma^2(\bar{\mu}-\beta^2\varepsilon); & i\gamma^2(\bar{\mu}_a-\beta^2\varepsilon_a); & 0 \\ -i\gamma^2(\bar{\mu}_a-\beta^2\varepsilon_a); & \gamma^2(\bar{\mu}-\beta^2\varepsilon); & 0 \\ 0; & 0; & \bar{\mu}_{\parallel} \end{pmatrix}, \tag{1.13}$$

$$(\bar{M})=\begin{pmatrix} \gamma^2(\bar{\varepsilon}-\beta^2\mu); & i\gamma^2(\bar{\varepsilon}_a-\beta^2\mu_a); & 0 \\ -i\gamma^2(\bar{\varepsilon}_a-\beta^2\mu_a); & \gamma^2(\bar{\varepsilon}-\beta^2\mu); & 0 \\ 0; & 0; & \bar{\varepsilon}_{\parallel} \end{pmatrix},$$

$$(\overset{\vee}{\bar{M}})=\begin{pmatrix} \gamma^2(\mu-\beta^2\bar{\varepsilon}); & i\gamma^2(\mu_a-\beta^2\bar{\varepsilon}_a); & 0 \\ -i\gamma^2(\mu_a-\beta^2\bar{\varepsilon}_a); & \gamma^2(\mu-\beta^2\bar{\varepsilon}); & 0 \\ 0; & 0; & \mu_{\parallel} \end{pmatrix}, \tag{1.14}$$

$$(N)=\gamma^2\begin{pmatrix} \varepsilon_a-\bar{\mu}_a); & i(\varepsilon-\bar{\mu}), & 0 \\ -i(\varepsilon-\bar{\mu}); & (\varepsilon_a-\bar{\mu}_a); & 0 \\ 0; & 0; & 0 \end{pmatrix},$$

$$(\overset{\vee}{N})=\gamma^2\begin{pmatrix} (\bar{\varepsilon}_a-\mu_a); & i(\bar{\varepsilon}-\mu); & 0 \\ -i(\bar{\varepsilon}-\mu); & (\bar{\varepsilon}_a-\mu_a); & 0 \\ 0; & 0; & 0 \end{pmatrix}. \tag{1.15}$$

Writing the 6-dimensional permittivity tensors in terms of four square 3-dimensional tensors, we reduce the constitutive equations of moving gyrotropic media to four vector equations:

$$\vec{D}=-(M)\vec{E}+i\beta(N)B, \tag{1.16}$$

$$\bar{H}=i\beta(N)\vec{E}+(\overset{\vee}{M})\bar{B}, \tag{1.17}$$

$$\vec{E}=-(\bar{M})\vec{D}+i\beta(\overset{\vee}{\bar{N}})\bar{H}, \tag{1.18}$$

$$\bar{B}=i\beta(\overset{\vee}{\bar{N}})\vec{D}+(\overset{\vee}{\bar{M}})\bar{H}. \tag{1.19}$$

In some cases it is advisable to introduce circularly polarized electromagnetic waves. Equations (1.16)—(1.19) then take the form

$$D_{\pm}=a_{\pm}E_{\pm}\pm i\beta b_{\pm}B_{\pm}, \tag{1.20}$$

$$H_{\pm}=\pm i\beta b_{\pm}E_{\pm}+\overset{\vee}{a}_{\pm}B_{\pm}, \tag{1.21}$$

$$E_{\pm}=a_{\pm}D_{\pm}\pm i\beta\overset{\vee}{\bar{b}}_{\pm}H_{\pm}, \tag{1.22}$$

$$B_{\pm}=\pm i\beta\overset{\vee}{\bar{b}}_{\pm}D_{\pm}+\overset{\vee}{\bar{a}}_{\pm}H_{\pm}, \tag{1.23}$$

$$D_3=\varepsilon_{\parallel}E_3 \quad B_3=\mu_{\parallel}H_3, \tag{1.24}$$

where

$$a_{\pm}=\frac{\gamma^2(\varepsilon_{\pm}\mu_{\mp}-\beta^2)}{\mu_{\pm}},\quad \overset{\vee}{a}_{\mp}=\frac{\gamma^2(1-\beta^2\varepsilon_{\pm}\mu_{\mp})}{\mu_{\mp}},\quad b_{\pm}=\frac{\gamma^2(\varepsilon_{\pm}\mu_{\pm}-1)}{\mu_{\mp}}, \tag{1.25}$$

$$\bar{a}_{\pm}=\frac{\gamma^2(1-\beta^2\varepsilon_{\mp}\mu_{\pm})}{\varepsilon_{\pm}},\quad \overset{\vee}{a}_{\pm}=\frac{\gamma^2(\varepsilon_{\pm}\mu_{\pm}-\beta^2)}{\varepsilon_{\pm}},\quad \overset{\vee}{b}_{\pm}=-\frac{\gamma^2(\varepsilon_{\pm}\mu_{\pm}-1)}{\varepsilon_{\pm}}. \tag{1.26}$$

Note that (1.16)—(1.19) yield 12 equations in 12 unknowns, but the rank of the matrix of this homogeneous system is $r=6$. It is therefore unsolvable. If we now add six linear equations of the variable electromagnetic field of the form (1.2), (1.3), the problem can be solved in principle. It is more convenient to replace equations (1.2), (1.3) with a system from which the vectors $\bar{D}$ and $\bar{B}$ have been eliminated. This system can be solved independently of (1.16)—(1.24), and the displacement and induction vectors can then be found from the constitutive equations of moving gyrotropic media (1.16)—(1.24). Applying (1.17) and (1.18), we reduce the linear equations (1.2) and (1.3) of a variable electromagnetic field in a longitudinally moving gyrotropic medium to a pair of vector equations:

$$-(\bar{M})[\vec{\zeta}\times\bar{H}]-i\beta(\overset{\vee}{N})\bar{H}+\vec{E}=0, \tag{1.27}$$

$$(\overset{\vee}{M})[\vec{\zeta}\times\vec{E}]+i\beta(N)\vec{E}-\bar{H}=0. \tag{1.28}$$

Resolving the vector of normal refraction into longitudinal and transverse components

$$\vec{\zeta}=\zeta_1\vec{e}_1+\zeta_3\vec{e}_3, \tag{1.29}$$

we expand equations (1.26) and (1.27) writing them in terms of the components of the electric and magnetic field vectors $\bar{E}$ and $\bar{H}$:

$$\begin{aligned}
&i\gamma^2[\zeta_3(\bar{\mu}_a-\beta^2\varepsilon_a)+\beta(\varepsilon_a-\bar{\mu}_a)]E_1-\gamma^2[\zeta_3(\bar{\mu}-\beta^2\varepsilon)+\beta(\varepsilon-\bar{\mu})]E_2-\\
&\qquad-i\zeta_1\gamma^2(\bar{\mu}_a-\beta^2\varepsilon_a)E_3-H_1=0,\\
&\gamma^2[\zeta_3(\bar{\mu}-\beta^2\varepsilon)+\beta(\varepsilon-\bar{\mu})]E_1+i\gamma^2[\zeta_3(\bar{\mu}_a-\beta^2\varepsilon_a)]+\beta(\varepsilon_a-\bar{\mu}_a)E_2-\\
&\qquad-\zeta_1\gamma^2(\bar{\mu}-\beta^2\varepsilon)E_3-H_2=0,\\
&\qquad\zeta_1\bar{\mu}_1E_2-H_3=0,\\
&i\gamma^2[\zeta_3(\bar{\varepsilon}_a-\beta^2\mu_a)-\beta(\bar{\varepsilon}_a-\mu_a)]H_1-\gamma^2[\zeta_3(\bar{\varepsilon}-\beta^2\mu)-\beta(\bar{\varepsilon}-\mu)]H_2-\\
&\qquad-i\zeta_1\gamma^2(\bar{\varepsilon}_a-\beta^2\mu_a)H_3+E_1=0,\\
&\gamma^2[\zeta_3(\bar{\varepsilon}-\beta^2\mu)-\beta(\bar{\varepsilon}-\mu)]H_1+i\gamma^2[\zeta_3(\bar{\varepsilon}_a-\beta^2\mu_a)-\beta(\bar{\varepsilon}_a-\mu_a)]H_2-\\
&\qquad-\zeta_1\gamma^2(\bar{\varepsilon}-\beta^2\mu)H_3+E_2=0,\\
&\qquad\zeta_1\bar{\varepsilon}_1H_2+E_3=0.
\end{aligned} \tag{1.30}$$

Equations (1.2), (1.3), and consequently (1.26), (1.27) and (1.16)—(1.24), obey Larmor's duality principle

$$\vec{E}\leftrightarrow\bar{H},\ \vec{D}\leftrightarrow-\bar{B},\ -(\varepsilon)\leftrightarrow(\mu),\ (M)\leftrightarrow(\overset{\vee}{M}),\ (\bar{M})\leftrightarrow(\overset{\vee}{M}),\ (N)\leftrightarrow(\overset{\vee}{N}). \tag{1.31}$$

The symmetric duality /4/ is also very useful:

$$\vec{D}\rightleftarrows\vec{E},\ \vec{B}\rightleftarrows\vec{H},\ \varepsilon\rightleftarrows\frac{1}{\varepsilon},\ \mu\rightleftarrows\frac{1}{\mu},\ (M)\rightleftarrows(\bar{M}),\ \overset{\vee}{(M)}\rightleftarrows\overset{\vee}{(\bar{M})},\ (N)\rightleftarrows\overset{\vee}{(\bar{N})}. \tag{1.32}$$

The symmetric duality establishes a relation between equations (1.16) and (1.18), (1.17) and (1.19), (1.20) and (1.22), (1.21) and (1.24), and also between the 6-dimensional permittivity tensors (1.12). The two duality principles are applied in the following sections to simplify the calculations if the solution of one of the two dual problems is known.

2. THE EQUATION OF NORMALS

System (1.30) of homogeneous linear equations for the components of the variable electromagnetic field is solvable if its determinant vanishes. Setting the determinant equal to zero, we obtain the characteristic equation for the vector of normal refraction $\vec{\xi}$, or in other words, the equation of normals for longitudinally moving gyrotropic media:

$$\begin{aligned}
&\frac{\zeta_1^4\gamma^4}{\varepsilon_\perp\mu_\perp}(1-\beta^2\mu\varepsilon_\perp)(1-\beta^2\varepsilon\mu_\perp)-\frac{1}{4}\frac{\zeta_1^4\beta^2\gamma^8}{\varepsilon\mu\varepsilon_\perp\mu_\perp}(1-\beta\zeta_3)^2(\varepsilon_+\mu_+-\varepsilon\mu_-)^2-\\
&-\frac{\zeta_1^2\gamma^2}{2}\left(\frac{\mu_\parallel}{\mu_+}+\frac{\varepsilon_\parallel}{\varepsilon_+}\right)(1-\beta^2\varepsilon_+\mu_+)\times\\
&\times\left\{1-\frac{\gamma^4}{\varepsilon_-\mu_-}[\zeta_3(1-\beta^2\varepsilon_-\mu_-)+\beta(\varepsilon_-\mu_--1)]^2\right\}-\\
&-\frac{\zeta_1^2\gamma^2}{2}\left(\frac{\mu_\parallel}{\mu_-}+\frac{\varepsilon_\parallel}{\varepsilon_-}\right)(1-\beta^2\varepsilon_-\mu_-)\times\\
&\times\left\{\frac{\gamma^4}{\varepsilon_+\mu_+}[\zeta_3(1-\beta^2\varepsilon_+\mu_+)+\beta(\varepsilon_+\mu_+-1)]^2\right\}+\\
&+\varepsilon_\parallel\mu_\parallel\left\{1-\frac{\gamma^4}{\varepsilon_+\mu_+}[\zeta_3(1-\beta^2\varepsilon_+\mu_+)+\beta(\varepsilon_+\mu_+-1)]^2\right\}\times\\
&\times\left\{1-\frac{\gamma^4}{\varepsilon_-\mu_-}[\zeta_3(1-\beta^2\varepsilon_-\mu_-)+\beta(\varepsilon_-\mu_--1)]^2\right\}=0.
\end{aligned} \tag{2.1}$$

Equation (2.1) is biquadratic relative to the transverse component of the normal-refraction vector and is of fourth order relative to the longitudinal component. Let us consider some particular cases. If the gyrotropic medium is at rest, i.e., $\beta=0$, equation (2.1) takes the simple form

$$\begin{aligned}
&\frac{\zeta_1^4}{\varepsilon_\perp\mu_\perp}-\frac{\zeta_1^2}{2}\left(\frac{\mu_\parallel}{\mu_+}+\frac{\varepsilon_\parallel}{\varepsilon_+}\right)\left(1-\frac{\zeta_3^2}{\varepsilon_-\mu_-}\right)-\frac{\zeta_1^2}{2}\left(\frac{\mu_\parallel}{\mu_-}+\frac{\varepsilon_\parallel}{\varepsilon_-}\right)\left(1-\frac{\zeta_3^2}{\varepsilon_+\mu_+}\right)+\\
&+\varepsilon_\parallel\mu_\parallel\left(1-\frac{\zeta_3^2}{\varepsilon_-\mu_-}\right)\left(1-\frac{\zeta_3^2}{\varepsilon_+\mu_+}\right)=0.
\end{aligned} \tag{2.2}$$

Equation (2.2) is biquadratic in either component of the normal-refraction vector, so that its solution gives two roots for each of these components. After some manipulations, equation (2.2) can be written

in the well-known form /1/

$$\left(\frac{\zeta_1^2}{\varepsilon_\perp}+\frac{\zeta_3^2}{\varepsilon}\right)\left(\frac{\zeta_1^2}{\mu_\perp}+\frac{\zeta_3^2}{\mu}\right)-2\zeta_3^2\left(1+\frac{\varepsilon_a\mu_a}{\varepsilon\mu}\right)-\zeta_1^2\left(\frac{\varepsilon_\perp}{\varepsilon_\parallel}+\frac{\mu_\perp}{\mu_\parallel}\right)+\varepsilon_\perp\mu_\perp=0. \tag{2.3}$$

When the propagation of the electromagnetic wave is parallel or anti-parallel to the motion of the gyrotropic medium, i.e., when $\xi_1=0$, equation (2.1) takes the simple form

$$\zeta_3(1-\beta^2\varepsilon_+\mu_+)+\beta(\varepsilon_+\mu_+-1)=\pm\gamma^2\sqrt{\varepsilon_+\mu_\pm}, \tag{2.4}$$

having (3.3) as its solution. When the electromagnetic wave propagates in the transverse direction, slightly departing from the transverse plane $\xi_3=\beta$, equation (2.1) reduces to an equation for the transverse component of the normal-refraction vector:

$$\left(\frac{\xi_1^2\gamma^2}{\mu_\parallel}-\varepsilon_\perp\right)\left(\frac{\zeta_1^2\gamma^2}{\varepsilon_\parallel}-\mu_\perp\right)=0. \tag{2.5}$$

If the moving medium is isotropic, (2.1) takes the elementary form

$$\zeta_1^2(1-\beta^2\varepsilon\mu)+\gamma^2[\zeta_3(1-\beta^2\varepsilon\mu)+\beta(\varepsilon\mu-1)]^2=\gamma^{-2}\varepsilon\mu, \tag{2.6}$$

which defines an ellipse

$$\frac{x^2}{a^2}+\frac{y^2}{b^2}=1$$

with the semi-axes a and b and a displaced center:

$$a=\frac{(1-\beta^2)\sqrt{\varepsilon\mu}}{(1-\beta^2\varepsilon\mu)},\quad b=\sqrt{\frac{\varepsilon\mu(1-\beta^2)}{(1-\beta^2\varepsilon\mu)}},\quad x=\zeta_3+\beta\frac{(\varepsilon\mu-1)}{(1-\beta^2\varepsilon\mu)},\quad y=\zeta_1. \tag{2.7}$$

The ellipse is slightly oblate, and its eccentricity is $e=\beta\sqrt{\frac{(\varepsilon\mu-1)}{(1-\beta^2)}}$. As the velocity of the isotropic medium is lowered to zero, the ellipse degenerates into a circle, and in the laboratory system the observer will record a transition from an anisotropic medium to an isotropic one. It should be emphasized that the similarity between the moving isotropic medium and the anisotropic one is not complete: the origin of the coordinates in the anisotropic medium coincides with the center of the ellipse, while this is clearly not so in moving media. The vector drawn from the origin to the ellipse defines the direction of phase propagation of the electromagnetic wave (of its normal or momentum), whereas the perpendicular to the tangent at the point where the ellipse meets the vector of normal refraction gives the vector of radial refraction (the radial vector or the Umov—Poynting vector /4/). The figure illustrates these geometrical constructions. Since the problem is symmetric about the longitudinal axis, we can maintain that the normal surface describes an ellipsoid of revolution in the three-dimensional space, whose plane

section is the ellipse defined by equation (2.7).

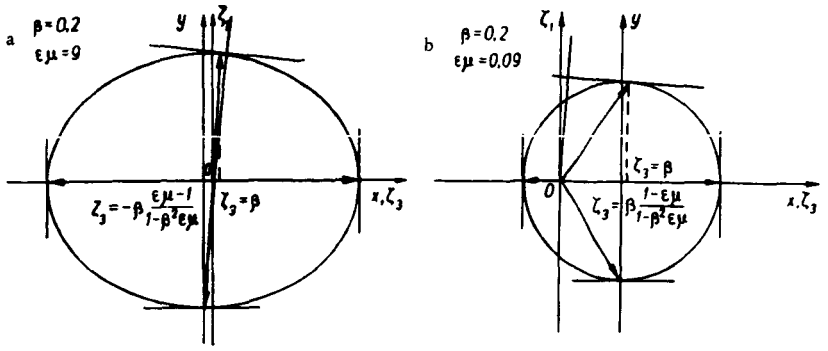

Normal ellipses for moving isotropic media

3. CIRCULARLY POLARIZED TEM WAVES

For longitudinal propagation of electromagnetic waves, the transverse component of the vector of normal refraction $\xi_1=0$. It therefore follows from (1.30) that the transverse components of the electromagnetic field are all zero, and we may introduce circularly polarized TEM waves which reduce equations (1.30) to

$$\pm i\gamma^2[\zeta_3(1-\beta^2\varepsilon_\pm\mu_\pm)+\beta(\varepsilon_\pm\mu_\pm-1)]E_\pm-\mu_\pm H_\pm=0, \tag{3.1}$$

$$\varepsilon_\pm E_\pm\pm i\gamma^2[\zeta_3(1-\beta^2\varepsilon_\pm\mu_\pm)+\beta(\varepsilon_\pm\mu_\pm-1)]H_\pm=0. \tag{3.2}$$

The characteristic equation of the system (3.1) and (3.2) is (2.4); its solution is the relativistic formula of vector addition:

$$\zeta_3=\frac{\zeta_0+\beta}{1+\beta\zeta_0},\quad \zeta_0=\pm\sqrt{\varepsilon_\pm\mu_\pm}. \tag{3.3}$$

Applying (3.1)—(3.3) and (1.21), (1.25), (1.22), we can easily find an expression for the field components of circularly polarized TEM waves:

$$D_\pm=\varepsilon_\pm^{ef}E_\pm, \tag{3.4}$$

$$B_\pm=\mu_\pm^{ef}H_\pm, \tag{3.5}$$

$$H_\pm=\pm i\sqrt{\frac{\varepsilon_\pm}{\mu_\pm}}E_\pm, \tag{3.6}$$

$$B_\pm=i\frac{\zeta_0+\beta}{1+\beta\zeta_0}E_\pm, \tag{3.7}$$

$$D_3=E_3=B_3=H_3=0. \tag{3.8}$$

In this case we can introduce the effective dielectric constant and the effective magnetic permeability

$$\varepsilon_{\pm}^{ef}=\pm\frac{\pm\sqrt{\varepsilon_{\pm}\mu_{\pm}}+\beta}{1\pm\beta\sqrt{\varepsilon_{\pm}\mu_{\pm}}}\sqrt{\frac{\varepsilon_{\pm}}{\mu_{\pm}}}, \tag{3.9}$$

$$\mu_{\pm}^{ef}=\pm\frac{\pm\sqrt{\varepsilon_{\pm}\mu_{\pm}}+\beta}{1\pm\beta\sqrt{\varepsilon_{\pm}\mu_{\pm}}}\sqrt{\frac{\mu_{\pm}}{\varepsilon_{\pm}}}, \tag{3.10}$$

$$\zeta_3=\sqrt{\varepsilon_{\pm}^{ef}\mu_{\pm}^{ef}}=n^{ef}. \tag{3.11}$$

The longitudinal axis x_3 is a main axis of the normal surface, so that phase propagation coincides with the direction of electromagnetic energy transfer:

$$\frac{p_3}{w}=\zeta_3,\quad \vec{p}=[\vec{D}\times\vec{B}],\quad w=\frac{1}{2}(\vec{D}\cdot\vec{E}+\vec{B}\cdot\vec{H}), \tag{3.12}$$

$$\frac{y_3}{w}=\xi_3=\frac{\xi_0+\beta}{1+\beta\xi_0},\quad \xi_0=\pm\frac{1}{\sqrt{\varepsilon_{\pm}\mu_{\pm}}},\quad \vec{y}=[\vec{E}\times\vec{H}]. \tag{3.13}$$

For gyrotropic media at rest, the difference $\Delta\zeta_0=\sqrt{\varepsilon_+\mu_+}-\sqrt{\varepsilon_-\mu_-}$ specifies the rotation of the plane of polarization of the initially linearly polarized wave. In longitudinally moving gyrotropic media an additional phase differences is contributed by (3.3), resulting in an additional relativistic rotation of the plane of polarization.

4. ABERRATION OF T M AND T E WAVES

Equations (1.30) are general for all waves propagating in moving gyrotropic media. It is advisable to divide them into two distinct groups characterizing two independent types of waves. This can be done, say, if one of the field components is zero. We may thus consider TM waves having $E_3=0$, and TE waves having $H_3=0$. The two subsystems of equations obtained from (1.30) by this technique are independent, as can be easily shown by means of the duality principle (1.31). To avoid repetition, we consider TM waves only. The equation of normals (2.1) is satisfied by a vector of normal refraction with the components

$$\zeta_3=\beta, \tag{4.1}$$

$$\zeta_1=\pm\sqrt{\mu_1\varepsilon_\perp}(1-\beta^2). \tag{4.2}$$

Substituting the normal-refraction components (4.1) and (4.2) in equation (1.30) defining the TM wave, we obtain

$$i\beta\varepsilon_a E_1-\beta\varepsilon E_2-H_1=0, \tag{4.3}$$

$$\varepsilon E_1+i\varepsilon_a E_2=0, \tag{4.4}$$

$$\varepsilon_1\bar{\mu}_1 E_2-H_3=0, \tag{4.5}$$

$$i\beta\mu_a H_1-i\zeta_1\gamma^2(\bar{\varepsilon}_a-\beta^2\mu_a)H_3+E_1=0, \tag{4.6}$$

$$\beta\mu H_1-\zeta_1\gamma^2(\bar{\varepsilon}-\beta^2\mu)H_3+E_2=0. \tag{4.7}$$

Solving this system in conjunction with the constitutive equations (1.18), (1.19), we find the following expressions for the electromagnetic field components:

$$D_1=0, \quad D_2=\varepsilon_\perp E_2, \quad D_3=0, \tag{4.8}$$

$$E_1=-i\frac{\varepsilon_a}{\varepsilon}E_2, \quad E_2\neq 0, \quad E_3=0, \tag{4.9}$$

$$H_1=-\beta\varepsilon_\perp E_2, \quad H_2=0, \quad H_3=\sqrt{\frac{\varepsilon_\perp}{\mu_\parallel}(1-\beta^2)}E_2, \tag{4.10}$$

$$\beta_1=-\beta E_2, \quad B_2=-i\beta\frac{\varepsilon_a}{\varepsilon}E_2, \quad B_3=\sqrt{\mu_\parallel\varepsilon_\perp}\,(1-\beta^2)E_2. \tag{4.11}$$

The momentum of the electromagnetic field has the following components in the longitudinal plane

$$p_1=\varepsilon_\perp\sqrt{\mu_\parallel\varepsilon_\perp(1-\beta^2)}E_2^2, \quad p_2=0, \quad p_3=\beta\varepsilon_\perp E_2^2 \tag{4.12}$$

and is collinear with the vector of normal refraction:

$$\frac{p_3}{p_1}=\frac{\zeta_3}{\zeta_1}=\frac{\beta}{\sqrt{\mu_\parallel\varepsilon_\perp(1-\beta^2)}}=\operatorname{tg}\vartheta_E. \tag{4.13}$$

The Umov—Poynting vector

$$Y_1=\sqrt{\frac{\varepsilon_\perp}{\mu_\parallel}(1-\beta^2)}E_2^2, \quad Y_2=-i\frac{\varepsilon_a}{\varepsilon}Y_1, \quad Y_3=\beta\varepsilon_\perp E_2^2, \tag{4.14}$$

divided by the energy density defines the vector of radial refraction $\vec{\xi}$:

$$\frac{Y_1}{w}=\sqrt{\frac{(1-\beta^2)}{\mu_\parallel\varepsilon_\perp}}=\xi_1, \quad \frac{Y_2}{w}=-i\frac{\varepsilon_a}{\varepsilon}\xi_1=\xi_2, \quad \frac{Y_3}{w}=\beta=\xi_3. \tag{4.15}$$

From (4.12)—(4.15) it follows that the direction of energy transfer by the TM wave, departing from the transverse direction by an angle ψ_E,

$$\frac{Y_3}{Y_1}=\beta\sqrt{\frac{\mu_\parallel\varepsilon_\perp}{(1-\beta^2)}}=\operatorname{tg}\psi_E, \tag{4.16}$$

is not collinear with the momentum of the electromagnetic field. However, in this case it can be easily shown that the vectors of the magnetic field and the magnetic induction are respectively perpendicular to the vectors of radial and normal refraction:

$$\frac{H_1}{H_3}=-\operatorname{tg}\psi_E, \quad \frac{B_1}{B_3}=-\operatorname{tg}\vartheta_E. \tag{4.17}$$

This particular case can therefore be considered as the case of normal TM waves. To sum up, in longitudinally moving gyrotropic media, TM waves propagate at an angle ϑ_E (4.13) to the transverse plane (aberration angle). If the electromagnetic wave makes an arbitrary angle with the longitudinal axis, it is best resolved into the normal waves TEM, TM,

or TE, as is the practice in the case of gyrotropic media at rest /1/, and is treated as a superposition of these simple waves.

In conclusion we should note that the relativistic aberration of electromagnetic waves is of some interest for isotropic, but inhomogeneous, plasma, when the dielectric constant becomes vanishingly small. The aberration angle (4.13) is then quite substantial; the laws of refraction are defined in terms of the vector of normal refraction, and therefore the additional rotation of the refraction vectors may become noticeable as the electromagnetic wave propagates through the inhomogeneous layers.

BIBLIOGRAPHY

1. GUREVICH, A.G. Ferrity na sverkhvysokikh chastotakh (Superhigh-frequency Ferrites).—Moskva. Fizmatgiz, 1960.
2. PETROV, A.Z. Prostranstva Einshteina (Einstein Spaces).—Moskva, Fizmatgiz. 1961.
3. TAMM, I.E.—Zhurnal Russkogo Fiziko-Khimicheskogo Obshchestva, Vol. 56: 248. 1924.
4. FEDOROV, F.I. Optika anizotropnykh sred (Optics of Anisotropic Media). — Minsk. 1958.

N67 15451

B. L. Kashcheev

THE DRIFT OF METEOR TRAINS

Observations of bright meteor trains helped to establish, back in the 19th century, that motions with velocities of several tens of meters per second prevail in the atmosphere at a height of 80—100 km. Manning observed /8/ that the drift of ionized meteor trains is fully consistent with the motion of neutral masses in the atmosphere. The study of winds in the upper atmosphere is one of the principal problems of geophysics; meteor trains provide us with a natural test body which, if traced by means of radio equipment, gives the whole picture of diurnal atmospheric circulation. Knowledge of regular and irregular motions in the atmosphere is also necessary for astronomic purposes. It has been established experimentally that atmospheric wind is one of the main sources of errors in radiant measurements by radio techniques /1/.

Systematic measurements of the drift of meteor trains have been made at Manchester /5/, Adelaide /4/, and Khar'kov /2/. The Manchester series is the most complete of the three. Note that Manchester and Khar'kov are located approximately at the same latitude (the difference being $\sim 3°$), so that comparison of results obtained at these two sites is highly significant in reconstructing the global motion in the atmosphere.

1. EQUIPMENT AND METHODS

The train drift was measured by the coherent-pulse technique at a frequency of 36.9 Mc/s. The equipment of the Khar'kov Polytechnical Institute was described in /3/. The radio reflections from the ionization trains were photographed, and Figure 1 is a specimen recording of an echo. Eight electron beams in cathode-ray tubes recorded the following data: 1) range of train; 2) three range-amplitude characteristics of three receiving channels, for radiant determination; 3) range-amplitude curves of the two direction-finding antennas (right, second from top); 4) three phase curves giving the period of Doppler beats at the base and at one field site, and also the sense of the radial velocity component, i.e., whether "to the observer" or "away from the observer". Time base, 0.17 sec.

No less than a few dozen readings of drift velocities must be taken every hour. The equipment parameters /3,5/ are such that drift

measurements must be made for three days in each direction (N—S and E—W). If the experiments are carefully staged and the results are accurately treated, the main error will be due to the width of the antenna

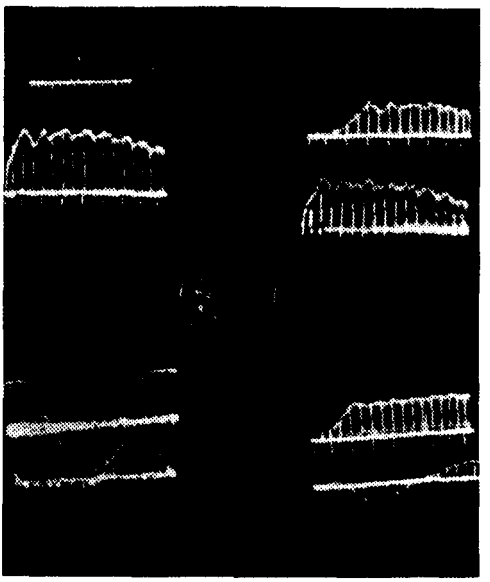

FIGURE 1

pattern in the horizontal plane. Considerable attention should therefore be paid to the choice of the antenna and to its tuning.

2. RESULTS OF MEASUREMENTS

In the period from March 1962 to March 1963, 133,721 individual values of the zonal component and 79,536 values of the meridianal component were obtained at the Khar'kov Polytechnic Institute. A distinct 12-hour (semi-diurnal) component with an amplitude of ~10—30 m/sec was observed on every single day. The constant component (the velocity of the prevailing wind) varies between wide limits, from 2 to 30 m/sec /2/. Figure 2 shows the smoothed curve of diurnal wind-speed variation (March—December 1962).

The yearly-average values of the zonal and the meridianal components are described by the equations

$$V = 8.0 + 5.6 \sin \frac{\pi}{12}(t - 8.5) + 14.9 \sin \frac{\pi}{6}(t - 5.8) + 3.7 \sin \frac{\pi}{4}(t - 7.1),$$

$$U = -3.1 + 2.3 \sin \frac{\pi}{12}(t - 2.2) + 13.8 \sin \frac{\pi}{6}(t - 2.4) + 3.7 \sin \frac{\pi}{4}(t - 4.2).$$

The prevailing wind veers from east to south approximately by 20°.

The velocity of the prevailing wind has a distinct character. Figure 3 plots the constant components in both directions (circles mark the values from March 1962 to March 1963, triangles the results obtained during the International Year of the Quiet Sun starting in December 1963). The results mainly apply to heights of 90-95 km. At this height the meridianal component is small, occasionally rising to 10 m/sec.

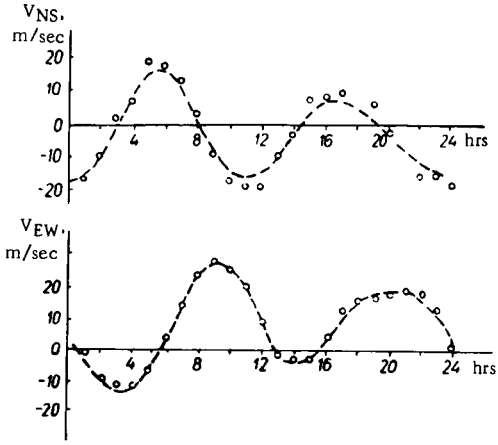

FIGURE 2

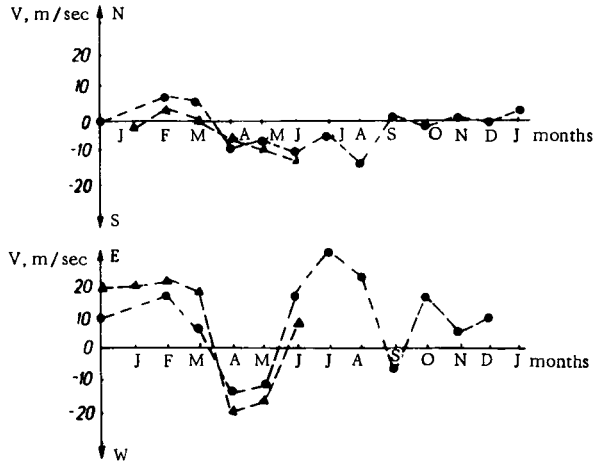

FIGURE 3

Figure 4 shows the variation in the amplitude of the 12-hour component in 1962-1963 (Figure 4, a). The results of the Jodrell Bank Experimental Station are given in Figure 4, b for purposes of comparison. Characteristically, the amplitudes of the zonal component do not differ much from the amplitudes of the meridianal one in any given month.

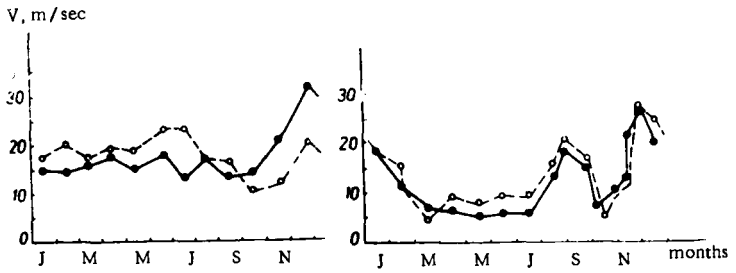

FIGURE 4

The 12-hour component can be represented as a vector commonly with clockwise rotation (this has been established experimentally). The phase difference between the northward and the eastward winds is close to three hours. In the period from January to June 1964, the phase difference was 3 ± 0.8 hrs.

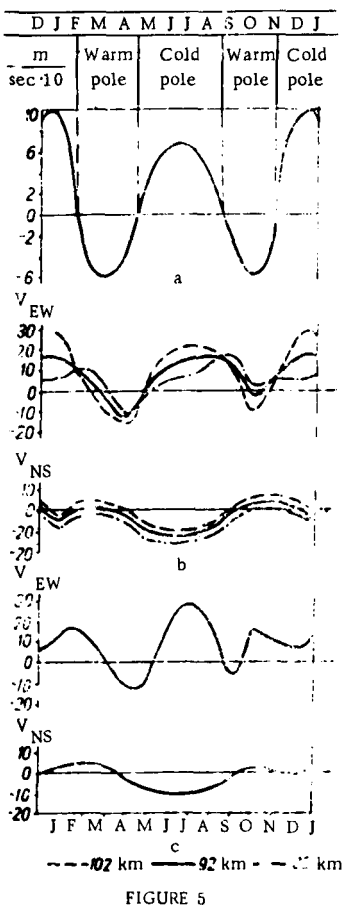

FIGURE 5

Month	Jan	Feb	March	April	May	June
Phase, hrs	2.9	2.2	3.1	3.8	3.9	2.2

The 8- and the 6-hour components are substantially smaller than the 12- and the 24-hour ones. For some months they are virtually negligible. The smooth curves in Figure 2 are a superposition of the constant component and three harmonics.

How are we to interpret the observed winds and their constant year-to-year recurrence? Theoretical analysis requires reliable data on the temperature at various points of the world, at various heights, and in different seasons. Unfortunately, no such data are available. The data for the range of heights from ~ 70 km (the range of meteorologic rockets) to ~ 200 km (the low of the satellite orbits) are particularly sparse /7/. The data for the meteor zone are unreliable.

The meteor zone is a sort of a transition layer between the mesosphere and the thermosphere. This zone is characterized by dissipation of oxygen, instability of temperature, high turbulence. Kellog /6/ developed a theory according to which a seasonal march of temperature should occur in the meteor zone above the pole. This possibly applies to lower latitudes also. Proceeding from this assumption, and also

applying the results on the height variation of the drift of meteor trains (Figure 5, b) and on velocity gradients (Figure 5, a), Kochanski proposed a model for the circulation in the upper atmosphere /8/. Seeing that the winds in the meteor zone are geostrophic, we can actually deduce from the Manchester (Figure 5, b) and Khar'kov (Figure 5, c) measurements that the temperature above the pole reaches a relative low from November to February and from May to August. The curve of the vertical velocity gradient has a six-month period, with maxima in winter and summer. The zonal components in Manchester and Khar'kov also vary in a six-month cycle (but the first minimum occurs in April—May, or in March in the case of the velocity gradient). The six-month variation of the N—S component is indistinct.

The enormous (relative to ground conditions) amplitude of the 12-hour component in the meteor zone may be attributed to resonance phenomena /9/. Resonance oscillations are produced by the sun. Calculations show that, in the light of modern motions on the vertical distribution of temperature, the period of resonance oscillations does not differ much from the 12-hour period (being approximately equal to 12.7 hrs).

The program scheduled for the International Year of the Quiet Sun will greatly advance our knowledge of the processes in the upper atmosphere.

BIBLIOGRAPHY

1. KASHCHEEV, B. L., V. N. LEBEDINETS, and M. F. LAGUTIN.—In: "Meteory", Vol. 1, p. 25. Izdatel'stvo Khar'kovskogo Universiteta. 1960.
2. KASHCHEEV, B. L., and I. A. DELOV.—DAN UkrSSR, Vol. 7:67. 1964.
3. KASHCHEEV, B. L. et al.—In: "Meteory", Vol. 1, p. 3. Izdatel'stvo Khar'kovskogo Universiteta. 1960.
4. ELFORD, W. G.—Planetary Space Sci., Vol. 1:94, 1959.
5. GREENHOW, J. S., E. L. NEUFELD.—Quart. Royal Meteorol. Soc., Vol. 87:472. 1961.
6. KELLOG, W. W.—J. Meteorol., Vol. 18:373. 1961.
7. KOCHANSKI, A.—J. Geophys. Res., Vol. 68:213. 1963.
8. Transactions of the International Symposium on Fluid Mechanics in the Ionosphere.—J. Geophys. Res., Vol. 64:2042. 1959.
9. WILKES, M. V.—Proc. Roy. Soc., Vol. 271:44. 1963.

N67 15452

E. N. Kramer

SOME PROBLEMS OF THE THEORY AND NEW METHODS OF OBSERVATION OF METEORS

One of the most topical problems of meteor astronomy is the investigation of the nature and the distribution of meteor matter. Of particular interest is meteor matter whose origin is connected with comets. Meteor particles of this class are now universally regarded as possessing a loose structure. This structural peculiarity is held responsible for the hypothetical fragmentation of meteors. Indirect evidence of fragmentation /1—3/ was obtained by comparing the results of observations with the theory developed for a single nonbreaking meteor body. In the following we consider one of the criteria of meteor fragmentation.

1. The fundamental equations of the physical theory of meteors

$$mj = -\Gamma S \rho v^2, \tag{1}$$

$$\frac{dm}{dt} = -\frac{\Lambda}{2Q} S \rho v^3, \tag{2}$$

$$I = -\frac{t_0}{2} v^3 \frac{dm}{dt} \tag{3}$$

in the case of an isothermal atmosphere

$$\rho = \rho_0 e^{-\frac{h}{H}} \tag{4}$$

and assuming an effective cross section

$$S = Am^{2/3}, \tag{5}$$

can be written in the form /4—6/

$$j = \frac{3}{2} j_M e^{-\frac{h-h_M}{H}} \left[1 - \frac{1}{3} e^{-\frac{h-h_M}{H}}\right]^{-1} \frac{v^2}{v_M^2}, \tag{6}$$

$$m^{1/3} = m_\infty^{1/3} \left[1 - \frac{1}{3} e^{-\frac{h-h_M}{H}}\right], \tag{7}$$

$$I = \frac{9}{4} I_M e^{-\frac{h-h_M}{H}} \left[1 - \frac{1}{3} e^{-\frac{h-h_M}{H}}\right]^2. \tag{8}$$

Here v, j, m, I are, respectively, the velocity, the acceleration, the mass, and the "visual intensity of radiation" /7/ at the height h; Γ, Λ, and t_0 are the drag, the heat-transfer coefficient, and the luminous efficiency; the subscript «м» is attached to quantities at the point of maximum emission, where

$$I_м = \frac{\Lambda\tau_0}{4Q} A m_м^{1/3} v^6 \rho_м, \tag{9}$$

$$\rho_м = \frac{3Q m_м^{1/3} \cos z}{AH\Lambda v_м^2}; \tag{10}$$

m_∞ is the initial mass of the meteor particle, z the zenith distance of the radiant, Q the latent heat of evaporation.

From equation (6) we can easily find the following relation for the extra-atmospheric velocity:

$$v_\infty = v_м\left(1 - \frac{2}{3}\frac{j_м H}{v_м \cos z}\right). \tag{11}$$

On the other hand, the velocities obtained in observations are generally interpolated by the formula

$$v = B + ce^{kt}, \tag{12}$$

where B is essentially the extra-atmospheric velocity v_∞ measured by some hypothetical direct means. Comparing the velocity v_∞ obtained from observations with the theoretical figure, we can judge to what extent the theory checks /5/. The deceleration index k is calculated directly from observations, and its theoretical value is easily found from (11) and (12):

$$k_{\text{theor}} = -\frac{j_м}{v_\infty - v_м} = \frac{3}{2}\frac{v_м \cos z}{H}. \tag{13}$$

Comparison of k_{theor} with k from Odessa and Harvard observations /8/ shows that k_{theor} increases with increasing k, but the deceleration index k calculated directly from observations is almost invariably somewhat greater than the theoretical figure k_{theor} /5/.

The energy radiated by the meteor between some initial height h_i and the final height h_f can be calculated from /9/

$$E'_{if} = \frac{9}{4} I_м \frac{H}{v \cos z}\left\{\left[1 - \frac{1}{3}e^{-\frac{h_i - h_м}{H}}\right]^3 - \left[1 - \frac{1}{3}e^{-\frac{h_f - h_м}{H}}\right]^3\right\}; \tag{14}$$

this formula is easily obtained by taking the integral of (8). In an isothermal atmosphere, meteors should theoretically appear at $h_i = \infty$. They vanish where

$$1 - \frac{1}{3}e^{-\frac{h_f - h_м}{H}} = 0.$$

Hence, the total visual energy radiated by a meteor is

$$E_{if} = \frac{9}{4} I_{\mu} \frac{H}{v \cos z}. \qquad (15)$$

Formula (14) is more convenient for comparison with observations, since it is not burdened by errors connected with the uncertainty in the sensitivity threshold of the photographic emulsion. However, measurements show that E_{if} calculated from (15) are but slightly greater than E'_{if} from (14).

Photographic observations of meteors make it possible to compare the actual luminosity curve with the theoretical function defined by equation (8). To evaluate numerically the agreement (or otherwise) between the observed and the theoretical curves, Levin /2/ introduced a parameter F, equal to the ratio of the measured and the theoretical trail lengths. We applied a somewhat different parameter, comparing the observed and the theoretical luminosity curves.

Let ε_{if} be the visual energy of radiation read off the observed curve. We can calculate the ratio

$$\Pi = \frac{E_{if} - \varepsilon_{if}}{E_{if}}. \qquad (16)$$

For most meteors $\Pi < 1$. The numerical values of Π cluster around $0.5 - 0.6$.

Π can be attractively interpreted as the luminosity deficit of the meteor: numerically, Πm_{∞} is equal to the so-called "residual luminous" mass. However, the I_{μ} in (14) and (15) (which have been obtained assuming (5)) corresponds to a real meteor, which may break up into a swarm of fragments. The concept of the residual luminous mass and the implied suggestion of a continuously evaporating meteor particle are not necessarily consistent with observations. Photographic methods in current use do not resolve the ambiguity surrounding the question of meteor fragmentation.

2. One of the shortcomings of the modern methods of meteor photography /10, 11/ is that the negative shows the trail produced by a flying meteor, but not the meteor itself (to use Astapovich's terminology /12/, this is a photometeor). The image of the meteor is absolutely indistinguishable. A shutter interposed in front of the objective (or elsewhere in the path of the light beam) cuts the photographic trail into separate streaks, so that if the shutter frequency is known, the velocity and the deceleration of the meteor can be calculated. A certain blurring of the gaps between the streaks is often observed in these photographs, which possibly points to a considerable linear size of the meteor. A meteor, having negligible breadth, often consists of a bright head and a comparatively faint tail. It is highly important to establish whether the tail is a manifestation of the afterglow of atoms and molecules or a column of glowing atoms escaping from the surface of the crushed dust particles. The length of the tail is variously estimated as ranging from several tens of meters to more than a kilometer.

The optics of the photographic equipment resolves objects whose linear size at a distance of $100 - 150$ km is greater than $20 - 50$ m. With a one

millisecond exposure, even a meteor moving with the velocity of 60—70 km/sec will have covered a distance much smaller than the linear size of some meteors. The meteor path will lie on the resolution threshold of the equipment. Working with sufficiently small exposures (the method of instantaneous exposure), we may hope to obtain a "pure" image of a meteor. The corresponding exposures should be as small as 10^{-3}—10^{-4} sec. Photographs taken by the method of instantaneous exposure will enable us to follow the formation and the development of the meteor tail.

It is noteworthy that the break-up of a meteor into comparatively large fragments is almost undetectable with long-focus equipment. First, increasing the focal distance generally narrows the angle of the equipment, so that the odds of photographing a meteor are reduced. Second, the transverse distance between the fragments lies below the resolving power of the objective even with focal distances of one or possibly two meters. The longitudinal separation of the fragments increases in time owing to differences in drag resistance and eventually the fragments become resolvable in principle; however, with ordinary photographic techniques, the successive images of the fragments are superimposed on one another, and the individual fragments are impossible to distinguish. The method of instantaneous exposure enables us to distinguish between the different fragments, to study their motion, and to calculate their respective masses.

The application of the method of instantaneous exposure in meteor photography does not involve any fundamental difficulties, since the method is a common one in other fields of study. However, the following points must be borne in mind when photographing meteors.

A. We never know in advance where and when a meteor will appear. The photographic equipment should therefore be designed for continuous operation over lengthy time intervals. The high-speed shutter will be tripped a great many times during each clear night. This obviously imposes certain requirements on the shutter design.

B. The instantaneous image of the meteor is aligned in the direction of its flight. Successive instantaneous images should therefore be appropriately spaced on the photographic record, to prevent overlapping. A technique approaching high-speed filming could be applied, but this is not easily feasible.

C. With ordinary photographic techniques, the meteor is allowed to produce a certain integrated effect on the emulsion. With instantaneous exposure, however, it covers a certain limited area and the photographic density correspondingly decreases. Furthermore, the bright-up background is also fainter, and the comparison stars are not as strong as could be desired.

All the preceding imposes certain requirements on the equipment design and on the actual technique of photographing meteors. Several methods of instantaneous meteor photography can be proposed.

A'. A fairly large disk is made to rotate in front of the objective. The disk is provided with a slit, whose width corresponds to the light cone of the objective (in practice, the slit is somewhat larger than the front lens diameter). If the distance of the light-admitting aperture from the center of the disk is R, and the radius of the aperture r, the effective exposure is given by $\eta = \frac{r}{\pi R \mu}$, where μ is the number of revolutions per second. The time between two successive photographs is $1/\mu$ sec. With meteor speeds

of 60 km/sec and linear dimensions $l = 1$ km, we must have $\mu \approx 50$ (the successive images of the meteor will not overlap). With an objective diameter $2r = 50$ mm and exposure of 10^{-3} sec, the disk radius may be as small as 320 mm. For larger apertures, the disk becomes proportionately larger, making the equipment unwieldy.

B'. Two moving grids are interposed in front of the objective, with alternating transparent and opaque bands. The grids can be easily made to move in a pattern ensuring an exposure of less than a millisecond and a spacing of 0.05—0.02 sec between successive photographs. This shutter instantaneously exposes the entire negative, which is advantageous for spectrographic investigation of meteors. The deficiencies of the technique are obvious: only 50% of the effective aperture is utilized, and the high accelerations applied to the shutter components limit the durability of the system.

C'. A new photographic camera is being used at the Odessa Astronomical Observatory, provided with special focal obturators interposed directly in front of the plate. A disk with one or two narrow slits (5 or 10° wide) rotates near the focal surface. With obturator velocities of 25—50 rev/sec, exposures close to 1/900—1/1800 sec are obtained. The stars and the background come out attenuated by a few stellar magnitudes, so that the camera is left running for several nights and a single negative is kept for some 20 hours.

A similar setup is now being assembled at the Tadzhik Astrophysical Institute.

Another system, utilizing electron-optical converters to photograph meteors, is in the design stage at the Odessa Astronomical Observatory. With this system it will be possible to photograph comparatively weak meteors, on the one hand, and to achieve instantaneous exposure with much less effort, on the other, since electric and magnetic (nonmechanical) signal modulation can be applied. Furthermore, the introduction of electron-optical converters will broaden the spectral range where meteors can be studied.

3. A highly topical problem is that of meteor-cometary relations. This is not only of theoretical significance: with the development of astronautics, the connection of meteor streams with comets continuously gains in importance. Nothing is known at present on the meteor hazards of interplanetary space. Comets, as it has been most convincingly demonstrated by S. K. Vsekhsvyatskii, are highly ephemeral formations. Once a comet has disintegrated, a meteor swarm follows its orbit for some time, and is gradually converted into a meteor stream. The region encompassed by the swarm or the stream presents the highest meteor hazard. Since at least in the first stages the trajectories of space ships will lie near the plane of the ecliptic, it is only natural to regard the intersection of the cometary orbits with this plane (the orbital nodes) as points of maximum meteor hazard. Anyhow, these points are of some interest in the investigation of meteor-cometary relations.

Table 1 lists the heliocentric coordinates for the nodes of all the cometary orbits meeting the plane of the ecliptic at distances of from 0.5 to 2 A.U. The second column gives the standard notation of the comet; the names of the periodic comets are also given (the abbreviations are expanded in the index, Table 2). The third column lists the node longitude (1950.0), and the fourth column gives the heliocentric distance of the node.

TABLE 1. Heliocentric ecliptic coordinates of the nodes of cometary orbits

No.	Comet	l_0	R_0	No.	Comet	l_0	R_0
1	−467 Halley	60.7	1.728	35	1145 Halley	51.1	1.588
		240.7	0.898			231.1	0.939
3	−240 Halley	57.6	1.722	36	1222 Halley	52.2	1.591
		237.6	0.898			232.2	0.938
4	−163 Halley	56.5	1.722	37	1231	203.5	1.248
		236.5	0.898	38	1240	134.4	0.712
5	−137 Borrelly II	249.1	1.018	39	1264	330.5	0.852
6	− 87 Halley	56.4	1.722	40	1299	116.2	0.835
		236.4	0.898			296.2	0.514
7	− 64	13.2	0.849	41	1301 Halley	53.1	1.618
8	− 12 Halley	55.4	1.683			233.1	0.905
		235.4	0.908	42	1337	281.6	0.828
9	+ 66 Halley	55.3	1.635	45	1366	46.6	0.991
		235.3	0.883	46	1378 Halley	55.3	1.628
10	141 Halley	54.2	1.683			235.3	0.886
		234.2	0.909	47	1385	96.4	0.784
11	218 Halley	54.2	1.683	48	1402	124.6	0.773
		234.2	0.909			304.6	0.747
12	240	212.9	0.653	51	1456 Halley	50.7	1.518
		32.9	0.864			230.7	0.915
13	295 Halley	54.1	1.683	52	1457 I Crom.	76.5	0.715
		234.1	0.909	53	1457 II	11.3	0.762
14	374 Halley	54.0	1.683	54	1468	77.8	1.232
		234.0	0.909	55	1472	292.6	1.633
15	451 Halley	53.4	1.703			112.6	0.692
		233.4	0.903	56	1490	115.2	0.899
16	530 Halley	52.8	1.683	57	1499	332.8	1.040
		232.8	0.909	58	1500	316.3	1.444
21	607 Halley	52.7	1.683	59	1506	139.1	1.446
		232.7	0.909			319.1	0.527
22	684 Halley	52.7	1.683	60	1531 Halley	51.3	1.499
		232.7	0.909			231.3	0.921
23	760 Halley	53.1	1.664	61	1532+	93.2	0.544
		233.1	0.914	62	1533	305.1	0.571
24	770	105.4	1.142			125.1	0.765
		285.4	1.278	63	1556	180.7	1.210
25	837 Halley	52.5	1.655			0.7	0.826
		232.5	0.894	64	1558	340.5	1.111
26	868	320.4	0.749	66	1580	24.3	1.191
		140.1	0.957			204.3	1.219
27	912 Halley	53.5	1.694	68	1585	42.8	1.166
		233.5	0.883	69	1590	170.6	0.705
28	962	9.5	0.939	71	1596	335.3	0.752
		189.5	1.254	72	1607 Halley	53.5	1.614
29	989 Halley	56.6	1.747			233.5	0.901
		236.6	0.858	73	1618 I	298.0	0.538
30	1006	51.2	1.242	74	1618 II	80.4	0.600
		231.2	1.099			260.4	1.110
31	1066 Halley	50.9	1.558	75	1652	92.3	1.128
		230.9	0.925	77	1664	85.2	1.243
32	1092	137.6	0.998	80	1672	122.0	1.042
33	1097	39.4	0.939	81	1677	240.6	0.668
34	1132	32.5	1.041	82	1678 de V.—S.	347.1	1.174

TABLE 1. (Continued)

No.	Comet	l_0	R_0	No.	Comet	l_0	R_0
83	1680	95.9	0.931	132	1783	58.0	1.462
84	1682 Halley	54.9	1.685	133	1784	59.1	0.800
		234.9	0.869	134	1785 I	86.5	1.203
85	1683	177.1	1.078	135	1785 II	247.0	0.532
		357.1	1.164	138	1787	109.1	0.829
86	1684	271.9	1.025			289.1	0.602
87	1686	357.7	0.589	139	1788 I	159.2	1.387
		177.7	0.782	140	1788 II Hr. - Rig.	354.7	0.813
90	1698	249.4	0.777	141	1790 I	355.1	1.057
91	1699	145.2	1.122	142	1790 II Tuttle I	90.8	1.099
92	1701	122.2	0.603	143	1790 III	215.4	1.070
93	1702	192.4	0.789	144	1792 I	13.0	1.360
94	1706	16.6	0.566	145	1792 II	105.5	1.050
		196.6	1.738	146	1793 I	110.4	1.624
95	1707	56.2	0.909			290.4	0.537
96	1718	131.2	1.028	149	1796	199.2	1.582
97	1723	17.4	1.064	150	1797	331.4	0.900
99	1737 I	229.3	0.534			151.4	1.269
100	1737 II	315.1	1.017	152	1798 II	71.6	0.857
101	1739	210.4	1.808	153	1799 I	101.6	1.868
		30.4	1.073			281.6	1.526
102	1742 G. - M.	188.3	0.828	154	1799 II	108.9	0.725
103	1743 I	89.8	0.864	156	1802	312.3	1.135
104	1743 II	188.9	0.704	157	1804	178.8	1.138
106	1746	162.9	1.006	159	1806 I Biela	73.3	0.998
108	1748 I	235.7	0.860	160	1806 II	144.4	1.272
109	1748 II	216.0	0.886	161	1807	268.8	0.647
110	1757	216.9	0.689	162	1808 I	324.9	1.083
		36.9	0.661			144.9	0.609
112	1759 I Halley	56.5	1.747	163	1808 II	206.2	0.731
		236.5	0.857	164	1810+	130.8	1.364
113	1759 II	142.3	1.500	165	1811 I	142.4	1.461
		322.3	1.720	166	1811 II	95.0	1.857
114	1759 III	82.5	1.270	167	1812 Pons-Brooks	74.9	0.799
115	1762	171.2	1.411	168	1813 I	62.5	0.704
116	1763	359.0	0.972	169	1813 II	224.6	1.275
		179.0	1.021	170	1815 Olbers	85.4	1.691
117	1764	122.7	1.492	172	1818 I Crom.	71.3	0.759
		302.7	0.884	173	1818 II	252.3	1.736
118	1766 I	246.7	1.247	174	1818 III	91.8	0.864
		66.7	0.850	177	1819 III P. - W.	295.0	0.791
120	1769	357.6	1.723	178	1819 IV	79.3	0.898
121	1770 I	314.5	0.771	180	1822 I	179.2	0.513
122	1770 II	111.2	1.270	182	1822 III	279.5	0.880
		291.2	0.904	183	1822 IV	274.5	1.145
123	1771	30.4	1.460	185	1824 I	236.1	0.623
124	1772 Biela	79.7	1.058	186	1824 II	281.0	1.939
125	1773	123.6	1.329	187	1825 I	201.9	1.389
126	1774	3.2	1.662	188	1825 II	14.7	0.884
127	1779	27.5	0.972	191	1826 I Biela	73.2	0.994
129	1780 II	144.4	1.386	194	1826 IV	45.7	0.865
		324.4	0.820	196	1827 I	6.3	0.540
130	1781 I	265.4	0.810	197	1827 II	319.2	0.827
131	1781 II	79.7	1.299	200	1830 I	208.0	0.924

TABLE 1. (Continued)

No.	Comet	l_0	R_0	No.	Comet	l_0	R_0
203	1832 II	254.1	1.239	268	1855 IV	52.9	1.349
204	1832 III Biela	69.9	0.987	269	1857 I	134.5	1.014
205	1833	325.1	1.103	270	1857 II Brorsen I	103.1	0.629
		145.1	0.802	272	1857 IV	22.1	0.747
206	1834	228.2	0.625	273	1857 V	196.3	0.716
209	1835 III Halley	56.8	1.751	274	1857 VI	320.6	1.011
		236.8	0.861	275	1857 VII d'Arrest	329.8	1.172
211	1840 I	121.5	0.948	276	1858 I Tuttle I	90.3	1.078
		301.5	1.780	277	1858 II P. - W.	294.8	0.785
212	1840 II	58.4	1.273	278	1858 III Tuttle II	176.4	1.197
213	1840 III	7.6	0.859	279	1858 IV	326.3	1.287
214	1840 IV	70.5	1.748			146.3	0.943
216	1842 II	209.3	1.985	280	1858 V Faye	31.0	1.732
		29.3	0.729	281	1858 VI	346.6	0.709
219	1843 III Faye	31.0	1.730	282	1858 VII	341.1	1.493
220	1844 I de V. - S.	65.3	1.755	284	1859	178.6	0.508
221	1844 II	33.1	0.922	285	1860 I	145.3	1.284
223	1845 I	158.2	1.278	286	1860 II	10.1	1.491
224	1845 II	168.6	1.319	287	1860 III	265.9	0.758
225	1845 III	339.3	0.644	288	1860 IV	46.1	0.818
		159.3	1.063	289	1861 I	211.2	1.001
227	1846 I	112.6	1.538	290	1861 II	280.2	0.881
228	1846 II Biela	67.4	0.969	291	1861 III	146.3	1 0.893
229	1846 III Brorsen I	104.1	0.658	293	1862 II	327.8	1.039
230.	1846 IV Vico-Skj.	79. 0	0.672	294	1862 III	318.7	1.018
232	1846 VI	261.8	1.571	295	1862 IV	177.0	0.982
233	1846 VII	263.3	1.516	296	1863 I	118.1	1.253
		83.3	1.079	297	1863 II	252.5	1.069
234	1846 VIII	6.1	1.785	298	1863 III	251.4	0.804
		186.1	1.554	299	1863 IV	98.7	0.707
238	1847 IV	78.2	1.895	300	1863 V	125.9	1.076
239	1847 V Br. - Mt.	132.3	0.594	302	1864 I	176.2	0.635
240	1847 VI	192.3	0.590	303	1864 II	276.4	0.970
		12.3	0.744	304	1864 III	213.0	1.157
241	1848 I	213.0	0.759	305	1864 IV	24.4	1.044
		33.0	0.553	306	1864 V	162.1	1.115
243	1849 I	36.6	1.019	309	1866 I	52.6	0.982
244	1849 II	204.0	1.262	310	1866 II Faye	30.9	1.720
245	1849 III	212.0	1.153	311	1867 I Coggia	79.6	1.578
246	1850 I	274.3	1.081	312	1867 II Tempel I	292.3	1.735
247	1850 II	207.4	0.780	314	1868 I Brorsen I	102.4	0.606
248	1851 I Faye	30.9	1.738	315	1868 II	233.3	0.725
249	1851 II d'Arrest	329.8	1.175	317	1869 I	294.7	0.798
250	1851 III	225.1	1.880	318	1869 II	132.6	1.237
253	1852 II	318.6	1.008	319	1869 III T. - S.	117.9	1.489
254	1852 III Biela	67 2	0.975	320	1870 I	322.9	1.035
255	1852 IV Westphal	347.6	1.600	321	1870 II	14.1	1.820
256	1853 I	70.9	1.982	322	1870 III d'Arrest	327.5	1.285
257	1853 II	222.3	0.935	323	1870 IV	95.9	0.787
261	1854 II	316.8	0.694			275.9	0.771
262	1854 III	349.0	1.023	324	1871 I	100.4	0.753
		169.0	1.766	325	1871 II	33.0	1.952
263	1854 IV	145.8	0.972	326	1871 III Tuttle I	90.4	1.083
266	1855 II	261.6	0.590	327	1871 IV	68.2	0.950

TABLE 1. (Continued)

No.	Comet	l_0	R_0	No.	Comet	l_0	R_0
330	1873 I Tempel I	259.8	1.808	396	1887 III	136.3	1.116
331	1873 II Tempel II	302.0	1.346	397	1887 IV	246.1	1.418
332	1873 III Faye	30.7	1.721	398	1887 V Olbers	85.4	1.668
333	1873 IV	51.7	0.806	399	1888 I	246.2	0.699
334	1873 V	177.6	1.882	401	1888 III	102.4	1.199
335	1873 VI Brorsen I	102.3	0.603	402	1888 IV Faye	30.5	1.781
336	1873 VII Crom.	70.9	0.761	404	1889 I	358.3	1.869
338	1874 II	275.2	0.942	406	1889 III	271.8	1.461
339	1874 III	299.8	0.717	407	1889 IV	287.0	1.056
340	1874 IV	36.9	1.810	408	1889 V Brooks	18.8	1.976
341	1874 V	72.6	1.878	409	1889 VI	331.3	1.847
342	1874 VI	283.0	0.519	412	1890 III	15.1	1.423
343	1875 I P. - W.	292.6	0.841			195.1	1.655
345	1877 I	188.3	0.818	414	1890 V d'Arrest	327.1	1.328
346	1877 II	317.6	1.308	415	1890 VI	281.0	1.289
347	1877 III	167.1	1.391	416	1890 VII Spitaler	45.9	1.833
348	1877 IV d'Arrest	327.2	1.322	418	1891 II Wolf I	27.2	1.597
349	1877 V	5.3	1.742	420	1891 IV	218.8	1.956
350	1877 VI	72.0	1.750			38.8	1.928
351	1878 I	283.3	1.393	421	1891 V Tempel-Swift	117.3	1.511
353	1878 III Tempel II	302.0	1.342	422	1892 I	241.7	1.075
354	1879 I Brorsen I	102.3	0.599	425	1892 IV P. - W.	284.9	0.890
355	1879 II	46.8	0.897	426	1892 V	27.2	1.442
356	1879 III Tempel I	259.8	1.807	427	1892 VI	85.3	1.504
357	1879 IV	33.4	1.803	430	1893 III	338.1	0.803
358	1879 V	268.2	1.384	431	1893 IV Finlay	53.3	1.123
360	1880 II	78.2	1.992	432	1893 V	175.7	0.822
362	1880 IV T. - S.	117.8	1.495	433	1894 I	85.2	1.314
363	1880 V	250.4	0.667	434	1894 II	207.2	1.085
364	1881 I Faye	30.6	1.781	435	1894 III Tempel II	302.0	1.352
365	1881 II	307.4	0.593	436	1894 IV de V. - S.	49.6	1.742
366	1881 III	271.9	0.771	438	1895 II	351.1	1.310
367	1881 IV	278.0	0.827	439	1895 III	83.8	1.138
368	1881 V	66.9	0.850	441	1896 I	209.6	0.585
369	1881 VI	275.1	0.904	442	1896 II Faye	30.6	1.758
372	1882 I	205.9	0.970	443	1896 III	179.0	0.566
374	1882 III	70.1	1.504	444	1896 IV	151.7	1.303
375	1883 I	99.1	1.120	445	1896 V	14.2	1.589
377	1884 I Pons-Brooks	75.0	0.797	446	1896 VI Brooks	18.8	1.984
378	1884 II	6.1	1.558	447	1896 VII Perrine	67.4	1.128
379	1884 III Wolf I	27.2	1.577	448	1897 I	267.2	1.068
382	1885 III	205.7	0.863	449	1897 II d'Arrest	327.2	1.331
383	1885 IV Tuttle I	90.6	1.077	450	1897 III	32.8	1.927
384	1885 V	263.1	1.191	451	1898 I	263.2	1.303
385	1886 I	217.3	0.805	452	1898 II P. - W.	281.6	0.927
386	1886 II	69.2	1.895	454	1898 IV Wolf I	27.2	1.607
		249.2	0.642	455	1898 V	167.6	1.560
387	1886 III	288.8	0.948	456	1898 VI	79.8	0.659
388	1886 IV	234.4	1.328	460	1898 X	277.0	0.974
390	1886 VI P. - W.	285.0	0.889	433	1899 III Tuttle I	90.6	1.070
391	1886 VII Finlay	53.4	1.136	464	1899 IV Tempel II	301.7	1.391
393	1886 IX	138.3	1.247	465	1899 V	272.9	1.802
		318.3	1.417	466	1900 I	41.1	1.394
395	1887 II	100.8	1.683	467	1900 II	328.7	1.027

TABLE 1. (Continued)

No	Comet	l_0	R_0	No.	Comet	l_0	R_0
468	1901 I Gia. - Z.	7.4	0.937	534	1914 V Tempel II	240.4	1.955
471	1902 I	232.9	0.542	536	1915 I Tempel II	301.2	1.326
472	1902 II Gr. - Skj.	224.5	0.753	537	1915 II	252.8	1.459
476	1903 III	33.8	0.500	538	1915 III P. - W.	279.9	0.976
477	1903 IV	294.2	1.675	539	1915 IV	78.2	1.712
478	1903 V Brooks	18.7	1.985			258.2	0.598
481	1904 III Tempel	301.6	1.390	540	1916 I	114.4	1.560
483	1905 II Borrelly I	77.5	1.400	541	1916 II Neujmin II	148.0	1.354
484	1905 III	158.0	1.055	542	1916 III	224.5	0.987
486	1905 V	43.6	1.254			44.5	0.839
489	1906 II	72.7	1.300	543	1916 IV	238.3	1.648
		252.7	1.629			58.3	1.386
491	1906 IV Kopff	264.3	1.733	544	1917 I	88.0	0.783
492	1906 V Finlay	53.0	1.095	545	1917 II	190.1	1.028
493	1906 VI	15.2	1.669	548	1918 II	198.3	1.118
494	1906 VII	85.4	1.220	550	1918 IV Borrelly I	77.3	1.401
496	1907 II G. - M.	189.8	0.996	551	1918 B Wolf I	27.2	1.586
497	1907 III Tuttle II	161.5	1.397	552	1919 I Kopff	264.2	1.741
498	1907 IV	143.6	0.724	553	1919 II Finlay	47.4	1.133
		323.6	1.744	554	1919 III Br. - Mt.	131.3	0.591
499	1907 V	55.2	1.392	555	1919 IV Sch.	91.1	1.335
501	1908 II Tempel-Swift	110.9	1.499	556	1919 IV	301.4	1.118
502	1908 III	283.7	0.950	557	1920 I	316.0	0.534
503	1909 I Borrelly	306.2	0.844			136.0	0.673
504	1909 II P. - W.	279.9	0.977	558	1920 II Tempel II	301.2	1.324
505	1909 III Perrine	62.9	1.185	559	1920 III	108.2	1.181
506	1909 IV	71.6	1.383	560	1921 I	246.4	1.932
507	1910 I	269.3	1.152	561	1921 II	268.7	1.409
508	1910 II Halley	57.8	1.799	562	1921 III P. - W.	278.5	1.047
		237.8	0.851	564	1921 V Neujmin II	148.0	1.354
510	1910 IV d'Arrest	326.9	1.273	565	1921 VI	94.9	0.810
511	1910 V Faye	26.8	1.689	566	1922 I Gr.-Skj.	215.9	0.890
512	1911 I Brooks	18.8	1.989	568	1923 I	82.3	1.681
513	1911 II	338.0	1.014	569	1923 II d'Arrest	323.9	1.355
515	1911 IV	89.3	0.886	570	1923 III	47.1	1.241
516	1911 V	293.5	0.518	572	1924 II	80.4	0.581
517	1911 VI	215.7	1.029			260.4	1.350
518	1911 VII Sch.	94.2	1.409	575	1925 II	318.4	1.228
519	1911 VIII Borrelly I	77.4	1.407	578	1925 V Tempel II	301.2	1.317
520	1912 I Wolf I	27.2	1.592	579	1925 VI Faye	26.6	1.650
521	1912 II	117.6	0.753	582	1925 IX Borrelly I	77.4	1.393
522	1912 III	324.3	1.896	583	1925 X Brooks	355.8	1.884
523	1912 IV Tuttle I	90.2	1.083	585	1925 XII	321.1	0.961
524	1913 I	303.4	0.701	586	1926 I	136.4	1.454
		123.4	0.971	587	1926 II Kopff	264.3	1.733
525	1913 II	315.6	1.820	589	1926 IV Tuttle I	90.1	1.084
526	1913 III	348.4	1.548	590	1926 V Finlay	45.6	1.169
527	1913 IV	337.9	1.851	591	1926 VI Gia. - Zin.	16.3	0.998
528	1913 V Gia. - Zin.	16.4	0.980	592	1926 VII	289.0	0.883
529	1913 VI Westphal	347.3	1.605	593	1927 I Neujmin II	148.0	1.352
530	1914 I	33.2	1.955	594	1927 II	199.1	1.280
		213.2	0.752	595	1927 III Comas Solá	65.9	1.925
531	1914 II	199.4	1.837	597	1927 V Gr. - Skj.	215.9	0.894
533	1914 III	0.9	1.416	598	1927 VI Gale	247.4	1.287
		180.9	1.437	599	1927 VII P. - W.	278.5	1.045

TABLE 1. (Continued)

No.	Comet	l_0	R_0	No.	Comet	l_0	R_0
600	1927 VIII Sch.	90.9	1.342	677	1941 VIII	256.7	1.619
601	1927 IX Vico-Skj.	257.6	1.101			76.7	1.905
602	1928 I Reinmuth	125.2	1.867	679	1942 II	171.6	1.346
604	1928 III	197.1	1.009	681	1942 IV	160.1	1.674
605	1928 IV Crom.	70.4	0.759	682	1942 V Gr. - Skj.	215.4	0.857
609	1930 I	147.8	1.189	686	1942 IX Coggia	78.5	1.596
		327.8	1.074	687	1943 I	100.0	1.531
610	1930 II	359.3	0.699	689	1943 III d'Arrest	323.6	1.389
611	1930 III	90.6	0.572	690	1943 IV Daniel	70.4	1.530
613	1930 V	278.6	1.298	691	1943 V Sch.	86.9	1.420
614	1930 VI	257.1	1.081	693	1944 II Comas Solâ	65.7	1.921
615	1930 VII	229.6	0.560	694	1944 III	202.4	1.940
		49.6	1.503	697	1945 II	178.7	1.272
616	1930 VIII	301.1	1.321	698	1945 III	254.3	1.700
617	1931 I	347.6	1.545	699	1945 IV P. - W.	274.5	1.166
619	1931 III	191.6	1.182	700	1945 V Kopff	253.0	1.579
622	1932 I	212.8	1.612	701	1945 VI	325.4	1.960
623	1932 II Gr. - Skj.	215.8	0.909	704	1946 II	301.3	1.060
624	1932 III Kopff	264.2	1.723	705	1946 III Tempel II	299.4	1.402
625	1932 IV Borrelly I	77.3	1.389	706	1946 IV Brooks II	257.7	1.902
626	1932 V	344.8	1.162	707	1946 V Gia. - Zin.	16.2	1.000
627	1932 VI	215.4	1.241	708	1946 VI	237.6	1.505
629	1932 VIII Brooks	357.7	1.893	709	1946 VI+	326.2	1.879
630	1932 IX Faye	26.5	1.653	711	1947 II Gr. - Skj.	215.4	0.854
631	1932 X	77.9	1.227	712	1947 III	142.3	1.920
632	1933 I	131.8	1.164	713	1947 IV	353.2	0.720
633	1933 II P. - W.	276.9	1.110	714	1947 V	232.2	1.410
634	1933 III Gia. - Zin.	16.2	1.004	718	1947 IX Faye	26.3	1.702
635	1933 IV	290.9	1.028	719	1947 X	134.6	0.820
636,	1933 V	8.8	0.989	722	1947 XIII Wirtanen	86.3	1.672
640	1935 I	91.7	0.832	723	1948 I	270.7	0.755
641	1935 II Reinmuth	125.2	1.865	726	1948 IV	23.1	1.550
643	1935 IV Comas Solâ	65.9	1.933	734	1948 XII Honda-Mrkos	53.0	0.558
645	1936 II	314.1	1.187	735	1948 XIII Neujmin I	347.1	1.565
646	1936 III	264.1	0.610	738	1949 III	278.6	1.472
647	1936 IV	344.2	1.492			98.6	1.431
649	1937 I Daniel	70.3	1.540	740	1949 V	135.5	1.970
651	1937 III Gr. - Skj.	215.6	0.909	743	1950 II d'Arrest	323.6	1.380
653	1937 V	238.5	1.215	746	1950 V Daniel	69.7	1.469
655	1938 I Gale	247.2	1.256	748	1950 VI	124.7	1.481
656	1939 I	108.8	0.724	750	1951 II	310.5	1.056
657	1939 II Kopff	264.1	1.865	752	1951 IV Tuttle II	165.6	1.218
658	1939 III	311.4	1.042	754	1951 VI P. - W.	274.4	1.165
		131.4	1.070	755	1951 VII Kopff	253.0	1.579
660	1939 V P. - W.	276.8	1.110	756	1951 VIII Tempel II	289.4	1.400
661	1939 VI Hr. - Rig.	355.1	0.799	757	1951 IX	127.9	1.490
662	1939 VII Brooks II	177.7	1.901	759	1952 II	76.2	1.490
665	1939 VII Tuttle I	89.8	1.077			256.2	1.470
666	1940 I Gia. - Zin.	16.2	1.000	760	1952 II	74.3	1.603
667	1940 II Faye	26.4	1.701	761	1952 III Sch.	86.4	1.418
671	1941 II	148.6	1.115	762	1952 IV Gr. - Skj.	215.4	0.857
673	1941 IV	42.3	1.614	763	1952 V	301.8	1.409
		222.3	1.541	765	1952 VII Comas Solâ	62.9	1.931
676	1941 VII	229.6	1.754	766	1953 I	40.8	1.682

TABLE 1. (Continued)

No.	Comet	l_0	R_0	No.	Comet	l_0	R_0
767	1953 II	162.9	1.216	783	1954 XI Wirtanen	86.5	1.653
768	1953 III	95.2	1.898	784	1954 XII	254.9	1.180
769	1954 IV Borrelly I	76.2	1.456	785	1954 XIII	145.6	1.840
770	1953 V Brooks II	357.7	1.889	787	1955 II	20.2	1.691
771	1953 VI	316.6	1.838	788	1955 III	48.5	0.585
772	1953 VII Finlay	45.4	1.155	789	1955 IV	302.8	1.450
775	1954 III Honda-Mrkos	53.1	0.557	790	1955 V	338.8	0.885
776	1954 IV	329.3	1.947	792	1955 VII Perrine I	62.6	1.162
777	1954 V	297.2	1.658	797	1956a Olbers	85.4	1.621
778	1954 VI Pons-Brooks	76.2	0.753	799	1956 Crom.	70.4	0.757
779	1954 VII	122.2	0.677	800	1957 I Tempel II	299.3	1.380
782	1954 X	182.3	0.955				

TABLE 2. Periodic comets

C	Comet	Abbr	Chronological number
1	Halley		1, 3, 4, 6, 8, 9, 10, 11, 13, 14, 15, 16, 21, 22, 23, 25, 27. 29, 31, 35, 36, 41, 46, 51, 60, 72, 84, 112, 209, 508.
3	Borrelly II		5, 503.
29	Crommelin	Crom.	52, 172, 336, 605, 799
56	de Vico-Swift	de V.—S.	82, 220, 436.
75	Grigg-Mellish	G—M.	102, 496.
96	Biela		124, 159, 191, 204, 228, 254.
114	Tuttle I		142, 276, 326, 383, 463, 523, 589, 665.
136	Pons-Brooks		167, 377, 778
112	Herschel-Rigollet	Hr.—Rig.	140, 661.
139	Olbers		170, 398, 797.
144	Pons-Winnecke	P.—W.	177, 390, 277, 425, 425, 452, 504, 538, 562, 599, 633, 660, 699.
176	Faye		219, 248, 280, 310, 364, 402, 442, 511, 579, 630, 667, 718.
183	Brorsen I		229, 270, 314, 335, 454.
184	de Vico-Skjellerup	Vico-Skj.	230, 601.
193	Brorsen-Metcalf	Br.—Mt.	239, 554.
201	d'Arrest		249, 275, 322, 414, 449, 510, 569, 689, 743.
205	Westphal		255, 529.
222	Tuttle II		278, 497, 752.
249	Coggia-Stephan	Coggia	311, 686.
250	Tempel I		312, 330, 356.
254	Tempel-Swift	T.—S.	319, 362, 421, 501.
262	Tempel II		353, 435, 464, 481, 536, 558. 578. 705. 756, 800.
296	Wolf I		379, 418, 454, 520, 551.
305	Finlay		391, 431, 492, 553, 590, 772.
319	Brooks II		408, 446, 478, 512, 583, 629, 662, 706, 770.
326	Comas Solá		416, 595, 643, 693, 765.
347	Perrine		447, 505, 792.
361	Giacobini-Zinner	Gia.—Zin.	468, 528, 591, 634, 666, 707.
364	Grigg-Skjellerup	Gr.—Skj.	472, 566, 597, 623, 651, 682, 711, 762.
372	Borrelly I		483, 550, 582, 625, 769.
379	Kopff		491, 519, 552, 587, 627, 657, 700, 755.
386	Daniel		506, 649, 690, 746.
393	Schaumasse	Sch.	518, 555, 600, 691, 761.
398	Neujmin I		526, 735

TABLE 2. (Continued)

C	Comet	Abbr.	Chronological number
408	Neujmin II		541, 564, 593.
439	Gale		598, 655.
440	Reinmuth		602, 641.
	Wirtanen		722, 783.
	Honda-Mrkos		734, 775.

For some comets the coordinates of two points are given, the ascending and the descending nodes, respectively. Table 2 is a list of periodic comets, indexing their chronological numbers in Table 1. This index enables easy cross-reference between the two tables. The first column in Table 2 lists the numbers of comets according to Yamamoto's catalog /15/. The node coordinates are marked on a network of polar coordinates. The trajectory of the object whose possible collision with meteor matter is being investigated is also plotted in the same coordinates. The numbers of the comets whose nodes are intercepted by the trajectory are then written out, and the problem of orbital encounter is solved. This can be done following the method of A. D. Dubyago /13/ or by other formulas, which are listed in /14/. The data of Table 1 can be fed to a computer which, given the equation of motion of the object in polar coordinates, will compute, in the first approximation, the distances of nodes from the trajectory. Second-approximation calculations require knowledge of the exact elements of the cometary orbit /15—17/. The data of Table 1 can thus be applied in new extra-atmospheric meteor research. In future one will have to compute an orbit that will carry an interplanetary station, at a small relative velocity, as close as possible to the head or the nucleus of a comet.

BIBLIOGRAPHY

1. JACCHIA, L. G. —AJ, Vol. 121:521, 1955; Smiths. Contr. to Astroph., Vol. 2:9. 1958.
2. LEVIN, B. Yu. O droblenii meteornykh tel (Fragmentation of Meteor Bodies). —AZh, Vol. 40:2, 1963.
3. McCROSKY, R. E. —Harv. Reprint, ser. 2, N 30; AJ, Vol. 63:3. 1958.
4. HAWKINS, G. S. and R. B. SOUTHWORT. —Smiths. Contr. to Astroph., Vol. 2:11, 1958.
5. VOROB'EVA, V. A. and E. N. KRAMER. —Geomagnetizm i Aeronomiya, Vol. 4:6, 1964.
6. LEVIN, B. Yu. Fizicheskaya teoriya meteorov (Physical Theory of Meteors). — Izd. AN SSSR. 1956.
7. OPIK, E. J. Physics of Meteor Flight in the Atmosphere. —Interscience Publ. Inc., N. Y. 1958.
8. JACCHIA, L. G. —Harv. Reprint, Ser. 2, N 44. 1952.
9. KRAMER, E. N. O raspylenii meteorov (Pulverization of Meteors). —Geomagnetizm i Aeronomiya, Vol. 5:1.1965.
10. WHIPPLE, F. L. —Harv. Reprint, Ser. 2, N 19. 1947.
11. KATASEV, L. A. Fotograficheskie metody meteornoi astronomii (Photographic Methods of Meteor Astronomy). — Fizmatgiz, 1957. [English translation by Israel Program for Scientific Translations, Jerusalem, 1964 (OTS 64-11021).]
12. ASTAPOVICH, I. S. Meteornye yavleniya v atmosfere zemli (Meteor Phenomena in the Earth's Atmosphere). — Fizmatgiz, 1958.
13. DUBYAGO, A. A. Opredelenie orbit (Determination of Orbits). —Fizmatgiz, 1950.
14. KRAMER, E. N. —Izvestiya Odesskoi Astronomicheskoi Observatorii, Vol. 3:163, 1953.
15. YAMAMOTO, A. S. Preliminary General Catalogue of Comets. Kyoto. 1936.
16. BALDET, F. and G. de OBALDIA. Catalogue general des orbites des comets. 1952.
17. VSEKHSVYATSKII, S. K. Fizicheskie kharakteristiki komet (Physical Characteristics of Comets). — Fizmatgiz, 1958. [English translation by Israel Program for Scientific Translations, Jerusalem, 1964 (OTS 62-11031).]

I.S. Astapovich

N67 15453

ON THE SUBJECT OF THE TRAJECTORY AND THE ORBIT OF THE TUNGUSKA COMET

INTRODUCTION

The appellation "Tunguska Comet", in view of the data on hand (see, e.g., /1/), seems to provide a more fitting description of what has been conventionally designated as the Tunguska Meteorite /2/. This suggestion was first advanced by the geophysicist F.J.W. Whipple /3/ in 1934, and then by the author in 1939 /4/. As early as 1939 the author wrote that this meteorite "is in fact a small comet" /5/, arguing that its retrograde orbital motion, considerable eccentricity of its orbit, and its large mass (over 10^4 tons) are all highly unusual in a meteorite; furthermore, the optical anomaly attendant on its fall (white nights) is attributable to dust particles of a size characteristic of cometary tails. Since 1951, when the last comprehensive review of data on the Tunguska Comet was published /2/, the major contributions to the subject have been made by K.P. Florenskii /6/ and especially by G.V. Plekhanov /7, 8/, the head of the General Independent Expedition which systematically worked through the area of the 1908 catastrophe in the years 1959—1964. Plekhanov's expedition included 73 members in 1960 and 59 in 1961; it was supported by the Siberian Branch of the USSR Academy of Sciences, and later by the Tomsk Division of the Academy of Sciences' All-Union Geographical Society. The research program of the expedition was coordinated by the Academy of Sciences' Meteorite Committee and its findings were discussed at the Meteorite Conference in Leningrad in 1962 and in Moscow in 1964. A.F. Kovalevskii examined the magnetograms of seventeen previously disregarded stations, and he found a magnetic explosion on a magnetogram of the Irkutsk Magnetic and Geophysical Observatory taken in the year 1908 /9/. V.K. Zhuravlev /10/, and also K.G. Ivanov /11/ tried to interpret this effect. The explosion apparently took place at a height of 10 ± 2 km /8, p.12/, or even as low as 5.5 km above the location $\varphi = +60°52'50''$, $\lambda = 101°55'0$ east /12/. Eyewitnesses who observed the comet's flight in the form of a fireball on 30 June 1908 are still alive, and it is urgent that they should be interrogated on the subject of the apparent fireball trajectory; the coordinates of the initial, the terminal, and the summit points of the trajectory above the horizon (the azimuth and the angular height) should be determined using a surveyor's dial or a tangent compass and an inclinometer, as is the common practice in meteorite trajectory determinations /13/. If the observer cannot give

full details (the event having occurred too far in the past or for other reasons), he should at least specify whether the fireball moved "from right to left" or "from left to right"; several accounts of this sort collected over an extensive area can be used to determine the azimuth of the trajectory's projection. Unfortunately, even this azimuth has not been determined yet, and the trajectory of the Tunguska Comet must be inferred very crudely from indirect considerations. Nevertheless, it must always be borne in mind that exact knowledge of the azimuth of the projection of the atmospheric trajectory of a comet and its inclination to the horizontal plane is all-important: if the time of flight is known, these two quantities give the position of the radiant in the equatorial system and, in the final analysis, the direction of the tangent to the comet's orbit at that time. If the velocity is also known, the heliocentric orbit of the comet can be determined.

However, "some details are apparently irretrievably lost" /14/.

FLIGHT AZIMUTH

The following data are available, bearing on the subject of the azimuth of the trajectory's projection (the fireball was observed over a large distance, and the trajectory was therefore exceptionally flat): 1) the coordinates of the points where optical phenomena were witnessed: the fireball was not observed in those locations where its trajectory was projected onto the part of the sky occupied by the sun; 2) the line of symmetry between the points where acoustical and mechanical phenomena were observed; 3) the sum total of eyewitness accounts on the direction of flight; 4) isolated observations making it possible to establish the coordinates of individual points of the trajectory and hence to derive the radiant and, consequently, the projection azimuth of the atmospheric trajectory. Voznesenskii's old data /15/ gave $a = +13°$ for the astronomical azimuth of the radiant. In a private conversation held in Leningrad in the '30's, Prof. A.V. Voznesenskii informed the author that in 1908, back in Irkutsk, while still under the immediate impression of the phenomenon, he came to the conclusion that none of the eyewitnesses doubted that the "meteorite" had actually passed from south to north over the then Central Siberia. He also added that no reports of the phenomenon had reached him from the areas to the east of Baikal, although those areas had been sufficiently densely populated. "The meteorite passed to the west from Irkutsk", said this meticulous scientist, who for 17 years would not allow publication of the data that he, as the director of the Irkutsk Magnetic and Meteorological Observatory, had obtained in 1908 for fear that his findings would be branded as fantastic; he published his information only after he had carefully collated it against the reports of the geologist S.V. Obruchev.

Voznesenskii's data on the direction of flight are confirmed by the findings of the Meteor Expedition of the Academy of Sciences which functioned as late as 1921—1922, in particular investigating "the lost Filimonovo meteorite" /16/. According to the reports of this expedition, based on the data collected in Kansk area, in Tomsk, and elsewhere, the meteorite passed in the general direction "from south to north" /17/.

This gives $a \approx 0°$. In 1930—1932, in the course of astronomical and geophysical expeditions in the basins of the rivers Angara and Lena, the author visited 27 of the 61 points mentioned by Voznesenskii and it was "clearly established that the meteorite flared up to the south from the trans-Siberian railway tracks, ... following ... a very flat trajectory" /18, p. 469/; the crude observations gave an azimuth anywhere from $a = -16°$ to $a = \pm 26°$. In /5, p. 19/, the radiant of the meteorite was calculated assuming an average azimuth $a = +10°$. If the points where detonations were heard are marked on a map (from Yenisei to Vitim and from Minusinsk to Baikal), the line of symmetry is seen to pass at $a = +3°$ /2/. The acoustical phenomena can be differentiated in terms of intensity, each being represented by an appropriate decibel value; this approach led to the charting of lines of equal loudness from 30 to 100 db. The ballistic (shock) wave which reached the earth from heights of 80-55 km somewhat distorted the concentric pattern of these isolines (centered in the area of the catastrophe, $\varphi = +60°53'$, $\lambda = 101°54'$ east), and their elongation corresponding to the projection of the trajectory gives $a = +4°$. This result is also obtained from Krinov's chart /19, pp. 28-29, Fig. 5/. Krinov himself apparently disregarded the line of symmetry and obtained $a = -43°$. Furthermore, electrophonic phenomena were recorded in six points, and the author, back in 1929, was the first to concentrate on these effects /20/, which are now being intensively studied in Europe and the USA /21—23/; the line of symmetry of these phenomena gives independently $a = +5°$. The author also treated the data on the hypergene tremor produced by the meteorite's flight; isoseisms of Rossi—Forel force IV, V, VI, VII, VIII were plotted /2, Fig. 2/, and they give the direction $a = 0°$. In a certain house near Tolstyi Mys (Baikal), some lamp-oil was spilt in the direction NNW—SSE when the tremor shook the icon-lamp there; this gives $a = -22°$.

Let us now consider the few observations from which information pertaining to the position of the apparent trajectory can be obtained.

No.	Place of observation	Observer	Position of apparent trajectory	Page in /19/
1	Znamenskoe, 270 km N of Irkutsk	L. Klykov	SW	32
2	Malyshevo, 160 km NW of Irkutsk	I. Nikol'skii	NE	
3	Kamenskoe (Kamenka)	A. Goloshchekin	"separated from the sun"	
4	Zaimskaya, 40 km SW of Kezhma*	T. Bryukhanov	NW, $h = 60°$	65
5	Kova, 85 km SW of Kezhma	S. Privalikhin	"summer sunset", $h < 45°$	57
6	Kezhma	K. Kokarin	SW to NE, $h = 45°$	51
7	Kezhma	A. Bryukhanov	Iridiscence in the trail when projected onto the solar disk	53
8	Kezhma	T. Naumenko	Projected onto the solar disk	53

* Krinov /19/ mistook this location for village Zaimka, some 190 km SW of Kezhma.

Calculations for $T_0 = 0^h16^m.2$ U.T. (the time of occurrence of the event) give $h = 27°$ and $a = -85°$ for the sun (Kezhma). There are several Znamenskoe's in the area; Krinov /19/ deals with Znamenskoe near

Yeniseisk, although there is another Znamenskoe nearer to Irkutsk, some 15 km to the northwest from Nizhneudinsk;* for the former, $h = 24°$, and Krinov's trajectory, like Voznesenskii's, passes at an unlikely height

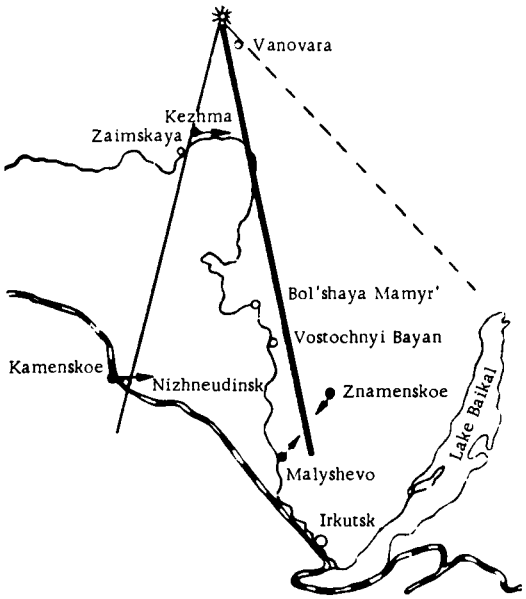

Flight trajectory of the Tunguska Comet

(270 km); in the second case, the first trajectory must be rejected, whereas the second is acceptable (75 km).

We thus have the point of the trajectory which appeared to be projected onto the solar disk in the various locations. Another point is the "ground point" of the trajectory, determined by the azimuth of the epicenter of the fallen wood area. Since the geographical position of the holocaust focus is known, the azimuth can be read off a map. The great circles of the celestial sphere through the ground point and the "sun point" for each location may give the radiant in the same coordinate system, if the observations are accurate and have been made at fairly distant locations. In our case, however, the observations are highly approximate (the azimuths of No. 4 and No. 5 are inconsistent, and the height of No. 6 is at variance with sun's height) and we shall therefore have to adopt a different approach. Observations in Nos. 1 and 2 show that the fireball trajectory passed b e t w e e n these two locations. Let us accept this conclusion for the time being, plotting the corresponding trajectory on a map. We used the standard Atlas of the USSR ("Atlas SSSR", maps 42 — 43, 1 mm to 3 km). Then from Kezhma, in the sun's azimuth, the horizontal distance to this projection is 90 km, and from Kamenskoe (Kamenka near Nizhneudinsk) the distance is 315 km; the corresponding linear heights in the atmosphere are 46 km and 154 km for the two locations; the two points are distant 225 km and 650 km from the epicenter. From these data we may plot the

* [There seems to be some confusion in the Russian original; reference to the map will immediately show that the settlement 15 km to the northwest from Nizhneudinsk is Kamenskoe, and not Znamenskoe, which is located some 300 km to the east. Unfortunately, having no access to Krinov's book /19/, we could not resolve the ambiguity.]

atmospheric trajectory, attaching a higher weight coefficient to Kezhma. The results are as follows. Since the terminal point of the trajectory did not touch the ground, but was actually located at a height of ~10 km, it must not be neglected in calculating the inclination i of the true trajectory to the horizon. For observations in Kezhma (No. 6), we have $i = 9°$, and for observations in Kamenka, $i = 13°$; this agreement is clearly more than could be expected on the basis of the primitive observations available. This seems to justify our hypothesis, i.e., the projection of the trajectory passed between Znamenskoe and Malyshevo, or actually between $a = -10°$ and $a = -4°$, as observed.

The author tends to accept an average azimuth, $a = -7°$. This trajectory easily satisfies the bulk of other observational data and, apparently, the pattern of the fallen woods also.

Acad. Fesenkov was right to observe that Krinov's conclusion concerning the flight azimuth was mainly based on the fact that in Kirensk the tail of the fireball had been observed in the vertical plane; in fact, this was the "mushroom" which, as we know now, is characteristic of any powerful explosion, and it was observed not only in Kirensk, but also in many other locations (e.g., Nizhne-Ilimsk /18, p. 481/). This phenomenon can no longer be regarded as the "tail" of the fireball, i.e., the meteor train. Furthermore, many other observations from the same area give the impression of a flat trajectory. The Teterya trading station lies precisely on the projection of the trajectory that we have just constructed; if our trajectory is true, then not one, but two "columns" must have been observed at the station — one from the explosion, another from the trail. And indeed, Obruchev /25/ actually reports that "fire columns" were observed there. In /19/, various observations contradicting Krinov's trajectory are disqualified as unreliable, although almost all of them satisfy Voznesenskii's "southern trajectory". All the foregoing forces us to reject the trajectory proposed by Krinov for the Tunguska Meteorite /19/, and leaves us with a task of reevaluating the pattern of the fallen wood.

INCLINATION

The angle i can be estimated independently on the basis of the difference between the heights of appearance and disappearance of the fireball and the length of the apparent path. Since the fireball was observed in Znamenskoe and Malyshevo, but nowhere to the south of Irkutsk, it seems to have appeared in the atmosphere somewhere near $\varphi = +54°$, $\lambda = 104°$ east, at a distance of 775 km to the SSE from the epicenter. Since the height of appearance of objects of this class has never been determined, especially not in daytime, we shall assume the limits of 100 and 150 km. Seeing that the explosion above the epicenter took place at a height of some 10 km, we find the extreme inclinations $i = 7°$ and $i = 10°.5$.

On the other hand, an independent, albeit crude, estimate of the inclination can be obtained from the fact that a dense group of settlements on River Angara (from Vostochnyi Bayan to Bol'shaya Mamyr'), where the first detonations were heard, is located approximately under the fireball's trajectory. According to Denning, the shock waves of "ordinary" detonating fireballs originate at a height of 55 km, while according to Schrödinger $3 \cdot 10^{-6}$ of the energy of the sound wave reaches us from heights of 80 km. Since the sonic boom in this case was fairly powerful, we shall

assume an upper limit of 80 km; since the distance from the southern boundary of this group of villages ($\varphi = +55°.5$) to the epicenter is 600 km, we have $\tan i = 80:600$, or $i = 7°$.

In conclusion, geometrical, geophysical, and astronomical techniques independently give $i = 7 - 13°$, or on the average some 10°.

RADIANT AND ORBIT

$0^h10^m.2$ U.T., astronomical azimuth $a = -8°$, and inclination $i = 10°$ correspond to $\alpha = 32°$ and $\delta = -18°$ (Cetus); this estimate is within the range of possible radiants of the meteorite obtained back in 1933 /18/. Parabolic heliocentric velocity corresponds to a geocentric velocity of 66 km/sec. This, as we know, is not inconsistent with observations. Furthermore, as I observed back in 1939 /5/, the theoretical radiant of comet 1874 II also lies in Cetus; this is a parabolic comet with similar orbital elements and a close value of Tisserand's constant (some −0.19). The larger comet 1874 II and the Tunguska Comet of 1908 possibly followed one orbit with a period of 34 years some time in the past, and once presumably comprised a single body.

This, as well as other questions raised in the paper, require further thorough study.

BIBLIOGRAPHY

1. FESENKOV, V. G. —Meteoritika, Vol. 20: 27—30. 1961; Vol. 21: 3—14. 1961; AZh, Vol. 38: 4. 1961.
2. ASTAPOVICH, I. S. —Priroda, No. 3: 13—23. 1951.
3. WHIPPLE, F. J. W. —Meteorol. Mag., Vol. 69: 145, July, 1934.
4. ASTAPOVICH, I. S. —AZh, 16(6): 32. 1939; Priroda, No. 6: 16. 1940; No. 4: 26. 1941.
5. ASTAPOVICH, I. S. —AZh, 16(6): 32. 1939.
6. FLORENSKII, K. P. et al. —Meteoritika, Vol. 12: 62. 1955; Vol. 19: 103—134. 1960; Geokhimiya, Vol. 3: 284—295. 1963.
7. PLEKHANOV, G. V. —Meteoritika, Vol. 24: 170—175. 1964.
8. Problema Tungusskogo meteorita (The Tunguska Meteorite), pp. 3—21. —Collection of papers published at the Tomsk University, Tomsk. 1963.
9. KOVALEVSKII, A. F. —In: "Problema Tungusskogo meteorita", pp. 187—194. Tomsk. 1963.
10. ZHURAVLEV, V. K. —In: "Problema Tungusskogo meteorita", pp. 195—197. Tomsk. 1963.
11. IVANOV, K. G. —Meteoritika, Vol. 24: 141—157. 1964.
12. ZENKIN, G. M., A. I. IL'IN, and L. F. SHIKALOV. —Paper delivered at the 10th Meteorite Conference of KMET, Leningrad, 1962.
13. ASTAPOVICH, I. S. —Meteoritika, Vol. 15: 34—35. 1958.
14. ASTAPOVICH, I. S. —AZh, 10(4): 465. 1933.
15. VOZNESENSKII, A. V. —Mirovedenie, 14(1): 25—38. 1925.
16. KULIK, L. A. —Mirovedenie, Vol. 11, No. 1(40): 74. 1921; No. 1(42): 80. 1922; No. 2(43): 143—144. 1922; No. 1(44): 6. 1923.
17. KULIK, L. A. —Izv. AN SSSR, pp. 391—410. 1922.
18. ASTAPOVICH, I. S. —AZh, 10(4): 467—486. 1933.
19. KRINOV, E. L. Tungusskii meteorit (The Tunguska Meteorite), Moskva— Leningrad. 1949.
20. ASTAPOVICH, I. S. —Mirovedenie, 18(6): 337—339. 1929.
21. ROMING, M. and D. C. LAMAR. —RAND Corporation Memorandum RM-3724—ARPO, 60 pp. California, July, 1963.
22. LAMAR, D. C. and M. ROMING. —Meteoritics, 2(2): 127—136. 1964.
23. DIGGELEN, J. V. —Hemel en Dampkring, pp. 53—60. 1964.
24. FESENKOV, V. G. —Meteoritika, Vol. 25: 163. 1964.
25. OBRUCHEV, S. V. —Mirovedenie, Vol. 14: 38—40. 1925.

I. A. Delov

N67 15454

TURBULENT MOTIONS IN THE UPPER ATMOSPHERE AT HEIGHTS OF 80—110 km ACCORDING TO RADIO OBSERVATIONS OF METEOR TRAINS

A considerable number of studies have recently dealt with the turbulent motions in the upper atmosphere at heights of 80—110 km. It has been established /1-6/ that the turbulence at these altitudes is highly complex, with distinctly anisotropic large-scale eddies. Data have been obtained on the structure of turbulence /3, 6/ and on the height /1, 6, 7/, as well as diurnal /8, 9/, variation of some parameters. Our information, however, is by no means complete, and hardly any data are available for some important relations.

In the present paper we discuss the results on turbulent motions at the height of 80—110 km obtained by radio observations of meteor trains; these observations were made at Khar'kov in 1962 according to the IGY program. A four-site coherent-pulse technique was applied. A pulse transmitter was installed in one of the sites (site B). Transmitter technical specifications: pulse power ~150 kW, pulse length ~15μsec, pulse frequency 500 c/s, transmitter wavelength ~8 m. Three sites A, B, C, were all on one east—west line, and the fourth site D was located ~9 km to the north from site B. Maximal site separation ~50 km. Transmitting antenna pointed either west or north.

The signals scattered by the meteor trains were received at the three field sites A, C, D, and also at the base B. The signals from the field sites were relayed to the base and then recorded on film. The radial velocity components could thus be measured at three distinct sections of the meteor train. The range-amplitude characteristics of the radio echo were recorded for four sections of the train.

The observations were made round the clock for 10—15 days during every month from March 1962 to January 1963. Some 200,000 wind-speed records were obtained. In 3000 cases, the reflections were recorded at no less than three "points" of the train. The analysis of the records enabled us to estimate the turbulence parameters in the meteor zone, and also to follow their vertical, seasonal, and other variations.

1. HEIGHT VARIATIONS

Base observations were mainly made in the east—west direction, so that the variation of the parameters with height was investigated for the westward direction only.

The curves of height variations were plotted proceeding from the experimental dependence /10/ of the vaporization height of meteor particles on their velocity. This dependence is shown in Figure 1 (where v is the velocity in km/hr). We plotted the vertical distribution of some turbulence parameters, and also of the mean wind velocity. Figure 2 gives the height variation of the eddy wind velocity gradient (Figure 2, a), of the rms velocity of turbulent motion (Figure 2, b), and also of the mean wind velocity (Figure 2, c). The curves were plotted from the data collected in the period between April and December 1962. Before the graphs could be actually constructed, the calculated eddy velocity gradient $\frac{\Delta U}{\Delta h}$ and eddy wind velocity (velocity fluctuations) u, as well as the measured horizontal wind velocity component V had to be divided into 11 groups depending on the meteor velocity. For each group we then calculated: 1) the arithmetic average of the eddy velocity gradient $\frac{\Delta U}{\Delta h}$; 2) the rms velocity fluctuations $u = \sqrt{\frac{\Sigma U^2}{n}}$, where U is the horizontal component of the wind velocity fluctuations, and 3) the mean value of the horizontal wind velocity component V.

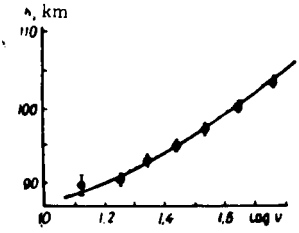

FIGURE 1. The vaporization height of meteor particles as a function of their velocity

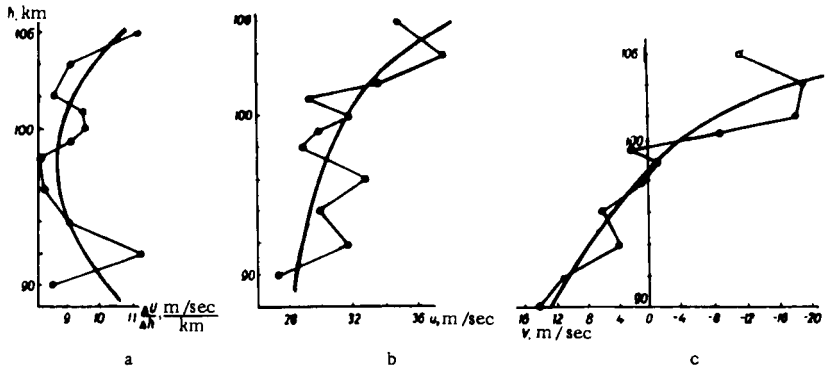

FIGURE 2. Height variation of the mean eddy velocity gradient (a), of the rms wind velocity fluctuations (b), and of the average horizontal wind speed (c)

It follows from the graphs in Figure 2, b, c, that the rms fluctuations and the average wind velocity increase exponentially with height. The highest value of u (38 m/sec) is observed at a height of ~106 km/sec, and the lowest (28 m/sec) at a height of ~ 90 km. The average eddy velocity gradient at those heights is ~0.6 m·sec^{-1}/km. The average wind velocity passes through zero at a height of ~98 km. Below this level westward winds are observed, their average speed dropping with height. Above the 98 km level, eastward winds blow, their average speed increasing with altitude.

The height variation of the eddy velocity gradient shown in Figure 2, a is characterized by a minimum at the height of 98 km. Above this level, the eddy velocity gradient increases with height, while below this level

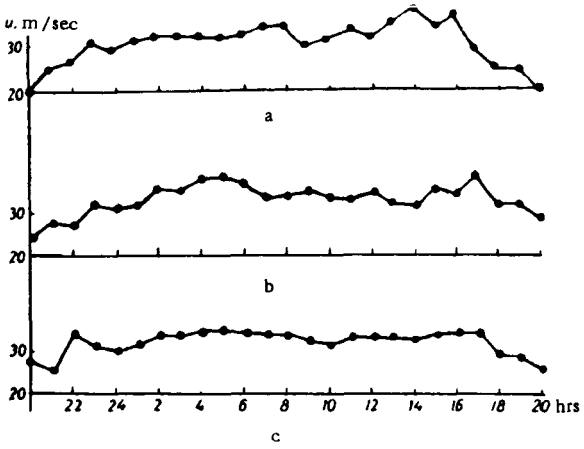

FIGURE 3. Diurnal march of the rms eddy velocity of east—west (a) and south—north (b) winds; diurnal march of the rms eddy velocity averaged for the east—west and the south—north directions (c)

its behavior is reversed. A calculation of the variation of the size of large-scale eddies l with height shows that l increases with altitude: it is equal to 5.8 km at a height of 92 km and to 9 km at the 106 km level.

The horizontal dimensions of large-scale eddies L were calculated by the correlation technique for the heights of ~ 103 and ~ 95 km. At the altitude of 103 km, $L \sim 300$ km, and at the 95 km level, $L \approx 150$ km. The height variation of L is very significant.

2. DIURNAL VARIATIONS

Figure 3 plots the diurnal variations of the rms eddy velocity of winds in the east—west (Figure 3, a) and the south—north (Figure 3, b) directions, and also the march of the average values in the two directions (Figure 3, c). The curves were plotted from the data obtained for the entire period of observations. The hour-by-hour values of u were calculated from the relation $u=\sqrt{\frac{\Sigma U^2}{n}}$, when no less than 40 observations per hour were available. The quantity U was found as the difference $U=V-\overline{V}$, where $\overline{V}$ is the hourly average wind speed, V the measured wind velocity.

We see from the graphs in Figure 3 that U does not vary much during the day. However, the E—W and the S—N winds show a noticeable minimum in the evening, near 20 hours (always local time).

Figure 4 shows the diurnal march of the eddy velocity gradient $\frac{\Delta U}{\Delta h}$, plotted from the results of observations in the westward direction for the period from April to December 1962. The general diurnal trend of the

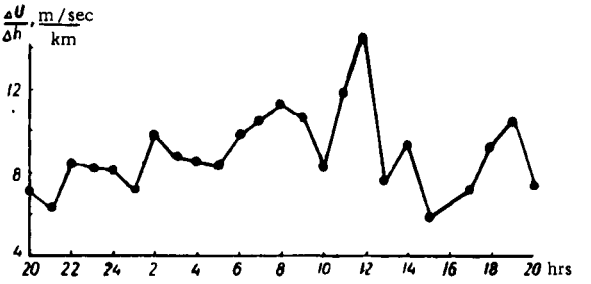

FIGURE 4. Diurnal march of the average eddy velocity gradient

gradient is approximately the same as that of u: an evening minimum and an indistinct maximum at noon.

To estimate the diurnal variation of the vertical extent of the large-scale eddies l, we plotted the correlation coefficient for the wind velocity at two points of a train as a function of Δh for the daytime period (from 6 hours to 21 hours) and for the night hours (from 22 to 5 hours). We found 7.7 km for the daytime l and 5.6 km for l at night.

We also estimated the horizontal extent of the large-scale eddies L in daytime and at night. The average daytime L at the heights of 95 and 103 km was found equal to 300 km, while at night $L = 200$ km. Both L and l show a distinct diurnal march.

Applying the well-known relation for the parameters of large-scale eddies $L = ut$, we estimated the eddy "lifetime" t during the day and at night. The daytime t was found to be ~ 150 min, and the lifetime at night ~ 100 min.

3. SEASONAL VARIATIONS

Figure 5 plots the seasonal variation of the rms eddy velocity of east—west (a) and south—north (b) winds.

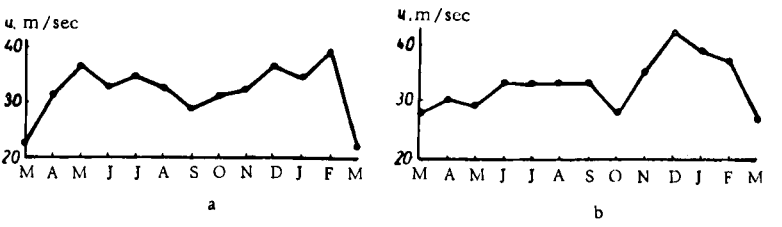

FIGURE 5. Seasonal march of the rms eddy velocity of east—west (a) and south—north (b) winds

The seasonal march of u in both directions shows a certain tendency to semiannual periodicity. The maxima occur in winter and in summer, the minima in spring and autumn. The amplitude of these variations is insignificant, reaching a mere ~20%. There is, however, a distinct difference in the seasonal march of east—west and south—north winds. The SN autumnal minimum occurs in October, while the EW minimum is in September.

Figure 6 shows the seasonal march of the average eddy velocity gradient $\frac{\Delta U}{\Delta h}$ in the east—west direction for the period from April to December 1962. Like u, $\frac{\Delta U}{\Delta h}$ shows a distinct month-to-month variation. $\frac{\Delta U}{\Delta h}$ also displays a tendency to periodic oscillation, with maxima in winter and summer and minima in spring and autumn. However, the smooth march is somewhat distorted by the abrupt variation of $\frac{\Delta U}{\Delta h}$ in May and June. To plot the seasonal march of the "lifetime" t of large-scale eddies, we determined a single value of t for one representative day of every month from April to December 1962. The lifetime t obtained from the autocorrelation curve by the method described in /9/ displays the same seasonal tendency as u and $\frac{\Delta}{\Delta h}$. However, t reaches its high in spring and autumn, with minima in summer and winter.

FIGURE 6. Seasonal variation of the average eddy velocity gradient

The value of l was determined by the correlation technique for the four seasons: summer (June, July, August), winter (November, December, January), spring (April, May), and autumn (September, October). Figure 7 is the graph of the correlation coefficient of the wind velocity at two points of a train as a function of Δh for summer (a), winter (b), spring (c), and autumn (d).

We see from the graphs that l is determined with high reliability, being equal to 6.3 km in summer, 6.2 km in winter, 6.3 km in spring, and 6.2 km in autumn. The scale l at the height of ~94 km thus remains virtually constant during the year, being equal to 6.2 km.

The horizontal scale L was calculated by the correlation technique for the cold season (October, November, December) and the hot season (May, June, July, August). L was determined from data at two altitudes, 103 and 95 km. The results obtained therefore represent the average value of L for these two heights. This average L remains virtually constant: ~275 km in the cold season and ~ 250 km in the warm season.

4. STRUCTURE OF TURBULENCE

The following parameters of large-scale eddies were obtained for the height of ~94 km (averages for the entire period of observations): u = = 33 m/sec, $\frac{\Delta U}{\Delta h}$ = 9.3 m · sec^{-1}/km, L = 150 km, l = 6.2 km, t = 63 min,

$Re = 3 \cdot 10^5$. The Reynolds number is very high, so that well developed turbulence may indeed be observed in the meteor zone.

Let us estimate the eddy dissipation energy ε. We shall apply the following relation between ε and the parameters of large-scale eddies:

$$\varepsilon = A\frac{u^2}{t}.$$

Setting $u = 33$ m/sec, $t = 63$ min, $A = 1$, we find $\varepsilon = 2.8 \cdot 10^3\,\mathrm{g \cdot cm^2 \cdot cm^{-3}}$.

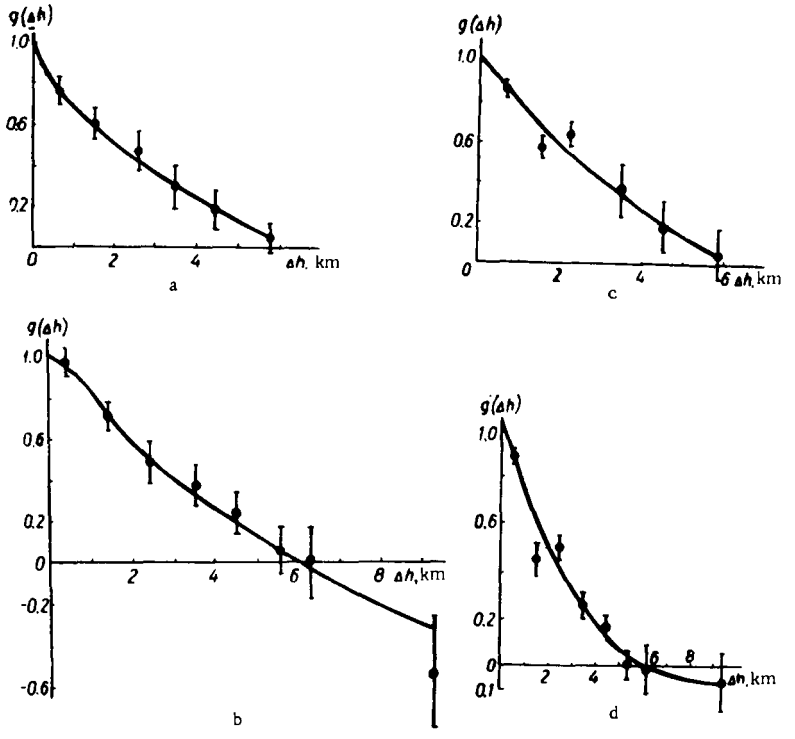

FIGURE 7. The vertical correlation function of the wind velocity in summer (a), winter (b), spring (c), and autumn (d)

A more reliable estimate of the energy ε can be obtained by introducing the dissipation ratio λ, related with ε by the expression

$$\varepsilon = \frac{15\delta u^2}{\lambda^2}.$$

According to the summertime correlation curve, $\lambda = 1200$ m. Then $\varepsilon = 1 \cdot 10^3\,\mathrm{g \cdot cm^2 \cdot sec^{-3}}$. Two independent estimates of ε thus give a value close to $2 \cdot 10^3\,\mathrm{g \cdot cm^2 \cdot sec^{-3}}$.

The parameters l, U_l, t_l were calculated using the relations

$$l = \left(\frac{\delta^3}{\varepsilon}\right)^{1/4}, \quad U_l = (\delta\varepsilon)^{1/4}, \quad t_l = \left(\frac{\delta}{\varepsilon}\right)^{1/2}.$$

The results obtained,

$$l = 8\,\text{m}, \quad U_l = 1.2\,\text{m/sec}, \quad t_l = 7\,\text{sec},$$

are in satisfactory agreement with the figures in /3, 9/.

5. DISCUSSION OF RESULTS

The height variation of the rms eddy velocity of winds is in satisfactory agreement with the data of /1/, and also with the theoretical results of /11/; it is attributable to gravitational waves agitated in the lower atmospheric layers and propagating upward /11/.

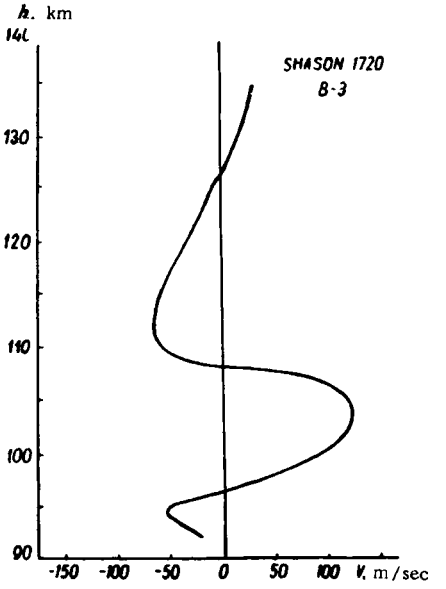

FIGURE 8. Height variation of wind velocity from rocket data /12/ (Rosenberg et al.)

The height variation of the average eddy velocity gradient $\frac{\Delta U}{\Delta h}$ is apparently due to changes in the structure of the turbulence field with height induced by the combined action of two opposing factors: the increase of the eddy wind velocity with height, on the one hand, and the increase

of the kinematic viscosity suppressing the smaller eddies, on the other. It is noteworthy that the highest values of the wind-velocity gradient obtained in /7/ also apply to the 100—110 km range.

Satisfactory agreement with the results of /1, 12/ is also observed for the height variation of the average wind velocity. Figure 8 is a reproduction of the vertical profile of wind speeds from /12/. We see from Figure 8 and Figure 2,c that the height variation of wind velocity according to our results is very close to the findings of /12/.

A remarkable feature is the considerable similarity between the height variation of the rms eddy velocity and that of the average wind velocity; no less remarkable is the existence of a sharp boundary observed at the height of ~100 km, as if separating between two regions displaying different height variations of u, $\frac{\Delta U}{\Delta h}$, and $\overline{V}$. This suggests that the height variation of the parameters being discussed is largely determined by the physical state of the atmosphere at the corresponding height and, in all probability, by the vertical temperature distribution in the atmosphere.

The vertical extent of large-scale eddies found for the ~94 km level is in good agreement with the data of /3, 6, 15/; it is numerically equal to the height of the homogeneous atmosphere H. As regards other altitudes, it should be remembered that H is directly proportional to height /14/, and l and H are very close to each other in the entire vertical range investigated. It is therefore suggested that l in the meteor zone is determined by the height of the homogeneous atmosphere H and is numerically equal to this quantity.

The foregoing assumption was applied to calculate the temperature profile in the relevant range of altitudes (Figure 9). The calculations were based on the well-known relation among T and H:

$$T = mgH/R.$$

Since l were available for the entire period of observations, the temperature profile plotted in Figure 9 gives the yearly average height variation of atmospheric temperature. The results in Figure 9 are in satisfactory agreement with rocket data /15/ obtained for middle latitudes.

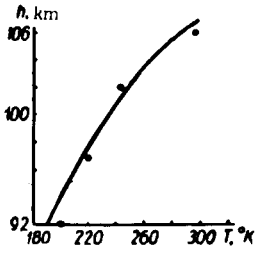

FIGURE 9. Height variation of temperature in the atmosphere

The horizontal extent L of large scale eddies at the height of ~95 km is consistent with the results of /4/. No comparable data have been published in the literature on the value of L at the 103-km level.

Applying the relation $L = ut$ for large-scale eddies, we shall estimate the eddy "lifetime" for the heights of 103 and 95 km. The rms velocity fluctuation u for the desired height is read off the curve in Figure 2. The lifetime t was found to be equal to ~130 min at the height of 103 km, and ~80 min at 95 km. The lifetime t also varies considerably with height.

Diurnal variations. The diurnal march of u, as well as that of $\frac{\Delta U}{\Delta h}$, is not very distinct, but these quantities nevertheless show a characteristic

hour-by-hour variation: a diurnal low in the evening and a gradual increase toward midnight (compare /12/). Our data are also in good agreement with the results in /8, 9/.

The observed change in the vertical extent of large-scale eddies l from day to night is apparently attributable to the diurnal march of the atmospheric temperature at the particular altitude. Setting $l=H$, we can estimate the amplitude of these day-to-night temperature variations. Applying the relation

$$T=mgH/R,$$

we find that the daytime temperature of the atmosphere is 250°K, while the temperature at night is 186°K. The daytime air temperature at the height being studied is thus greater almost by 35% than the temperature at night, which is consistent with the data in /10/.

Seasonal variations. Figure 10 shows the seasonal march of the semidiurnal wind obtained in this study. The seasonal march is plotted for two directions: east—west (a) and south—north (b). There is a certain

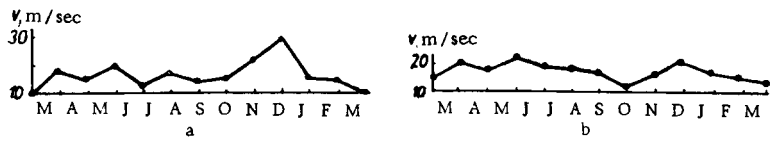

FIGURE 10. Seasonal march of the semidiurnal wind: east—west (a) and south—north (b)

likeness between the seasonal variation of the semidiurnal wind and that of the rms eddy velocity. Both these quantities display a tendency to a semiannual periodicity. They reach a high in winter and summer, passing through the respective minima in spring and autumn. There is also a certain phase shift in the autumnal minima for the east—west and the south—north directions. The observed similarity between the seasonal march of the rms eddy velocity and the semidiurnal wind is apparently a reflection of a common mechanism producing these variations. This mechanism may be supplied by the temperature variations in the upper atmosphere at the particular altitudes.

Somewhat unexpected were the results on the lack of seasonal variation of the vertical extent of large-scale eddies l. Since in the meteor zone $l=H$, then according to the hypothesis of /16/, and also on the basis of the experimental seasonal march of the quantities u, T, $\frac{\Delta U}{\Delta h}$, L, and the semidiurnal wind, the parameter l could also be expected to vary from season to season. However, l remained virtually constant during all the four seasons, being equal to 6.2 km. This fact apparently can be accounted for if we assume that the seasonal variation of l is slight, and does not emerge from the smoothed measurements taken for each season. The seasonal variation of the other parameters of turbulence is apparently determined by appropriate changes in the physical state of the upper atmosphere, and primarily by the march of temperature.

Possible sources of turbulence in the meteor zone. Owing to the strong stabilizing influence of the Archimedes forces in the meteor zone, the mean wind cannot be regarded as the source of turbulence. This conclusion is corroborated by estimates of Richardson numbers, which in our case are equal to ~100; by experimental data, turbulence sets in in the presence of a wind velocity gradient only if Ri<1. Neither we nor the authors of /3/ could find a relation between the rms eddy velocity and the mean wind, or between the rms velocity and the prevailing wind gradient.

One of the possible sources of turbulence in the meteor zone, according to /11/, are the gravitational waves generated elsewhere in the atmosphere, in an environment lacking thermal or hydrodynamic equilibrium. Tides and general-circulation winds in the atmosphere may act as an infallible source of energy for the gravitational waves with various wave numbers. The nonlinear transfer of energy from large to small scales proceeds as in the homogeneous atmosphere.

The following conclusions can be drawn from our results:

1. The turbulence observed at the height of 80—110 km displays a sharply pronounced large-scale anisotropy, which increases with altitude.

2. The yearly average values of the parameters of the large-scale eddies at the height of ~94 km are: $L = 150$ km, $l = 6.2$ km, $t = 63$ min, $u = 33$ m/sec, $\frac{\Delta U}{\Delta h} = 9.3\,\text{cm}\cdot\text{sec}^{-1}/\text{km}$, $\text{Re} = 3\cdot10^5$.

3. The parameters of the large-scale eddies vary with height. The nature of the height variation is apparently determined mainly by the vertical distribution of atmospheric temperature at the particular height.

4. The parameters of the large-scale eddies show a slight diurnal march. The large-scale eddies are generally larger in daytime than at night.

5. The parameters of the large-scale eddies, with the exception of their vertical extent, display a seasonal variation.

BIBLIOGRAPHY

1. LILLER, W. and F. L. WHIPPLE. Rocket Research in the Upper Atmosphere. — [Russian translation p. 135. 1957.]
2. GREENHOW, I. S., E. L. NEUFELD—J. Geophys. Res., Vol. 64: 2129. 1959.
3. GREENHOW, I. S., E. L. NEUFELD—J. Atm. Terr. Phys., Vol. 16: 384. 1959.
4. GREENHOW, I. S., E. L. NEUFELD—Proc. Phys. Soc., Vol. 75: 228. 1960.
5. DELOV, I. A., B. L. KASHCHEEV, and L. I. BOROVICH. —DAN UkrSSR, Vol. 8: 56. 1964.
6. BLAMONT J. E. and J. IAGER—Geophys. Res., Vol. 67: 313. 1962.
7. KAMPE, H. I., M. E. SMITH, R. M. BROWN—J. Geophys. Res., Vol. 67: 4243. 1962.
8. GREENHOW, I. S., E. L. NEUFELD—Proc. Phys. Soc., Vol. 74: 1. 1959.
9. DELOV, I. A., M. F. LAGUTIN, and A. LYSENKO. —Izv. vuzov. Radiofizika, Vol. 7: 225. 1964.
10. GREENHOW, I. S. and J. S. HALL—J. Atm. Terr. Phys., Vol. 18: 203. 1960.
11. HINES, C. O. —J. Geophys. Res., Vol. 64: 2210. 1959.
12. COSPAR Sixth Plenary Meeting and Fourth International Space Science Symposium, Poland—Warsaw 2—2—12 June 1963.
13. GUL'MEDOV, KH. —Geomagnetizm i Aeronomiya, Vol. 2: 313. 1963.
14. KHVOSTIKOV, I. A. —Fizika Ozonosfery i Ionosfery, Vol. 11: 498. 1963.
15. MIKHNEVICH, B. V. —UFN, 63(1b): 197. 1957.
16. KOCHANSKI, A. —J. Geoph. Res., Vol. 68: 213. 1963.

THE KIEV SEMINAR ON COMETARY PHOTOMETRY

An All-Union Seminar on Cometary Photometry, organized by the IQSY Comet Section and the Kiev University, was held at the T. G. Shevchenko Kiev State University on 15 – 18 June 1964. Astronomers specializing in cometary research and representatives of Soviet observatories participating in the cometary survey network and the IQSY comets program took part in this seminar. Thirty-five participants were registered. The seminar was opened by Prof. S. K. Vsekhsvyatskii, chairman of the comets section, who dwelt on the urgent need of improving the current techniques of photometric, polarimetric, and spectro-photometric cometary observations and harnessing the full potential of the observatories with the object of more comprehensively recording the various processes in comets which have bearing on the conditions prevailing in the interplanetary space and on fundamental geophysical problems.

Papers were read by Prof. O. V. Dobrovol'skii, Cor. Memb. Tadzhik Acad. Sci. (visual photometry of comets), L. N. Kolesnik, Cand. Phys. Math. Sci. (photometric systems and stellar magnitude standards), D. A. Rozhkovskii, Dr. Phys. Math. Sci., V. P. Konopleva, Cand. Phys. Math. Sci. (brightness distribution in cometary heads and tails), V. G. Rijves (photographic photometry of comets), V. I. Cherednichenko (problems of cometary spectrometry), Prof. V. A. Dombrovskii (problems of cometary polarimetry), L. V. Ksanfomaliti, Cand. Phys. Math. Sci. (electronic instruments in cometary photometry and polarimetry), Sen. Eng. O. I. Bugaenko, M. A. Eritsyan, Cand. Phys. Math. Sci. (photoelectric photometers). E. B. Kostyakova, Cand. Phys. Math. Sci., presented the results of the spectrophotometry of comet Arend–Roland 1956 h. O. V. Dobrovol'skii reported on cometary conferences in East Germany in 1963, and some reports were read on the scope of cometary observations and studies at the observatories linked to the cometary survey network – Abastumani, Alma-Ata, Byurakan, Leningrad University Observatory, Dushanbe, Kiev (Ukrainian Acad. Sci.), L'vov, Crimea, Odessa, Shemakha. On 18 June, the participants visited the Goloseev Observatory of the Ukrainian Academy of Sciences and familiarized themselves with its potential as regards cometary research.

The lively atmosphere at the seminar greatly contributed to its success; many interesting discussions were held and several important recommendations and resolutions were passed in the final session. All were agreed that similar seminars should be organized in future.

The following recommendations and resolutions were passed at the seminar.

1. The next cometary seminar is to take place during the first months of 1965.

2. The Astronomical Committee and the Interdepartmental Geophysical Committee will provide the necessary funds.

The seminar proceedings will be published; the IQSY Comets Section will take the necessary steps; the Astronomical Committee and the IGC are requested to extend their assistance.

3. All the observatories are requested to proceed with the treatment of observational data obtained in past years with the object of utilizing the results in current and future research; observers of comets are requested to prepare for publication the results obtained in past years and to present short communications for publication in the cometary circular.

4. The seminar urges the development of the following "standard" equipment for cometary survey observatories:

a) a parabolic reflector 1.00 – 1.25 m in diameter (1/5 – 1/7 speed) with necessary auxiliary equipment for photographic, visual, photometric, and spectroscopic observations of weak comets and automatic guiding;

b) 0.5 – 0.7-meter reflector with an improved photoelectric photometer for continuous recording of the intrinsic brightness of comets in the UBV system and in individual emission lines, as well as for polarimetric observations (with automatic guiding);

c) a double astrograph ($F = 1.0 – 1.5$ m, 1/4 – 1/7 speed) with a selection of wide-angle high-speed cameras for photographic and spectroscopic observations of bright comets.

5. Soviet observatories should maintain a closer contact with Czechoslovakian and other foreign observatories.

6. Visual photometric observations and brightness estimates of comets should be constantly made and improved. The seminar suggests the application and further improvement of the following techniques for estimating the intrinsic brightness of comets: a) extrafocal comparison with stars, b) the Volokhov – Beyer method (where the system is unfocused until the image vanishes), and c) other methods of comparison.

7. S. K. Vsekhsvyatskii and I. S. Astapovich are requested to prepare a manual for large-scale amateur determination of comet brightness.

The Dushanbe group (O. V. Dobrovol'skii) is requested to carry on their researches on systems of reduction allowing for the size and the structure of the comet, the sky background, the particular instrument being used, etc.

The Alma Ata group of comet watchers is requested to build a model of the Schering-type visual photometer for the determination of the intrinsic brightness of comets and to prepare an instruction manual for actual manufacture of this photometer and its application in comet brightness estimates.

It is highly desirable that the amateur astronomers operating under the All-Union Astronomic and Geodetic Society should be called upon to give more attention to visual observations of comets. Nebulae and star clusters listed in the catalogs of Messier and Holetschek are suggested as objects of comparison for some comets.

The Main Astronomical Observatory of the Ukrainian Academy of Sciences is requested to prepare lists of photometric standards which can be applied for purposes of brightness estimates in the cometary survey. These lists are to be published in the cometary circular.

The Astronomical Committee is requested to prepare lists of all the existing standards in the UBV system for distribution to all the observatories participating in the cometary survey. The Committee will also prepare and publish its recommendation for photographic determinations close to the UBV system.

8. V. G. Rijves and the Tartu group are requested to present in the nearest future their recommendations for optimal exposure times with cameras of different models with the purpose of ensuring high-precision determinations of the intrinsic brightness of comets. A very urgent project in the opinion of this seminar is the development of appropriate techniques for focal and integral-light photometry of comets with small and ultra-short-focus cameras.

It is suggested that V. G. Rijves should compare his photographic magnitudes of comets with other published data obtained photographically and by visual or photoelectric techniques.

The Kiev group is requested to develop an efficient technique for estimating the color-indices of comets.

The Alma Ata group (D. A. Rozhkovskii) is requested to present their recommendations concerning the design of a special eyepiece for the guiding of comets and to lay a foundation for the creation of a special system of automatic cometary guiding.

All participants of the cometary survey are urged to report regularly their results on the photometry of comets in the cometary circular (Kiev).

9. The observatories in Abastumani, Byurakan, Leningrad University, Odessa, Alma Ata, Kiev, Pirkuli, Dushanbe, and elsewhere will proceed with the development of photoelectric techniques of brightness determination and polarization measurements of comets; it is suggested that different observation procedures be applied at the different observatories.

V. A. Dombrovskii and L. V. Ksanfomaliti will help to the best of their ability to all observers interested in the application of photoelectric and polarimetric techniques.

It is suggested that photoelectric and photographic determinations of the brightness of weak comets be made in parallel, with the object of pinpointing the systematic errors in the calculation of the intrinsic brightness of comets fainter than 11th or 12th magnitude.

10. The seminar views with concern the highly inadequate state of spectroscopic observations of comets in the Soviet observatories, although these observations are invaluable for the solution of various fundamental problems of the interplanetary space and solar physics. The seminar seeks the guidance of the Crimean Astronomical observatory in all that concerns observation of bright and weak comets with 50" and 102" telescopes; it is suggested that spectroscopic cometary observations should be made on a larger scale with the telescopes of the Shternberg Astronomical Institute's Crimean station and the Byurakan Observatory.

All observatories are urged to take cometary spectra with objective prisms.